Biologically Inspired Radar and Sonar Target Classification

Alessio Balleri

Supervisors:

Prof.   H.D. Griffiths
Prof.   C.J. Baker

A thesis submitted for the degree of
Doctor of Philosophy
of
University College London

Department of Electronic and Electrical Engineering
University College London
6th December 2010

I, Alessio Balleri, confirm that the work presented in this thesis is my own and has not been submitted in any form for another degree or diploma at any university or other institute of tertiary education. Information derived from other sources has been indicated in the thesis.

Alessio Balleri

London, December 6, 2010

Abstract

Classification of targets is a key problem of modern radar and sonar systems. This is an activity carried out with great success by echolocating mammals, such as bats, that have evolved echolocation as a means of detecting, selecting and attacking prey over a period of more than 50 million years. Because they have developed a highly sophisticated capability on which they depend for their survival, it is likely that there is potentially a great deal that can be learnt from understanding how they use this capability and how this might be valuably applied to radar and sonar systems. Bat-pollinated plants and their flowers represent a very interesting class of organisms for the study of target classification as it is thought that co-evolution has shaped bat-pollinated flowers in order to ease classification by bats. In this thesis, the strategy that underpins classification of flowers by bats is investigated. An acoustic radar has been developed to collect data to perform a floral echoes analysis. Results show that there is a relative relevance of specific parts of the flower in displaying information to bats and show that there are different characteristics in the flowers' echo fingerprints, depending on age and stage of maturity, that bats might use to choose the most suitable flowers for pollination. We show that, as suggested by the floral echoes analysis, a more intelligent way to perform target classification can result in improved classification performance and, investigate biologically inspired methods and ideas that might become important tools for the study and the development of radar and sonar target classification.

To Mamma e Babbo....

Acknowledgements

Contents

List of Figures

8

11

14

15

16

17

18

List of Tables

List of Acronyms

CF   Continuous Frequency

HFM   Hyperbolic Frequency Modulation

HRRP   High Range Resolution Profile

IID   Interaural Intensity Differences

IR   Impulse Response

ISAR   Inverse Synthetic Aperture Radar

ITD   Interaural Temporal Differences

K-NN   K Nearest Neighbour

LFM   Linear Frequency Modulation

MLS   Maximum Likelihood Sequence

PCA   Principal Component Analysis

PRF   Pulse Repetition Frequency

PRI   Pulse Repetition Interval

RADAR   RAdio Detection And Ranging

SAR   Synthetic Aperture Radar

SAS   Synthetic Aperture Sonar

SCAT   Spectrogram Correlation And Transformation

SNR   Signal to Noise Ratio

WAF   Wideband Ambiguity Function

List of Symbols

τ Time Delay

T Pulse Duration

R Range

c Speed of Propagation

B Pulse Bandwidth

R_r Range Resolution

v Target Velocity

f_0 Carrier Frequency

f_i Instantaneous Frequncy

f_D Frequency Doppler Shift

χ Ambiguity Function

η Doppler Compression Factor

γ Chirp Rate

h_H Hilbert filter response

X Fourier transform of the signal $x(t)$

$\hat{x}$ Analytic signal associated to x

$\dot{x}$ Complex envelope of x

ϕ	Instantaneous signal phase
ϕ_0	Phase offset
$Re\{\}$	Real part
$Log\{\}$	Logarithm operator
K_{nn}	K-Nearest Neighbour
$F(X,Y)$	2D Fourier transform of the function $f(x,y)$
p_ϑ	Projection of $f(x,y)$
P_ϑ	Fourier transform of p_ϑ
ω	Radial target velocity
P	Mean power
t	Time
f	Frequency
λ_0	Wavelength corresponding to the frequency f_0

Chapter 1

Introduction

1.1 Overview and motivations

In recent years with the development of high range resolution radar and sonar systems, the desire to be able to identify targets under all weather and clutter conditions has become of great importance. This is an activity carried out with considerable success by echolocating bats that are able to detect, select and attack prey even in a dense clutter environment [3] [4] [5]. Bats have evolved echolocation as a means of detecting, selecting and attacking prey over 50 million years, and there is (potentially) a great deal that can be learnt from understanding how they use these capabilities and how this might usefully be applied to radar and sonar systems. Although classification of targets is a very important task for modern radar and sonar systems and much has been published on these topics, there have been rather limited efforts to learn from nature. Target recognition performance obtained by modern radar and sonar systems is a long way short of that obtained

by bats. Limitation can result from the fact that typical classifiers do not take into account the characteristics of the targets that they have to recognize, and more importantly do not operate under any particular strategy aimed at maximizing classification performance. The common approach to classification of targets consists of comparing radar measurements, such as high resolution range profiles (HRRP), ISAR images or Doppler modulations, with templates contained in reference libraries which have been created in advance and are used to perform classification [6] [7] [8] [9] [10]. However, the problem associated with these libraries is that they require a significant amount of data to be stored. This approach leads to classification performance that appears not to be robust, as small changes in the target (such as an open door in a car, or a slightly different way of training the classifiers) could lead to significantly different results in terms of classification performance [11]. Although some feature extraction algorithms, such as Principal Component Analysis (PCA) and Fisher's Linear Discriminant Analysis, have been developed, none of them was realized to best perform with any particular targets of interest [12]. Common sense suggests that concentrating on features such as specific parts or particular behaviours of targets could reduce the complexity of the classification process and at the same time could enhance classification performance. In nature, echolocating mammals such as bats, whales, and dolphins have an imperative to detect, recognise and attack prey in order to feed. Thus it seems there is a great deal that could be learnt by investigating how the natural world operates.

Classification of insects by bats has been reported in the literature [13] [14]. This classification is performed through the combined information available

27

in both the time and the frequency domains. The amount of power reflected from targets gives the bats information on the size of the target itself. The bigger the target, the greater the fraction of power that is reflected. The same type of information can be obtained by looking at modulations in the amplitude of the echo. It has been shown that there is a positive correlation between body size and wing beat period in insects. Also, the periodic amplitude modulation by moving the wings is directional, giving the bats information on the look angle. Doppler shift and micro Doppler modulations are of great interest as well. It has been shown that each species of insect has a characteristic micro Doppler signature even when the wing beat frequency is the same [13] [14]. Although several works have looked at how bats recognize moving targets, the literature shows a lack of knowledge on how these mammals perform classification of static targets. Nectar feeding bats play an important role in the process of pollination of plants. Bat-pollinated plants and their flowers represent a very interesting class of organisms for the study of target classification as it is thought that co-evolution has shaped bat-pollinated flowers in order to ease classification by bats. Firstly, flowers are motionless and silent so that bats cannot rely on Doppler information or passive echolocation based on target sounds, and secondly their habitat is often a densely cluttered environment. Although classification of flowers in such an environment is demanding, nectar-feeding bats succeed in their pollination task. Finding and approaching a flower is a gradual process that involves all the bats' senses. Long range attraction is by scent and the bat's excellent spatial memory [15]. However, their sense of smell is not accurate enough to localize and approach the flower and bats have to rely largely on

28

echolocation to plan their approach flight and detect the flowers against the cluttered background. Evidence of this is provided in [16]. Choosing the most suitable flowers to be visited within a plant is a task that cannot be done by scent and is therefore mainly carried out by echolocation [2] [17].

1.2 Aim

The aim of this thesis is therefore to better understand the methodologies used by bats to perform classification of static targets and how these can be usefully applied to radar and sonar systems by an analysis of floral echoes. Specifically, this work aims at understanding the strategies that underpin the process of classification of flowers of bat-pollinated plants by bats and investigates whether the common idea that co-evolution between these two organisms enables high level classification performance is plausible. The final goal is to open up a discussion and a first investigation of how lessons from nature might be applied directly or indirectly, i.e. in the form of other supporting techniques, to radar and sonar systems to enhance target classification performance.

1.3 Thesis layout

This thesis is organised as follows. Chapter 2 contains a review of the main publications on the methods used to perform target classification in modern radar and sonar systems, and a review of the main publications on the methodologies deployed by bats to recognise objects and, in particular, the

targets they depend on for their survival. A detailed review of the publications that focus on the relation between bats and bat-pollinated plants is also given and their weaknesses highlighted to motivate the necessity of this research work.

Chapter 3 contains a description of the main concepts used in typical modern radar and sonar systems necessary to understand how the results reported in this thesis were obtained and assessed. In Chapter 4 a typical series of echolocation calls is analysed to provide the reader with a direct example of the type of echolocation calls deployed by bats in real scenarios. A preliminary analysis of floral echoes is given in Chapter 5 where a dataset provided by the University of Bristol is analysed. This allowed us to identify weaknesses of previous data collection procedures and to understand how to build a more efficient acoustic radar to gather the data that was needed to improve this study. This chapter concludes with a detailed description of the acoustic radar instrument which has allowed collection of all the floral data that was analysed to produce the results of this thesis. Results from the floral echoes analysis are given in Chapter 6 and Chapter 7. In Chapter 8 a bio-inspired intelligent strategy to gather target data and perform classification of targets is described and classification results assessed on the flower data. In Chapter 9 airborne ultrasound tomographic images are generated to investigate whether they can be successfully used to create images of very small objects. Finally in Chapter 10 it is investigated how ultrasound data might be used for the study of classification of radar and sonar targets, and the bio-inspired approach to target classification in tested on scaled man made targets. The conclusion of this work and the suggestions for future research

are given together in Chapter 11.

1.4   Achievement of this work

The work presented in this thesis represents a novel interdisciplinary study that, as such, has resulted in achievements on both biological aspects and radar and sonar systems aspects.

- In Chapter 4 it is shown that the use of harmonics can enhance the characteristic of the ambiguity function of typical radar and sonar waveforms.

- In Chapter 5 it is shown that the output of a multi-perspective classifier testing floral targets presents close similarities with respect to the output obtained when classical radar targets are tested.

- In Chapter 6 experiments show the relative importance of specific parts of the flower in displaying information to bats and that, in particular, pistils and petals may add critical components to the echo fingerprint that might contain the information bats use to decide to visit specific individuals flower.

- They also show that echoes from wilting flowers and closed buds present characteristics that are very different from those of the open flower.

- These findings are related to a typical bat trajectory and it is shown that the angular perspectives explored during an approach flight are

in agreement with the angular windows in which the scattering from flowers' features are very obvious.

- Experiments show that open flowers are highly directional on both the horizontal and the vertical plane with respect to closed buds and flowers without the corolla (Calyx) within an inflorescence. They also show that scattering from open flowers at the angle of interest is higher than that generated by closed buds. Results support the commonly accepted idea that, as in nature, radar and sonar systems should operate adaptively with the target in space and time.

- In Chapter 8 it is shown that a bio-inspired intelligent approach to radar and sonar target classification can result in a significant improvement in classification performance.

- In Chapter 9 it is shown that the acoustic radar is capable to capture detailed information of small static targets and in particular allow detection of differences due to small changes in their shape. We also show that bio-inspired ultrasound tomographies in air are possible and can lead to good imaging of small static targets.

- In Chapter 10 first results aiming to show that there are close similarities between RF data and ultrasound data are presented. It is argued that the acoustic radar can be deployed to gathered data from real scaled targets to carry out preliminary analysis of classification performance and produce predictions for real scenarios.

It is my hope that the results reported in this thesis and our suggestions for future works may play an important role for future studies in this highly challenging and motivating topic.

1.5 Publications arising from this research work

The following publications have resulted from the work presented in this thesis.

Journal Papers

1. A. Balleri, C.J. Baker, K. Woodbridge and M.W. Holderied, "Flowers classification by bats: radar comparisons", *IEEE Aerospace and Electronic Systems Magazine*, vol. 24, no. 5, pp. 4-7, May 2009.

International Conference Papers

1. A. Balleri, H.D. Griffiths, C.J. Baker and M.W. Holderied, "Bat-Inspired Multi-Harmonic Waveforms", in *2010 International Waveform Diversity and Design Conference*, Toronto, Canada, 8-13 Aug. 2010.

2. A. Balleri, H.D. Griffiths, C.J. Baker, K. Woodbridge and M.W. Holderied, "Impact of flight trajectory on the detection and selection of flowers by nectar-feeding bats", in *2nd International Workshop on Cognitive Information Processing*, Elba Island, Italy, 14-16 June 2010.

3. A. Balleri, H.D. Griffiths, C.J. Baker, K. Woodbridge and M.W. Holderied, "Bat-inspired ultrasound tomography in air", in *International Radar Conference 2010*, Washington DC, USA, 10-14 May 2010.

4. A. Balleri, C.J. Baker, H.D. Griffihts, K. Woodbridge and M.W. Holderied, "Bat-pollinated plants: feature extraction for target recognition in the natural world", in *International Radar Conference - Surveillance for a Safer World, 2009.*, pp. 1-5, Bordeaux, France, 12-16 Oct. 2009.

5. A. Balleri, H.D. Griffiths, C.J. Baker, K. Woodbridge and M.W. Holderied, "Nectar feeding bats: feature identification for target recognition in the natural world", *NATO Workshop on Machine Intelligence For Autonomous Operations*, Lerici, Italy, 7-8 Oct. 2009.

6. A. Balleri, C.J. Baker, K. Woodbridge and M.W. Holderied, "Classification of flowers by bats: comparison with the radar case", in *2009 International Waveform Diversity and Design Conference*, pp. 1-3, Orlando, USA, 8-13 Feb. 2009.

Chapter 2

Research context

The idea of developing a system capable of detecting objects by sending electromagnetic waves and receiving the corresponding echoes started to grow at the beginning of the last century. Since the 1930s there has been a lot of interest in investigating and improving the capabilities of these systems, which a few years later took the name of RADAR (RAdio Detection And Ranging). The basic task of a radar system was to detect the presence of a target by sending an electromagnetic waveform and waiting for a possible echo. More sophisticated systems have then been developed to satisfy the more demanding need of being able to localise and identify the target as well [18].

Classification is a very important task to be accomplished by radar systems and there has been considerable interest and substantial published research on radar target classification, not all with much success. Classification of targets by radar and sonar systems is a very difficult task to accomplish. Firstly, all the desired information on the targets of interest is not commonly

available. Secondly, even when some information is available, the data depends significantly on the target aspect angle and on small changes in the target as well. In addition to this, in some applications, targets are counter designed to be stealthy with respect to the task of target classification and are designed to reflect the least possible energy and information. Finally, radar and sonar systems commonly operate against highly cluttered backgrounds that together with weather conditions deteriorate the quality of the data significantly.

Here the reader is taken through some of the main publications on radar target classification with a particular emphasis on techniques concerning high range resolution profile target classification. The main publications on echolocation by bats and its role in target selection and recognition are then reviewed so that both the similarities and any differences can be extracted and understood.

A very good insight on the topic is given in the books by Tait [19], by Duda [12] and by Looney [20]. The word *classification* started to appear in the radar scene in the early 1970s when the international radar community became interested in exploiting resonance frequencies of targets [21] [22]. Attention on this technique was fueled by the fact that resonance frequencies are practically independent of aspect angle and hence it was hypothesised that they could be used to perform robust recognition with high performance. Unfortunately this technique proved not to be too practical as high powers are required to stimulate the frequencies of interest [23].

After high resolution radars became available, research on classification of targets by resonance frequencies slowed down considerably and the attention

started focusing on techniques such as high range resolution profile classification. This looks at the shape of the target echo response as a function of range. A way to look at exploiting the shape of a target is to use a two dimensional signature (2-D) obtained by SAR or ISAR processing. A very good overview of high resolution radar techniques is given in [24] and excellent references covering the wide literature on high range resolution profiles methods can be found in [25], [26], [27], [7] and [28]. In [8] and [6] multi perspective target classification using high range resolution profiles was performed and the authors showed that it is possible to obtain better classification performance by increasing the number of aspect angles. However, whilst this work used real radar data and targets, the targets were located on a turntable and were free from multipath and clutter (i.e. ideal conditions).

The main problem associated with the use of high range resolution profiles is their dependency on aspect angle and the difficulty of building a reliable reference library to be used to train the classifiers. For example, a small change physically in the target, such as opening a car door, can have a disproportionally large effect on the echo.

Because of these problems higher order spectra techniques for feature extraction, such as radially, axially and circularly integrated bispectra [29] [30] [31], were studied in order to resolve the time shift sensitivity of HRRPs and to reduce the library data set complexity [32][33]. Calculation of bispectra resulted in a significant computational overhead. Attempts to resolve this were presented in [34] where a method for calculating the Euclidean distances in the higher order spectra feature space was proposed. This avoided calculating the higher order spectra with a resulting drop in computation complexity

and storage requirements.

Methods exploiting full and micro motion have also been examined [35][10] [36] [37] [38]. Recently there has been the attempt to classify targets by using micro-Doppler signatures, i.e. time varying frequency modulations that are generated by moving parts of the targets. The advantage of this technique is that it does not require high resolution and is easily applied even to cheaper and older systems (legacy). In [9] and [39], classification results of a wheeled vehicle, a tracked vehicle and a walking person showed that micro-Doppler can provide crucial information leading to enhancement of performance up to correct classification probability peaks of about 96%.

Echo locating mammals, and in particular bats, have been studied for many years and there is a huge body of research published. Indeed the text by Altringham provides an excellent introductory treatment of the subject [5]. Bats use a wide range of signals designs in echolocation [3]. Factors such as frequency bandwidth, pulse interval and intensity are all shaped by natural selection according to environmental features in the bat's surroundings [4]. So strong is the influence of environmental features in shaping signal design, that bats in different evolutionary lineages have evolved similar signals to orientate and find prey in similar environments [3] [40]. Classification in bat echolocation is defined as the use of patterns of information in echoes to categorize targets [41]. In the past years a lot of research has focused on bats that emit continuous frequency (CF) signals. Figure 2.1 shows an example of a CF waveform that is composed of three main harmonics at about 30 kHz, 60 kHz and 120 kHz that are initiated and terminated by frequency modulated sweeps. It has been argued that the portions at the beginning and end of the
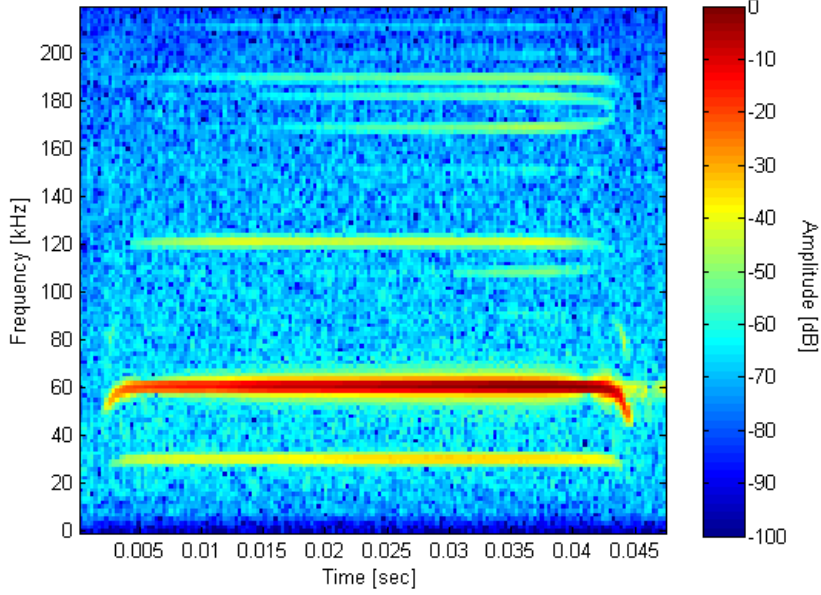
Figure 2.1: Example of a multi-harmonic CF signal with initial and final sweep.

waveform function in target localization, while the long constant frequency component eases the detection and the classification of targets [42]. Indeed, this type of waveform is not being used by any radar system and the fact that mammals perform amazingly by using it makes worth exploiting the impact that its use would have on radar target classification. In flight most species of CF bats, such as horseshoe bats, lower their call frequency in relation to their flight speed in order to compensate for Doppler shifts induced by their own movement so that echoes always return at a best suited frequency for the hearing of the bats [43]. Bats that emit CF signals can detect and classify fluttering insects from amplitude and frequency modulations of the echoes caused by the movement of the insect's wing [44][45]. These modulations, called 'acoustical glints', potentially provide information about the

wing beat rate and flight angle, and are very specific for each species of insect. Glints turn out to be useful not only for the detection of the prey but also for the identification of it. Amplitude modulations are the result of the fact that echo strength is strongest when the insect wings are perpendicular to the sound source and gets weaker as the insect wing moves away from the perpendicular position. Interestingly, the precise timing of the glint depends on the angular orientation of the insect [13], then amplitude modulations give information about the target elevation that affect the timing of the glint production [46]. Figure 2.2 shows an example of amplitude modulated echo from a flying moth *Autographa gamma* at three different angles with equidistant starting phase. In the figure the amplitude modulation is given with its corresponding wingbeat phase at each time. In the experiment the loudspeaker was placed at the same height as the insect. The plot shows that at 90 degrees the glint is produced at the top of the stroke, i.e. when the moth wings are perpendicular to the sound source. At 0 degree (frontal) and 180 degrees (rear), the glint occurs two phases after the upstroke suggesting that, in both cases, the same part of the wings produces the glint [13]. The wing movement towards and away from the receiver induces Doppler shifts in the echoes, taking information of wing beat movement, that are important signatures for species identification since insect wing beat frequency scales with body size [47]. Because the way in which a given insect species moves its wings is highly specific, the structure of glints varies across different species and even insects with the same wing beat may provide different spectral signature in the echo [14]. Figure 2.3 shows the spectrogram of four echoes from four different insects: *Deilephila elpenor*, *Scotia exclamationes*, *Melolontha*

41
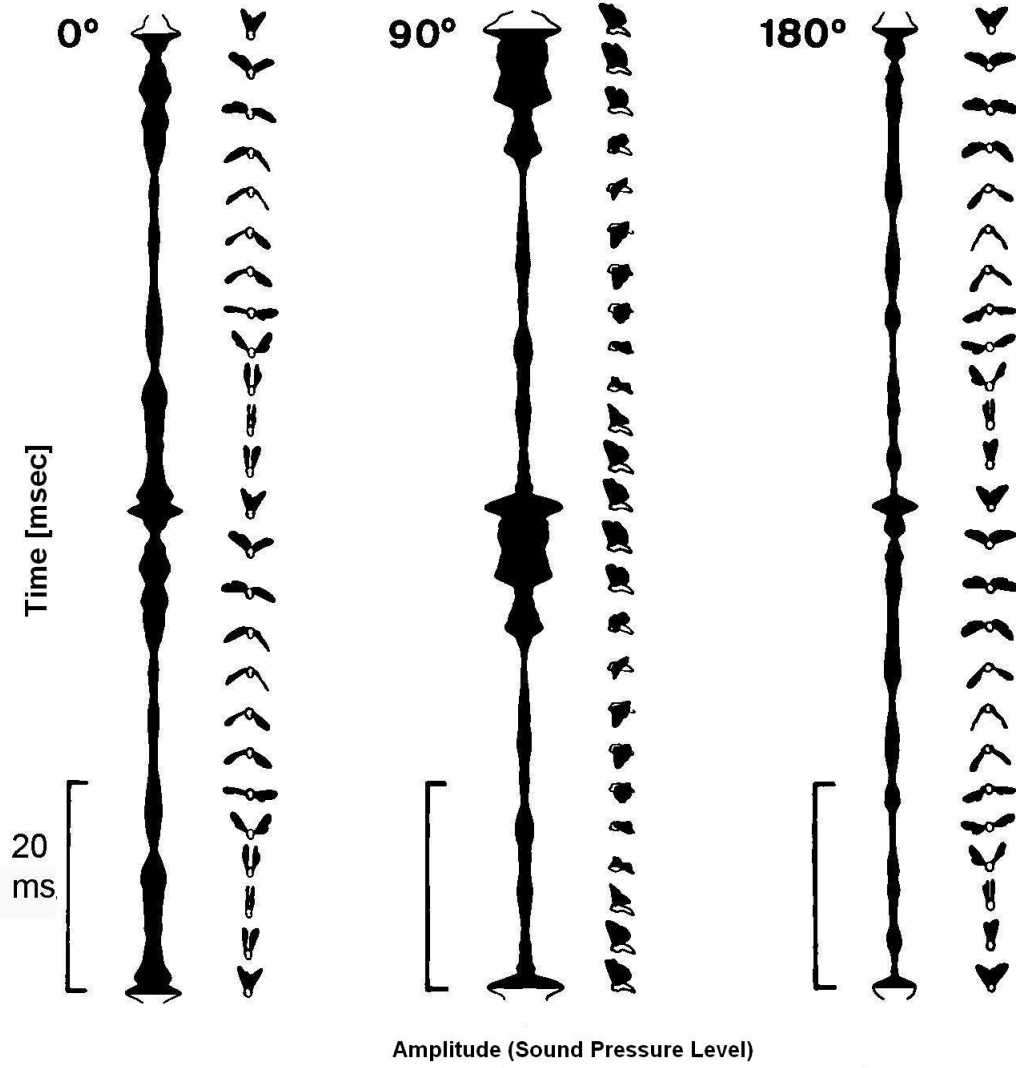
Figure 2.2: Amplitude-modulated echoes from a flying *Autographa gamma* at three different angles with equidistant phases of 2 wing beat cycles and their corresponding wingbeat phases. At 90 degrees the glint is produced at the top of the stroke, i.e. when the moth wings are perpendicular to the sound source. At 0 degree (frontal) and 180 degrees (rear), the glint occurs two phases after the upstroke suggesting that, in both cases, the same part of the wings produces the glint. Taken from [13].
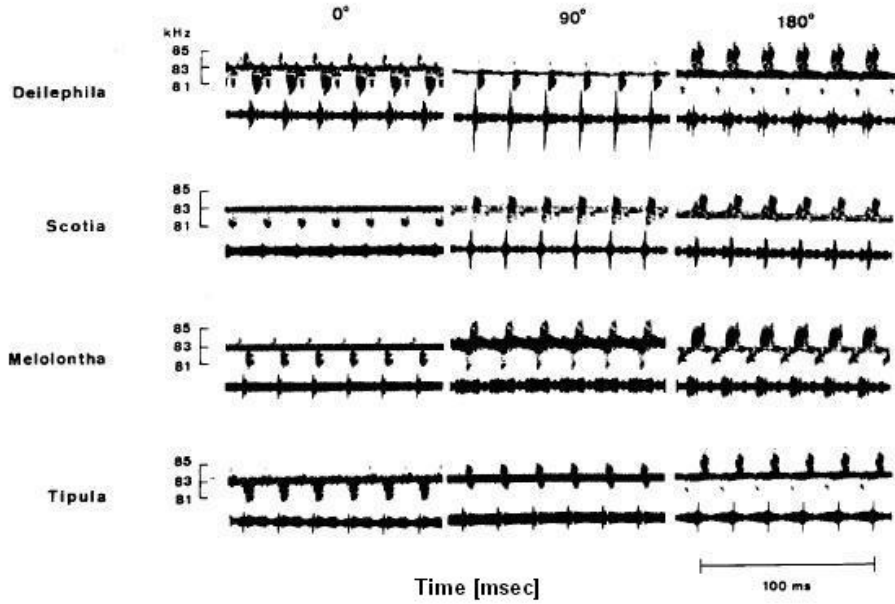
Figure 2.3: Echoes from four insect species all fluttering at 50 Hz but with different spectral patterns in echoes from their wing beats. For each insect, the upper trace represent the spectrogram of the echo and the lower trace the time oscillation. Taken from [14].

melolontha and *Tipula oleracea*. These were flying with the same wing rate and were illuminated from 0, 90 and 180 degrees with respect to the sound source. The figure shows that spectrograms related to each species present different characteristics, although the fluttering frequency is the same. It also shows that for the same insect the property of the spectrogram are also dependent on the angle from which the sound source was coming, confirming that spectral cues provide information on angular position as well [46] [48]. Finally, the trace of the time oscillation confirms that the same considerations are valid in the time domain. Schnitzler showed that at 0 degrees (i.e. frontal view) spectral broadenings in echoes due to glints, typically fall below the carrier frequency (i.e. the micro-Doppler signature concentrated below

43

the carrier frequency), while at 180 degrees they show negative and positive Doppler shift, and that the width of the broadening is related to the wing beat frequency of the insect [48]. Roverud showed that bats that use shorter signals need greater differences in wing beat frequencies than bats that emit longer signals, in order to discriminate between different fluttering targets [49]. However, behavioural experiment tests show that neither amplitude or frequency modulations alone are sufficient to achieve recognition of insects and that differences in glints from series of echoes play an important role in target classification. This highlights the fact that whilst it is clear that bats are able to use echo location sources in a comprehensive way, it is not fully understood how they do this. For example, von der Emde and Schinitzler showed that greater horseshoe bats are even able to discriminate insects of a given species when presented with echoes from the insect illuminated at angles that they had not previously experienced [14].

The way which CF bats classify fluttering insects has a very close parallel with the attempt, in radar systems, to classify targets by using micro-Doppler information in the echo spectrogram. A big difference though is that bats are able to combine information that derives, at least, from both amplitude modulations and frequency modulations and manage to obtain remarkable performance in a very difficult task. Bats, in fact, have shown a peculiar ability to distinguish between insects that present the same wing beat rate and that have very similar dimension and obtain performance which currently is enormously better than what a radar system can do. It is evident that all this might open the way to a new branch of research that not only looks at the micro-Doppler signature of a moving target but also at how this

movement modulates the amplitude of the echo and at how this information can be possibly combined and utilized to enhance radar target classification performance.

Although most research has focused on classification of fluttering targets by bats that emit CF signals, bats that emit broadband signals have the same ability to do so [50] [51] and there is a lot interest in understanding how they classify targets as well. Since for these species of bat the duration of the call is often too short and produced at low rates, Sum and Menne, and Grossete and Moss argued that the bats perform discrimination after receiving two different echo components, one from the stationary part of the targets and the other from the fluttering component of the target. These species of bats can transmit multi-harmonic frequency modulated signals, mostly LFM (Linear Frequency Modulated) and HFM (Hyperbolically Frequency Modulated), whose main component (i.e. the component which contains most of the energy) is not always the fundamental harmonic [3]. Krumbholz and Schmidt argued that multi harmonic calls allow bats to perceive local spectra changes in echoes that result from the effect of glints interference on each individual harmonic, allowing the bats to extract extra information from echo call consisting of a single harmonic. Moreover they showed that narrow spectral notches are particularly perceivable in echoes from multi harmonic calls [52]. Indeed, another hypothesis is that harmonics could be used for different individuals to distinguish their calls in a multi-signal environment [53].

Accuracy in measuring echo delays is strongly dependent on the transmitted waveform bandwidth, and it was shown that delay acuity (precision of estimation of the delay) declines in relation to the reciprocal of the relative echo

45
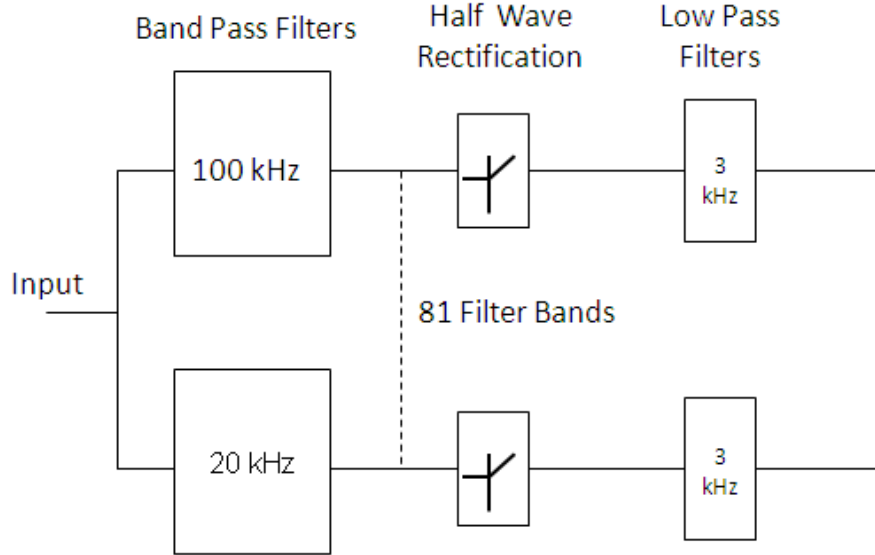
Figure 2.4: Diagram of the cochlear block of the SCAT receiver. The input signal is first processed by a bank of 81 parallel 10-th order Butterworth IIR filters with constant 4 kHz bandwidth. Each bandpass filter is followed by half-wave rectification and filtering with a 3 kHz low-pass filter. Taken from [56].

bandwidth [54]. An ideal receiver functions by cross-correlating the emitted signal and the incoming echo to produce a time-domain representation where, if an echo returns from a point target, the autocorrelation function of the signal approximates the cross-correlation function of the acoustic transmission and echo accurately [55] i.e. the equivalent to matched filtering in radar. The most sophisticated model of auditory computations used in ranging by broadband echolocation has been the spectrogram correlation and transformation (SCAT) model developed by Saillant [56] and also described by Simmons [57]. As shown in Figure 2.4, the SCAT model assumes that the bat's cochlea breaks up the frequencies in calls into parallel bandpass-filtered

channels, half-wave rectifies and then smooths the resulting frequency segments of sounds, and then triggers neuronal responses from these excitation patterns. The simulated neuronal responses triggered from auditory spectrograms can then be used in computations to reconstruct the positions of echo sources along a range axis. The SCAT model consists of three processing blocks that represent signal processing characteristics at different levels within the bat's auditory system. First there is a cochlear block, and then two parallel pathways for processing temporal features (spectrogram correlation block) and spectral features (spectrogram transformation block) in echoes. The model therefore includes consideration of how glints along the range dimension create interference patterns in echoes, and how spatial images of range can be represented. Finally, it considers how the auditory system's representation of spectral features can be transformed into a quite different time-domain metric that gives the bat an image of shape. The SCAT model was developed to give a plausible mechanism by which bats can distinguish ideally two echoes. In reality, echoes from a target are composed of many echoes returning from lots of reflecting surfaces. The sum of all these echoes is called the impulse response (IR) of the target. Bats are able to evaluate statistical property IRs and possibly able to classify by using these properties [1]. Grunwald et al. considered IRs from foliage targets and showed that the phyllostomid bat *Phyllostomus Discolor*, which emits multi-harmonic broadband echolocation calls, was able to classify phantom echoes that contained up to 4000 stochastically distributed reflections [1]. Figure 2.5 shows the time plot and power spectrum of the three different IRs that were used in the experiment by Grunwald. Every IR has the same time duration of 16.4

47
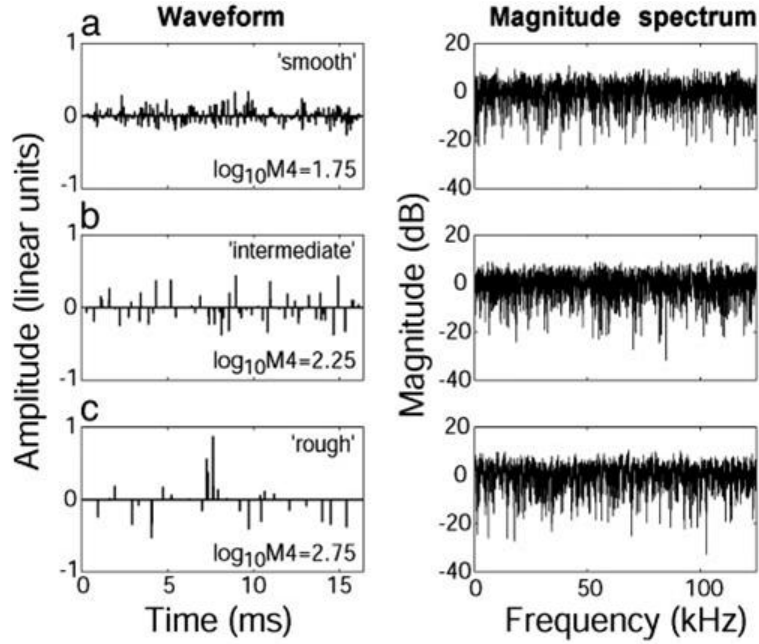
Figure 2.5: Representation of complex echoes with different degrees of roughness as impulse responses (IRs) as in [1].

msec but a different degrees of roughness (variability). The magnitude spectrum is frequency independent showing the fact that the bats can actually classify by using stochastic properties without any frequency information. Indeed it is claimed by Simmons [57] that bats can resolve targets spaced at a distance much closer that the bandwidth implies. There is no common agreement on how this could be achieved.

Another class of organism that is particularly interesting for the study of object classification by echolocation is bat pollinated plants and their flowers, which have evolved to attract nectar feeding bats not only by their scent and appearance but also by their echo acoustic signature. There has been some research focusing on species of flower that provide nectar for bats, since it is thought that co-evolution eases the bat's task of finding and exploiting these

48

flowers. Finding and approaching a flower is a gradual process that involves all the bats' senses. Long range attraction will be by scent and the bats's excellent spatial memory [15]. However, their sense of smell is not accurate enough to localize and approach flowers on a plant and bats have then to rely largely on echolocation to plan their approach flight, to detect flowers against the vegetation background, and to find the opening of the nectarium. Evidence of this was provided by von Helversen and von Helversen in [16]. Here the authors, to exclude the role of visual and olfactory cues, altered with unscented cotton pads the echo-reflecting properties of the *Mucuna holtonii* flower (without altering the smell of the flower) and counted the number of visits by bats to both original flowers and altered ones. Results showed that very few manipulated flowers were visited (17% of the total number of visits) with respect to the intact ones (66%). Nectar-feeding bats approach flowers in fast flight, slowing down over the last centimetres to accurately reach the flower's nectarium, which often measures only a few millimetres. Von Helversen and Winter showed that hovering flights last only fractions of seconds, during which the bats extract nectar from the flower [58], and von Helversen and von Helversen also have shown that, in nature, bats often inspect a flower in a first approach and that they return a few seconds later for the actual feeding visit [59]. Recognition of flowers turns out to be a very challenging task for bats. Firstly flowers are motionless and silent so that bats cannot rely on Doppler information or hearing and secondly their habitat is often a dense cluttered environment. Even if recognition of flowers seems to require a lot of effort, bats show remarkable performance. However, this performance has not been fully quantified. For example, von

Helversen found that with artificial objects nectar-feeding bats were not only able to discriminate between different types of artificial hollow forms, but even generalized certain shapes independent of absolute size [60]. Simon et al. showed that size discrimination of hollow hemispheres requires a constant size difference of approximately 16% of the radius, irrespective of the actual size of the hemispheres as if bats based object discrimination on the spectral cues generated by size-specific interference [17]. Von Helversen and von Helversen showed that the long-tongued bat *Glossophaga commissarisi* could find the flowers of the bat-pollinated vine *Mucuna holtonii* with the help of echolocation and could even recognize the degree of ripeness of the bud [59]. In order to complete the pollination task, nectar feeding bats have firstly to identify and localize the flower and then have to get a fine image of its structure in order to decide the best strategy of approach. Many flowers grow on stems or branches and usually closer to the plant, but because of several echo acoustic cues the flower manage to be unique and thus recognizable. Von Helversen and von Helversen showed that floral echoes last longer and can be stronger that echoes from leaves because of their bell shape and that for the same reason the echo field produced by flowers is often omnidirectional [58] [16]. Moreover, von Helversen and Holdereid showed that because flowers are complex targets and consist of many different reflectors at different distances, interference generates specific peaks and notches in the echo spectra, giving them a coloured spectral appearance [2]. This literature review has had the aim to give evidence of the ability of bats to detect and classify flowers, but there has been rather little research that has aimed to understand what are the factors that allow bats to achieve such great per-

formance. It is evident that further research exploiting in more detail the characteristics of the echoes from these particular flowers and possible critical features in their shape that might allow correct classification, is required, and this is one of the main topics of our research. Also, a better understanding on the strategy behind flower recognition such as instantaneous position of the bat with respect to the flowers and transmitted waveform is necessary to address the problem. All this might be applied to automatic radar target recognition to attempt to improve classification performance.

Finding the entrance of the flower and the nectarium requires some structural perception of the floral object behind the echo. The duration of the echo is a good indicator of the depth of the flower [2] but additional information about the structure of the flower derives from the fact that the bat receives two different echoes at its two ears. These differences, called binaural disparities, are quoted as being important perceptual cues for object recognition [61] [62]. Differences in magnitude between the two echoes received at each ear, called *interaural intensity differences (IIDs)*, give information about the orientation of the flower, and Holderied and Helversen showed that such *IIDs* may allow the bat to discriminate flower's orientation with a resolution of below 1 degree at a distance of 20 cm [61]. On the other hand, differences in time between reflection from different part of the flower, called *interaural time differences (ITDs)* allow the bat to reconstruct the position of these reflectors on the horizontal plane [61]. Figure 2.6 shows the reconstruction of a horizontal 2D flower structure from impulse responses received at the two ears for eleven angle between -5 and 5 degrees. At 3 degrees the echo received at the right ear presents two main glints, one of which is split into

two parts at the left ear, meaning that the left ear only can resolve two separate scatterers from the corolla. To better understand the detailed results a careful reading of [61] is recommended. This research show that binaural differences do exist and are likely to be used to elaborate a fine image of the target. It is evident that this could be applied to automatic recognition of targets by sensors as well, and specifically to image reconstruction and could open the way to research in the radar field that has to further investigate its possible advantages and disadvantages.

2.1   Summary

In this chapter the main publications on radar target classification and the main publications on the role that echolocation by bats has in target selection and recognition have been reviewed. Similarities and differences have been noted in order to understand which methodologies, successfully deployed by bats, can then be applied to radar (and sonar) systems to improve classification performance. This analysis has raised a few questions of great interest. It was shown that CF bats use a type of waveform composed of constant frequency harmonics initiated or terminated with a frequency sweep. These type of waveforms are not used in radar systems and suggest that further investigation is required to exploit how their use might impact on radar target classification performance. These species of bat perform classification of fluttering targets, in particular insects, combining information that derives at least from both amplitude and frequency modulations that are induced on the echo by the insect wing beat. Classification by using micro-Doppler
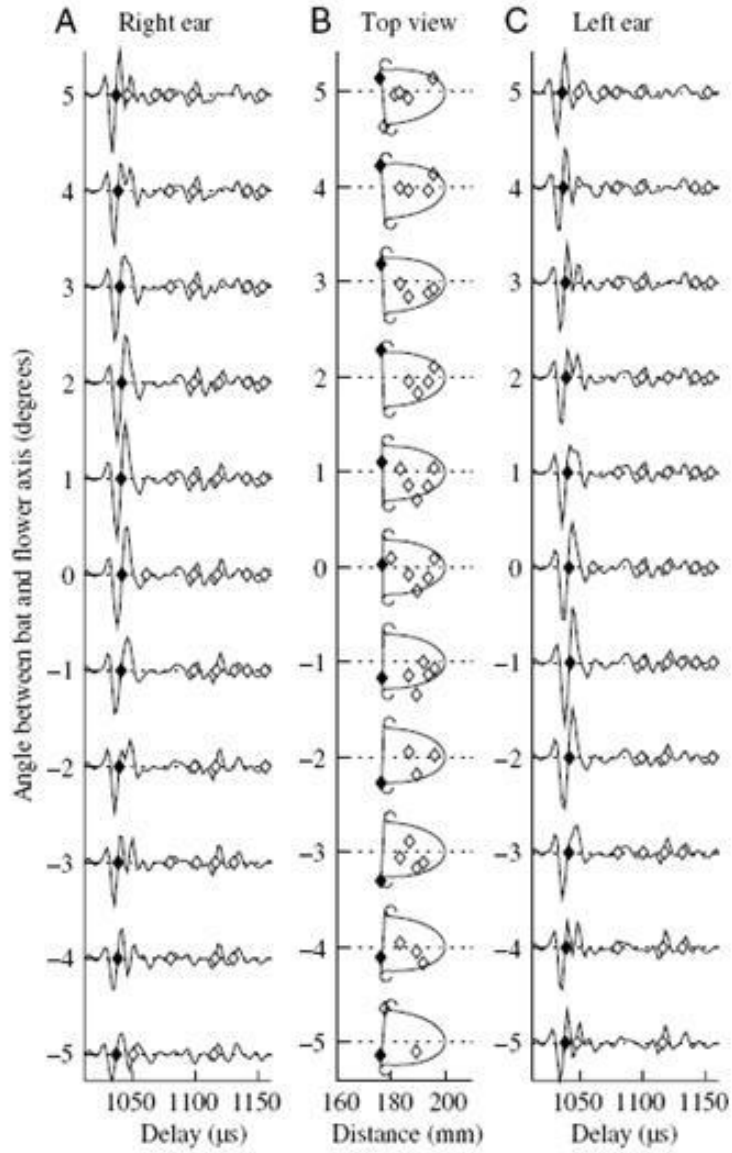
Figure 2.6: Reconstruction of horizontal 2D flower structures from impulse responses of V. gladioliflora for eleven different angles between bat and flower axis from -5 to 5 degrees. (A) Impulse responses picked up by right ear. (C) Impulse responses picked up by left ear. At 3 degrees the echo received at the right ear presents two main glints, one of which is split into two parts at the left ear, meaning that the left ear only can resolve two separate scatterers from the corolla [61].

signatures is a very close parallel in radar system, but there is a lack in understanding how multiple information can be combined in order to improve classification performance. Bats that emit broadband waveforms were then reviewed in order to understand how amazingly these bats can detect and classify complex static targets, such as flowers suitable for pollination, even in dense clutter environments. There has been rather little research that aims to understand what the factors that allow such performance are. Research looking at crucial features that characterize these flowers and further comparisons with radar targets is necessary and is likely to generate an important understanding on target classification. Moreover, the trajectory strategy of the bats with respect to the flower and relative transmitted waveforms as function of the trajectory itself, are likely to contribute to enhance classification performance and then require some detailed investigations. Indeed, this thesis opens a discussion on these last two topics and present the related results. Finally research on binaural differences was reviewed in order to understand how these might be used to create a fine image of an object. Further research exploiting how this could be applied to automatic target recognition represents another area of interest of this thesis.

Chapter 3

Fundamentals of radar and sonar systems

In this Chapter a number of processing concepts that are used in the subsequent chapters, and that the reader needs to understand in order to be able to comprehend this work are introduced.

3.1 Range resolution

In the previous chapter the ability of bats to resolve targets has been reviewed. As well as for bats, for a radar system there is the necessity of
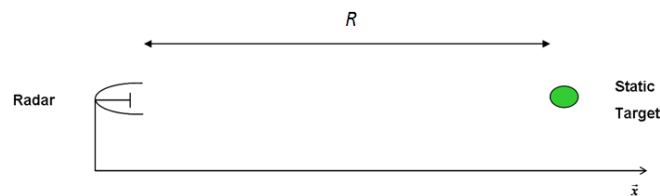
Figure 3.1: Example of a reflection from a static target.

knowing the minimum separation of two targets in order for the radar to resolve them as two separate identities, and this is a fundamental parameter to characterise a radar system. The range resolution R_r is defined as the minimum distance $d = |R_2 - R_1|$ that there must be between two targets in order for the radar to be able to distinguish them. Because the echo from a target arrives at the radar after a delay $\tau = 2R/c$ (see Figure 3.1), it is easy to show that two echoes from two different targets do not overlap when they obey the relation

$$R_2 - R_1 \geq \frac{cT}{2}, \tag{3.1}$$

where c is the speed of propagation and T is the pulse duration. This definition, however, leads to the need to clarify what is meant by saying that two echoes are distinguishable from each other. It is self evident that when two echoes do not overlap they are distinguishable. The traditional Rayleigh criterion, for example, establishes that two echoes are distinguishable when their whole main lobes do not overlap. In practise, it is often assumed that two echoes are distinguishable when their main lobes at -3 dB do not overlap. According to the latter criterion, when the receiver uses a filter matched to the transmitted signal, the range resolution is given by

$$R_r = \frac{c}{2B}, \tag{3.2}$$

where c is the speed of propagation and B is the bandwidth of the transmitted signal. The formula shows that the range resolution is a function of the bandwidth of the transmitted signal, and in particular that the range resolution increases as the bandwidth becomes wider. Figure 3.2 shows a
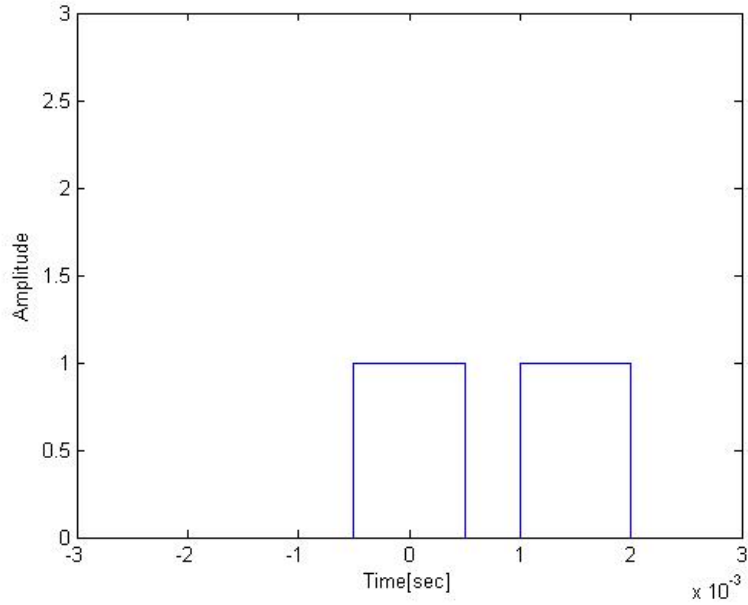
Figure 3.2: Example of two non-overlapping reflections from two targets delayed by 1.5 msec before the matched filter.

simple example of two non overlapping reflections of a square waveform of duration $T = 1$ msec, received with a delay equal to 1.5 msec, whose main lobes (the line at -3 dB is indicated by the red line) are distinguishable after matched filtering.

3.2 Doppler shift and Doppler resolution

A good number of publications have argued that bats can classify targets by looking at frequency modulations in the received echo that are induced by moving targets such as insects. Indeed, there is very close parallel in radar systems. When two targets cannot be resolved in range, and in other words belong to the same range cell, radars have still the ability to try to detect
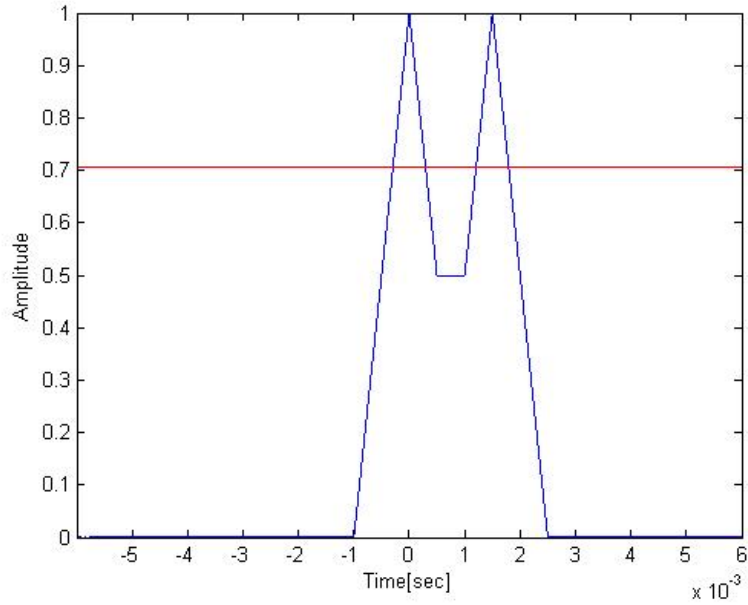
Figure 3.3: Output of the matched filter when the input is represented by two non-overlapping reflections delayed by 1.5 msec.

them by looking at a shift in the frequency domain, called Doppler shift, that is induced by the motion of the target. In this section the concept of frequency Doppler shift is introduced and the definition of Doppler resolution given. If the target of Figure 3.1 starts moving with a velocity $\vec{V}$ towards the target as in Figure 3.4 it produces an echo whose delay $\tau(t)$ is a function
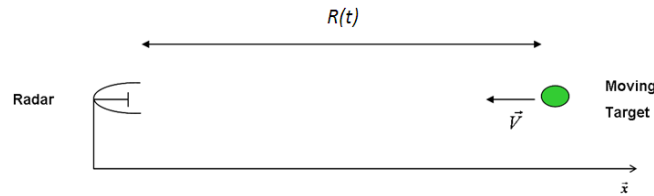
Figure 3.4: Example of reflection from a moving target.

of time t and given by the formula

$$\tau(t) = \frac{2(R - vt)}{c} \tag{3.3}$$

and then the received signal $r(t)$, if the radar emits a continuous waveform of frequency f_0, is

$$r(t) = \cos\left(2\pi f_0\left(t - \frac{2(R - vt)}{c}\right)\right). \tag{3.4}$$

The instantaneous frequency of the signal f_i, which is related to the time derivative of the phase, is given by the expression

$$f_i = f_0 + \frac{2f_0 v}{c}, \tag{3.5}$$

and therefore has been shifted by a quantity f_D, called Doppler shift, equal to

$$f_D = f_i - f_0 = \frac{2f_0 v}{c}. \tag{3.6}$$

The Doppler Resolution is defined as the minimum difference that there must be between the Doppler shifts induced by two distinct targets in order for the radar to distinguish them in the frequency domain.

3.3   Wideband ambiguity function

A fundamental tool that is widely used for the analysis of radar signals in order to assess their range and Doppler characteristics is the ambiguity

function [63]. In this section the mathematical basis that are necessary to understand the theory behind the definition of ambiguity function are given and then the ambiguity function is defined for both narrow band and wide band waveforms.

Given a real signal $x(t)$ with mean value equal to zero, its corresponding analytic signal $\dot{x}(t)$ is defined as

$$\dot{x}(t) = x(t) + j\hat{x}(t) \tag{3.7}$$

where $\hat{x}(t)$ is obtained by filtering $x(t)$ with a Hilbert filter

$$\hat{x}(t) = x(t) \otimes h_H(t). \tag{3.8}$$

In Eq. 3.8, $h_H(t)$ represents the impulse response in time of a Hilbert filter whose Fourier Transform is given by $H_H(f) = -jSign(f)$. Thus Eq. 3.7 and Eq. 3.8 lead to the relation:

$$\dot{X}(f) = \begin{cases} 2X(f) & f \geq 0 \\ 0 & f < 0. \end{cases} \tag{3.9}$$

Eq. 3.9 describes how the Fourier transform $X(f)$ of a real signal $x(t)$ is related to the Fourier transform $\dot{X}(f)$ of its analytical signal $\hat{x}(t)$ and shows that the Fourier transform of an analytic signal is equal to zero for negative frequencies.

From Eq. 3.7 it is very easy to derive that given an analytical signal the

correspondent signal $x(t)$ can be obtained as

$$x(t) = Re\{\dot{x}(t)\}, \tag{3.10}$$

which can be also expressed in polar coordinates as

$$x(t) = Re\{a(t)e^{j\phi(t)}\}, \tag{3.11}$$

where $a(t)$ and $\phi(t)$ represent the amplitude and the phase of $\dot{x}(t)$ respectively. The instantaneous frequency $f_i(t)$ of the signal $x(t)$ can now be defined as

$$f_i(t) = \frac{1}{2\pi}\frac{d\phi(t)}{dt}. \tag{3.12}$$

If a signal $x(t)$ is the input of a linear and invariant filter with impulse response $h(t)$, the analytic signal of the output $y(t)$ given by the formula

$$\dot{y}(t) = \int_{-\infty}^{\infty} \dot{x}(\tau)\dot{h}(t-\tau)d\tau, \tag{3.13}$$

where $\dot{x}(t)$ and $\dot{h}(t)$ are the analytical signals of the input $x(t)$ and the impulse response of the filter $h(t)$ respectively. When the filter is designed to match to the signal $x(t)$, and then $\dot{h}(t) = \dot{x}^*(-t)$, the expression above (Eq. 3.13) can be written as

$$\dot{y}(t) = \int_{-\infty}^{\infty} \dot{x}(\tau)\dot{x}^*(\tau-t)d\tau. \tag{3.14}$$

In radar and sonar systems the ambiguity function has been defined to exploit the property of the possible echo signals that can be measured at the receiver after filtering the transmitted waveform with a filter that is matched

to the transmitted signal itself. The ambiguity function represents the time response of a filter matched to a given finite signal, when that signal is received with a delay τ and a Doppler shift f_D, relative to nominal delay and Doppler (0,0) [64].

When a narrow band signal is reflected by a static target the received signal is a delayed and attenuated copy of the transmitted waveform. If the target moves, the Doppler effect induces a shift in frequency of the echo dependent on the target velocity as in Eq. 3.6. The ambiguity function for these types of signals is defined as

$$|\chi(\tau, f_D)| = \left| \int_{-\infty}^{\infty} \dot{x}(\tau)\dot{x}^*(\tau - t)e^{j2\pi f_D\tau}d\tau \right|. \tag{3.15}$$

When the transmitted signal is a wideband waveform, the echo from a static target is still a delayed and attenuated copy of the transmitted waveform but when the target moves the Doppler effect induces a time compression of the signal. The ambiguity function in this case is defined as

$$|\chi(\tau, \eta)| = \frac{1}{|\eta|} \left| \int_{-\infty}^{\infty} \dot{x}(t)\dot{x}^*(\eta(t - \tau))dt \right| \tag{3.16}$$

in order to take this effect into account. In the equation, η is the parameter that represents the Doppler compression and is equal to $\eta = \frac{c+v}{c-v}$, where c is the speed of propagation and v is the target velocity. It is self evident that the ambiguity function is directly related to the range and Doppler resolution. Indeed, the range resolution corresponds to the width of the main lobe of the ambiguity function as a function of τ computed in $f_D = 0$ ($\chi(\tau, 0)$) and, the

Doppler resolution is the width of the main lobe of the ambiguity function as a function of f_D computed in $\tau = 0$ ($\chi(0, f_D)$). Some examples of ambiguity functions are given in the next section where frequency modulated signals are introduced together with a detailed discussion on their ambiguity functions.

3.4   Amplitude and frequency modulations

The literature review has shown how bats can be mainly divided into two classes depending on the type of signals they transmit. There are, in fact, bats that echolocate by using a CF waveforms often composed of a few harmonics characterized by an initial or final sweep, and bats that instead use broadband waveforms. Indeed, in the latter class, a further classification can be made in relation to the type of frequency modulation these bats use in their echolocating calls. There are in fact bats that use linear frequency modulated calls and others that use hyperbolic modulated ones. These two types of waveform have been very much studied for radar systems and linear chirps are currently widely used in existing radar systems. In this section the theory that is needed in order to understand the concepts of amplitude and frequency modulation is given with particular attention to linear and hyperbolic chirps as these are common waveforms used by bats. The mathematical expressions for these two waveforms are also given and their properties and differences discussed.

A signal $x(t)$ is amplitude-only modulated if the instantaneous frequency

$f_i(t)$ is constant and can be expressed as

$$x(t) = Re\{a(t)e^{j2\pi f_0 t + \phi_0}\} = a(t)cos(2\pi f_0 t + \phi_0). \tag{3.17}$$

Similarly a signal $x(t)$ is frequency-only modulated when its amplitude is constant, and can be expressed as

$$x(t) = Re\{Ae^{j\phi(t)}\} = Acos(\phi(t)). \tag{3.18}$$

3.4.1 Linear frequency modulation

A signal $x(t)$ that obeys the expression

$$\begin{aligned} x(t) &= Rect\left(\tfrac{t-T/2}{T}\right) cos(2\pi(f_0 t + \gamma t^2)) \\ &= Rect\left(\tfrac{t-T/2}{T}\right) Re\left\{e^{j2\pi\gamma t^2}\right\}, \end{aligned} \tag{3.19}$$

is characterized by an instantaneous frequency equal to

$$f_i(t) = f_0 + 2\gamma t, \tag{3.20}$$

and therefore takes the name of Linear Chirp or linear frequency modulated (LFM) signal. From Eq. 3.20 it is easy to derive the expression for the bandwidth of signal, defined as the magnitude of the difference between the initial and the final frequency of the sweep, which is given by

$$B = |f(0) - f(T)| = f_1 - f_2 = 2\gamma T. \tag{3.21}$$
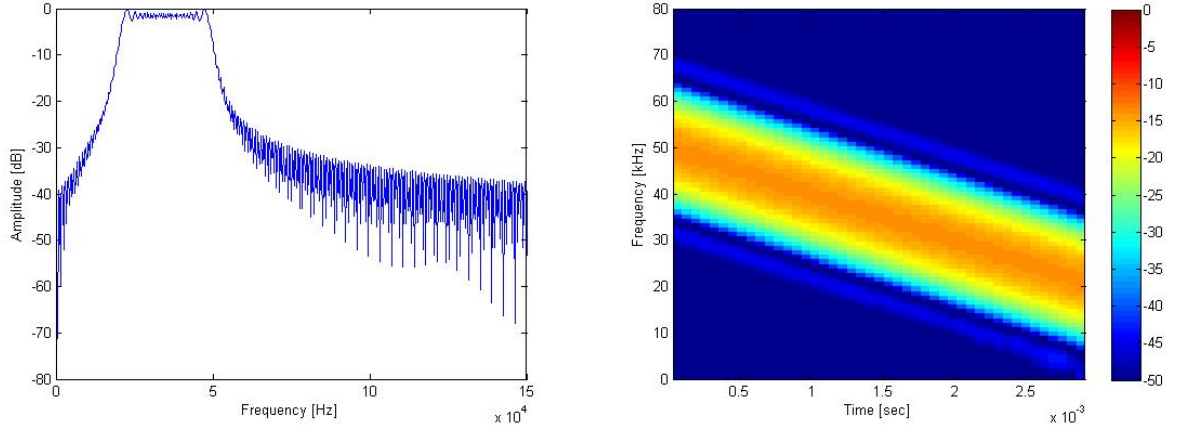
Figure 3.5: Power spectrum and spectrogram of a linear down-chirp spanning the frequencies from 50 kHz to 20 kHz. The duration of the pulse is 3 msec and the bandwidth, defined as the magnitude of the difference between the initial and the final frequency of the sweep, is 30 kHz.

Figure 3.5 plots the power spectrum and the spectrogram of a LFM signal with $f_1 = 50kHz$ and $f_2 = 20kHz$ respectively, and shows clearly how the instantaneous frequency in the spectrogram changes linearly as a function of time.

3.4.2 Hyperbolic frequency modulation

Similarly to a linear chirp, a signal $x(t)$ defined as in Eq. 3.19 is characterized by an instantaneous frequency that changes hyperbolically with time (3.20) and is called Hyperbolic Chirp or hyperbolic frequency modulated signal (HFM).

$$
\begin{aligned}
x(t) &= Rect\left(\tfrac{t-T/2}{T}\right) cos(2\pi a \log(1-kt)) \\
&= Rect\left(\tfrac{t-T/2}{T}\right) Re\{e^{j2\pi a \log(1-kt)}\}
\end{aligned}
\tag{3.22}
$$

The expression for the bandwidth of a hyperbolic chirp is given in Eq. 3.24

$$f_i(t) = \frac{ak}{kt - 1} \qquad (3.23)$$

$$B = f(0) - f(T) = f_1 - f_2 \qquad (3.24)$$

and its parameters can be easily derived accordingly (Eq. 3.25).

$$\begin{cases} a = -\frac{f_1}{k} \\ k = \frac{f_2 - f_1}{f_2 T} \end{cases} \qquad (3.25)$$

Figure 3.6 plots the power spectrum and the spectrogram of a HFM signal with $f_1 = 50kHz$ and $f_2 = 20kHz$ respectively and show clearly how the instantaneous frequency in the spectrogram changes hyperbolically as a function of time. Interestingly, one of the consequences of the non linear chirp is that power/unit bandwidth is not constant and therefore the spectrum is not flat.

3.4.3 Comparison of LFM and HFM ambiguity function

In the last two sections amplitude and frequency modulations have been described giving particular emphasis to linear frequency modulated (LFM) and hyperbolic frequency modulated (HFM) signals as these are the waveforms bats use for echolocation. In section 3.1 the definition of range resolution has been given and has highlighted that range resolution is a function of the bandwidth of the transmitted signal and in particular that the range
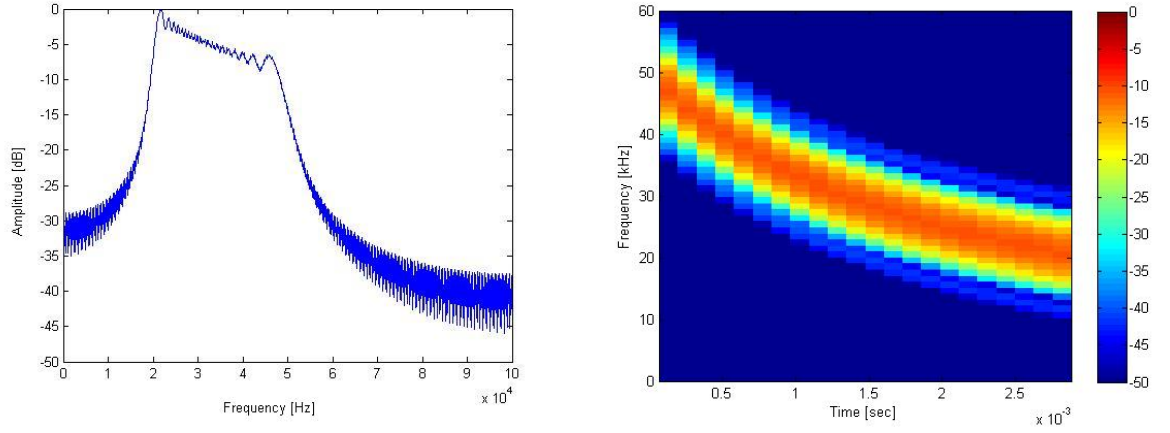
Figure 3.6: Power spectrum and spectrogram of a hyperbolic chirp spanning the frequencies from 50kHz to 20 kHz. The duration of the pulse is 3 msec and the bandwidth, defined as the magnitude of the difference between the initial and the final frequency of the sweep, equal to 30 kHz.

resolution improves as the bandwidth increases. This is the main reason why frequency modulated signals have been deployed in radar systems, as they allow to reach wider bandwidths without varying the duration of the pulse. In this section the differences and the advantages of using LFM or HFM are investigated by looking at their wideband ambiguity functions.

Figure 3.7 and Figure 3.9 plot the wideband ambiguity functions for a linear chirp and an hyperbolic chirp that sweep the frequencies between 50 kHz and 20 kHz, respectively. In both cases the bandwidth and the duration of the pulse are the same ($B = 30$ kHz, $T = 3$ msec). The plots of their relative $\chi(\tau, 0)$ and $\chi(0, f_D)$ function are given in Figure 3.8 and Figure 3.10. As expected, because the bandwidth of the two signals is the same, the $\chi(\tau, 0)$ plots show that the range resolution is approximately the same for both the signals. The $\chi(0, fD)$ plots instead show that the hyperbolic frequency modulation is desirable as it provides a better Doppler tolerance

67
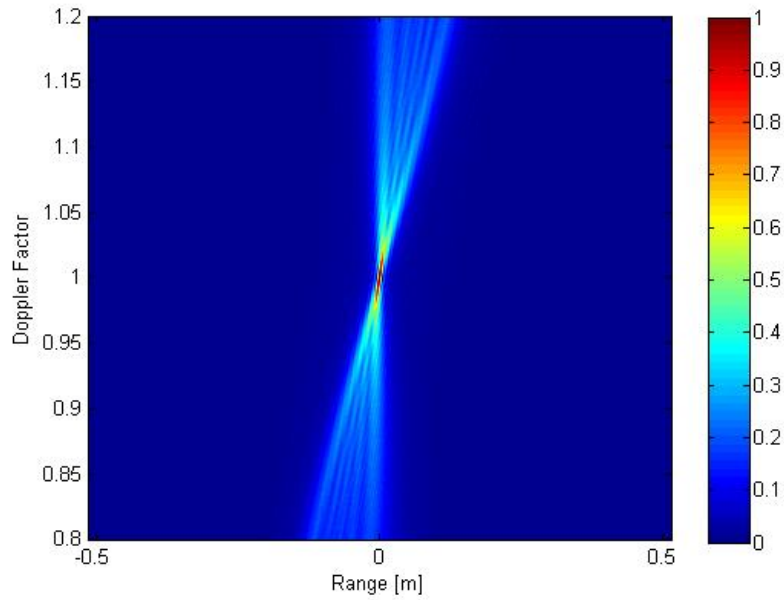
Figure 3.7: WAF for a linear chirp with a bandwidth equal to 30 kHz which spans the frequencies between 50 kHz and 20 kHz.
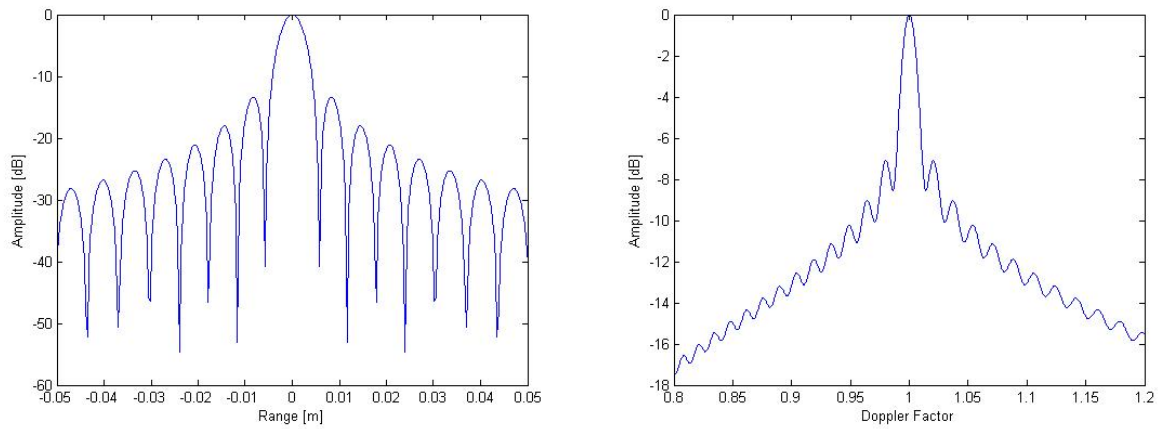
Figure 3.8: Range and Doppler cuts of the WAF of a linear chirp with a bandwidth equal to 30 kHz which spans the frequencies between 50 kHz and 20 kHz.
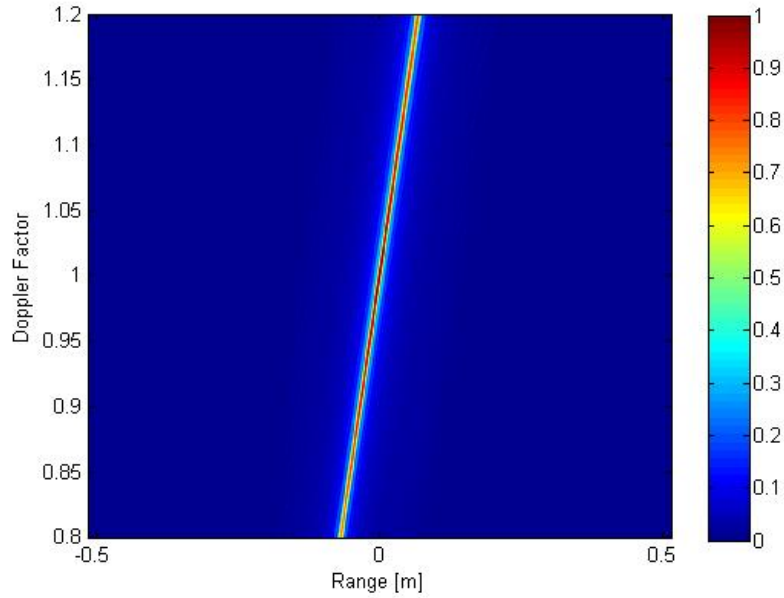
Figure 3.9: WAF for a hyperbolic chirp with a bandwidth equal to 30 kHz which spans the frequencies between 50 kHz and 20 kHz.
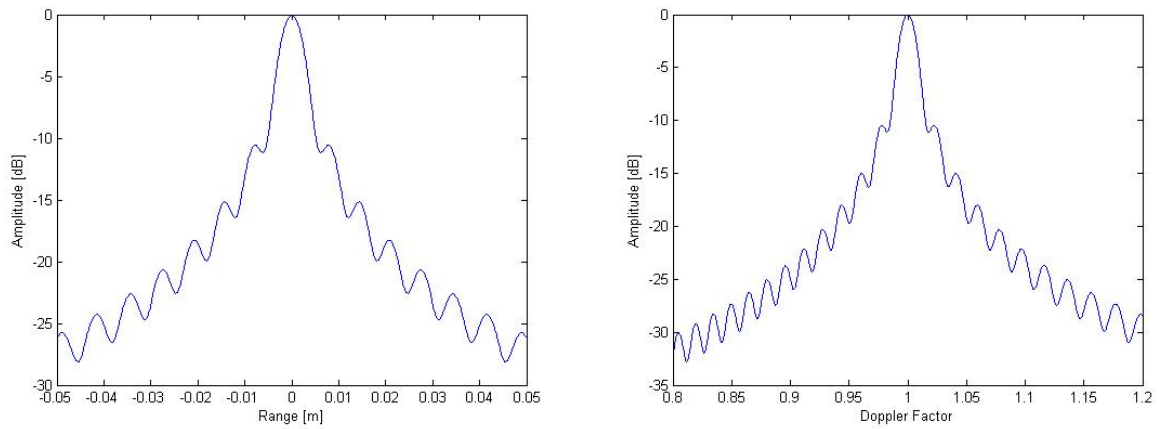
Figure 3.10: Range and Doppler cuts of the WAF of a hyperbolic chirp with a bandwidth equal to 30 kHz which spans the frequencies between 50 kHz and 20 kHz.

69

[65].

3.5 Basis of automatic target recognition

3.5.1 High Range Resolution Profiles

The literature review has highlighted how much research has been done on radar target classification with particular emphasis to high range resolution profile target classification (HRRP). Since high range resolution radar became available, in fact, these new techniques have had a great impact on latest research because of the simplicity which range profiles can be collected.

As range profiles will be widely used for the purpose of this thesis, in this section the concept of range profiles is introduced together with a description of how HRRPs are measured.

Consider a target on a platform as shown in Figure 3.11. A radar that illuminates the target receives an echo from the target itself. Since real targets are composed of many scatterers the echo that the radar receives is a complex signal that in first approximation, supposing that the target behaves as a linear system, can be seen as the sum of the echoes from each scatterer. As the echo enters the receiver it is usually matched filtered and then sampled into a vector $\vec{y} = (y_1, y_2, ..., y_N)$ that forms the range profile. When the distance between these main scatterers is greater than the range resolution the echo will present peaks corresponding to each scatterer. Range profiles are strictly dependent on the angle at which the radar is looking at the target. It
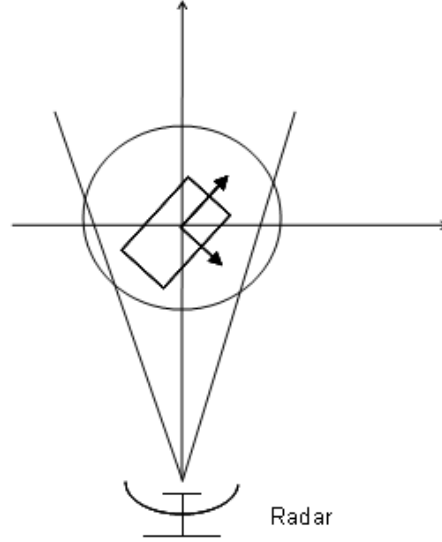
Figure 3.11: Radar measuring a range profile

is evident that range profiles might give a lot of information about the structure of the targets such as number of scatterers, distance in range between them, orientation of the target etc. Because of these properties range profiles, usually referred as High Range Resolution Profile (HRRP) to highlight that the radar is operating with a high resolution, have been widely studied for radar target classification. In this thesis, HRRPs will be referred to as the baseband version of the output of the matched filter, with both amplitude and phase information.

3.5.2 Classifiers

Classification of objects, or targets for the radar case, is the process of assigning a particular element to a set of known objects called a *class*. Figure

Figure 3.12: Block diagram of the classification process.

3.12 shows in a block diagram the main steps of the classification process. The raw data measured by the radar, or a sensor in general, are given as an input to a feature extraction block that has to reduce the dimensionality of the raw data by identifying the main features of the targets that will be used to perform classification. A few feature extraction algorithms, such as Principal Component Analysis (PCA) and Fisher Linear Discriminant [12], have been studied and tested to serve this purpose. Once the main features of the targets have been extracted the actual classification takes place in the classifier. The book by Duda [12] gives an insight on the different types of classifier that are present in the literature. Classifiers can be mainly divided into two types: parametric and non-parametric. Parametric classifiers assume that the raw data are governed by one or more stochastic parameters that present a particular probability density distribution (PDF). The classification task is performed under the assumption of having prior knowledge of the distribution of these parameters and then use their estimates to classify the object. Non-parametric methods are much more direct and mostly do not require any *a priori* knowledge on the properties of the data. Here, for simplicity reason and because there was no simple probability distribution that well fitted our data, a non-parametric classifier, called K_{nn}, is introduced.

3.5.3   K-Nearest Neighbour classifier

As introduced above, classification is performed by using a pattern, such as a process realization or a feature vector extracted from a process realization, that is given as an input to a classifier that has to automatically decide for the class the object belongs to. A few classifiers have been developed and implemented to serve this purpose. In this thesis, a non-parametric method called K-Nearest Neighbour classifier K_{nn} is used to assess classification performance. The approach consists of computing the K nearest distances between the input pattern, called test, and a number of patterns from each class known by the classifier. It is evident that in order to work the classifier needs to have what is called a *a priori* knowledge, represented by these training patterns, that is fundamental to *train* the classifier. Once all the possible distances between the test and the trainers are calculated the K nearest ones are selected for each class and then ordered from the smallest to the greatest in a vector $\vec{V}$ of NK elements, where N is the number of classes C_i. The last step consists of looking at the K smallest elements of the vector $\vec{V}$ and then choosing for the class that has a greater number of elements between them. Figure 3.13 shows that choosing the number K is quite a critical aspect for the K_{nn} classifier. In this particular example, for instance, choosing $K = 1$ would lead to assigning the test element to *Class 1* while choosing $K = 2$ would result in deciding for *unknown*. $K = 3$ would result in deciding for *Class 2*. There is not an optimal way to decide the value of K and an approach that can be used is testing some known patterns and then choosing the number K that give sufficient performance for them.
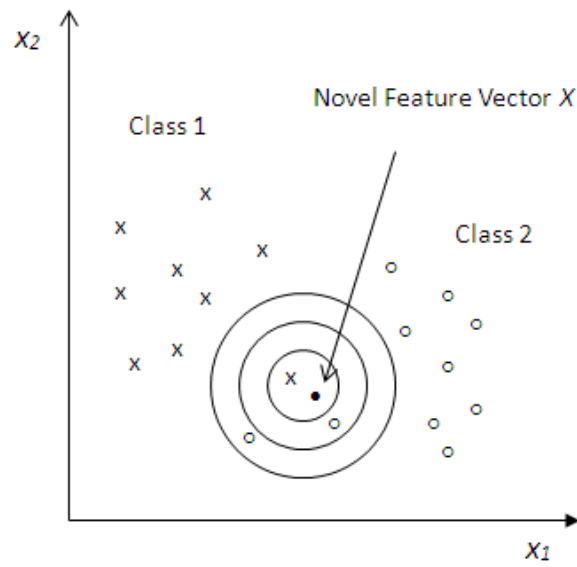
Figure 3.13: Example of K_{nn} classification [12] highlighting the importance of the selection of the parameter K. Choosing $K = 1$ would lead to assigning the test element to *Class 1* while choosing $K = 2$ would result in deciding for *unknown*. $K = 3$ would result in deciding for *Class 2*.

3.6 Imaging

In the previous section classification performed by processing HRRPs has been introduced and described. However, as the discussion carried out in Chapter 2 has shown there is a lot of ongoing research that is exploiting how to improve target classification and target recognition by looking at images of the targets themselves. In this section two algorithms that are widely used to perform imaging of targets, such as tomographies and SAR processing, are given.

3.6.1 Tomography

Given a function $f(x, y)$ in the two variables x and y, the projection of $f(x, y)$ over the line described by relation $x cos(\vartheta) + y sin(\vartheta) = r$ is defined as

$$p_\vartheta(r) = \int_{-\infty}^{+\infty} \int_{-\infty}^{+\infty} f(x, y) \delta(x cos(\vartheta) + y sin(\vartheta) - r) dx dy. \qquad (3.26)$$

The Fourier transform of the function $p_\vartheta(r)$

$$P_\vartheta(R) = \int_{-\infty}^{+\infty} \int_{-\infty}^{+\infty} \int_{-\infty}^{+\infty} f(x, y) \delta(x cos(\vartheta) + y sin(\vartheta) - r) e^{2\pi Rr} dx dy dr, \qquad (3.27)$$

after a simple mathematical calculation can be expressed as

$$P_\vartheta(R) = \int_{-\infty}^{+\infty} \int_{-\infty}^{+\infty} f(x, y) e^{2\pi(x R cos(\vartheta) + y R sin(\vartheta))} dx dy, \qquad (3.28)$$

which corresponds to the 2-D Fourier transform $F(X, Y)$ of the function $f(x, y)$ calculated at the spatial frequencies $(R cos(\vartheta), R sin(\vartheta))$. The relation

$P_\vartheta(R) = F(Rcos(\vartheta), Rsin(\vartheta))$ is well known with the name of the Fourier Slice theorem.

Let us now suppose that the image of an object described by a 2-D function $f(x,y)$ has to be reconstructed given a set of projections $p_\vartheta(r)$. The relation between the function $f(x,y)$ and its 2-D Fourier transform, given by

$$f(x,y) = \int_{-\infty}^{+\infty} \int_{-\infty}^{+\infty} F(X,Y)e^{2\pi(xX+yY)}dXdY, \qquad (3.29)$$

can be expressed as

$$f(x,y) = \int_0^\pi \int_{-\infty}^{+\infty} p_\vartheta(R)|R|e^{2\pi R(xcos(\vartheta)+ysin(\vartheta))}dRd\vartheta. \qquad (3.30)$$

This has been obtained after a simple variable transformation from cartesian co-ordinates to polar co-ordinates $(X = Rcos(\vartheta), Y = Rsin(\vartheta))$. Let us now define the function $W(t)$ as the convolution between the projections $p_\vartheta(r)$ and a filter whose frequency response is given by $H(R) = |R|$. The Fourier trasform $W(R)$ of $W(t)$ is given by

$$W(R) = p_\vartheta(R)|R|, \qquad (3.31)$$

and the function $W(t)$ can then be re-written (through a simple Inverse Fourier Transform) as

$$W(t) = \int_{-\infty}^{+\infty} p_\vartheta(R)|R|e^{2\pi Rt}dR. \qquad (3.32)$$

Eq. 3.30 can now be expressed as

$$f(x, y) = \int_0^\pi W(xcos(\vartheta) + ysin(\vartheta))d\vartheta \qquad (3.33)$$

to show that the image of the object represented by the function f(x,y) is only dependent on the projections of the object. In a real scenario where only a finite number of projections is available the expression above can be well approximated with

$$f(x, y) = \sum_{i=1}^{N} W(xcos(\vartheta_i) + ysin(\vartheta_i)). \qquad (3.34)$$

3.6.2 Synthetic aperture radar (SAR)

Synthetic Aperture Radar (SAR) is a technique that is widely used in radar systems to improve azimuth or cross-range resolution of a target scene with respect to that obtained by using a single antenna of length L illuminating the same area. This technique can be used for sonar systems as well and in this case it takes the name of Synthetic Aperture Sonar or SAS.

The angular azimuth resolution of a linear antenna of length L can be approximated as $\vartheta z = \frac{\lambda_0}{L}$ and thus the antenna footprint on the ground ΔX at a distance R is given by $\Delta X = \frac{\lambda_0}{L} R$. Many applications of radar and sonar systems require a much higher cross range resolution and thus new techniques looking at improving azimuth resolution without changing the physical size of the antenna have become an imperative. Synthetic aperture radar processing is a technique that allows improvement of cross range resolution by, as its name suggests, synthesising a longer aperture or antenna.

Suppose that an antenna moving a constant speed v transmits and receives
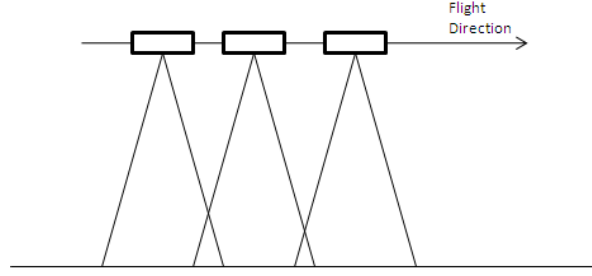
Figure 3.14: Sketch of a sensor illuminating the ground while flying on a straight line.
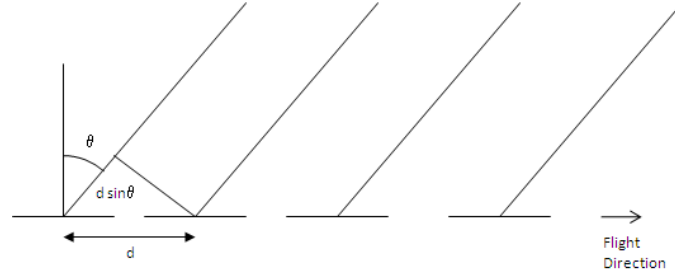
Figure 3.15: Received signal coming from an angle ϑ. This is given by the sum of the signals received at each flight step.

a pulse with a time period equal to T as described in Figure 3.14.

The received signal, given by the coherent sum of all the received pulses, can be expressed as

$$S_r(t) = e^{j2\pi f_0(t - t_0 - \frac{2nds\sin(\vartheta)}{c})}, \tag{3.35}$$

where $d = vT$ is the distance that the antenna has covered between two consecutive transmissions (Figure 3.15). After some calculations Eq. 3.35 can be expressed as

$$S_r(t) = e^{j2\pi f_0(t - t_0)} \sum_{n=0}^{N-1} e^{-\frac{4\pi nds\sin(\vartheta)}{\lambda_0}}. \tag{3.36}$$

It can be shown that for small values of ϑ the amplitude of the expression above can be written as

$$|S_r(t)| = \frac{|sin(\frac{N2d\pi\vartheta}{\lambda_0})|}{|sin(\frac{2d\pi\vartheta}{\lambda_0})|}. \qquad (3.37)$$

Eq. 3.37 shows that echoes arriving from different directions are attenuated as a function of the angle ϑ and in particular that the first zero point corresponds to the look direction $\vartheta = \frac{\lambda_0}{2Nd}$, where the quantity Nd corresponds to the azimuth resolution of the real aperture (equal to $\frac{\lambda_0}{L}R$). The azimuth resolution that can be achieved by a SAR system is then defined as

$$R_{azimuth} = \frac{\lambda_0}{2Nd}R = \frac{L}{2}, \qquad (3.38)$$

which is considerably higher than the one given by a single antenna of length L as desired.

Another interesting way to introduce SAR processing is to look at it from a Doppler point of view. Suppose that the sensor is carried by a platform that is moving with a constant velocity v as described in Figure 3.16 and to be transmitting continuously a tone at a frequency f_0 . In this case, the received signal

$$S_r(t) = e^{j2\pi f_0(t - \frac{2R(t)}{c})} \qquad (3.39)$$

will arrive at the receiver with a variable time delay that depends on the distance $R(t)$, equal to

$$R(t) = \sqrt{R_0^2 + (vt)^2} \approx R_0 + \frac{(vt)^2}{2R_0}, \qquad (3.40)$$

79
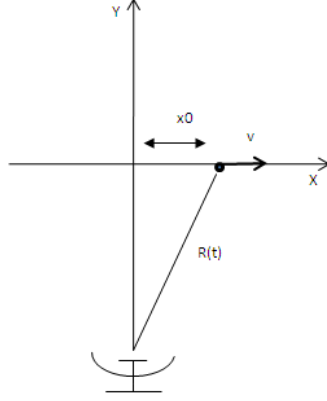
Figure 3.16: Target moving on a straight line with respect to a static sensor.

between the transmitter and the receiver at each instant. It is easy to show
that the instantaneous Doppler frequency

$$f_D(t) = f_i(t) - f_0 = -\frac{2}{\lambda_0}\frac{dR(t)}{dt} = -2\frac{v^2 t}{\lambda_0 R_0} \qquad (3.41)$$

depends on the position in azimuth of the target and thus it shows that two
targets can ideally be resolved by looking at their correspondent Doppler
shift. It is also interesting to highlight that the Doppler bandwidth

$$\Delta f_D = 2\frac{v^2 T}{\lambda_0 R_0} \qquad (3.42)$$

does not depend on the azimuth position of the target and that it remains
constant if the velocity is constant. Because the resulting return is a linear
frequency modulated chirp, the process of forming the synthetic aperture is
one of matched filtering the Doppler history.

The theory described above can be extended to the case of a static sensor
that is looking at a moving target. SAR processing, in fact, suggests that
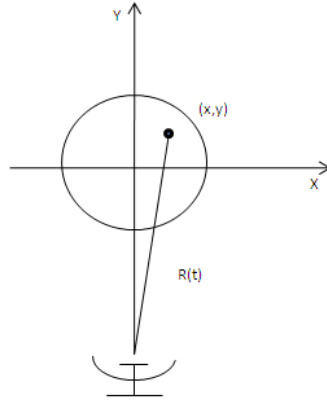
Figure 3.17: ISAR. Target rotating on a turntable with respect to a static sensor. Movement of the target allows imaging of the target itself.

when a radar or sonar system cannot move there is still some type of information that can be extracted from a moving target. In this case SAR processing takes the name of Inverse SAR (ISAR) and can be divided in two different classes; co-operative ISAR and non co-operative ISAR. It is cooperative when the motion related to the target can be somehow controlled, and non co-operative when the motion of the target is not controlled and thus all the parameters that describe its trajectory and any small changes in the position have to be estimated. Below, the simple case of a target placed on a turntable that rotates with a constant angular velocity w is described and some results are given.

Consider the situation as described by Figure 3.17 in which a scatter located in the point (x, y) of a 2-D plane is rotating with a constant angular velocity w. If the distance of the radar from the centre of rotation R_0 is much greater than the length of the radious r the instantaneous distant between

the scatterer and the radar can be approximated as

$$R(t) = R_0 - rsin(\vartheta), \qquad (3.43)$$

and thus its instantaneous Doppler shift is given by

$$f_D = -\frac{2}{\lambda_0}wrcos(\vartheta) = -\frac{2}{\lambda_0}wx. \qquad (3.44)$$

As for the case of a moving sensor the Doppler frequency is directly proportional to the position of the scatterer in cross range and thus this method can be used to resolve two moving scatterers in azimuth by looking at their Doppler shifts.

3.7 Summary

In this chapter the basic concepts of signal processing and radar theory that are useful for the reader to comprehend the results of the thesis were given. The concepts of range and Doppler resolution were defined and explained together with the definition of the ambiguity function, useful to exploit radar signal properties. By using the ambiguity function a deeper analysis LFM and HFM waveforms was carried out and differences and similarities of these two signals were discussed. These concepts will be used in Chapter 4 to exploit the properties of the waveforms deployed by bats to detect and select targets. An explanation of what range profiles are and how these can be collected and deployed for classification of targets was given together with an introductory discussion on the classifiers. In particular, a non-parametric

classifier, the K-Nearest Neighbour, was described in details. This will be used in Chapter 5 and Chapter 8 to support our classification performance analysis. Finally, two common algorithms used to perform target imaging, such as tomographies and SAR-ISAR, were given as well to support the analysis carried out in Chapter 9.

Chapter 4

Analysis of an echolocation buzz

In this chapter a feeding buzz sequence as emitted by a *Epetesicus nilssoni* bat while first searching and then attacking a slow moving target is analysed, and results are discussed in order to give the reader the necessary knowledge to fully comprehend and enjoy the topics of this thesis. Part of the data analysed in this chapter was already processed prior to the commencement of this work and the results relative to this first study can be found in [66] [67]. The goal of this research was to repeat the processing of the data in order to consolidate the results and to open up a more detailed discussion that could be part of a wider study like the one presented in this thesis.
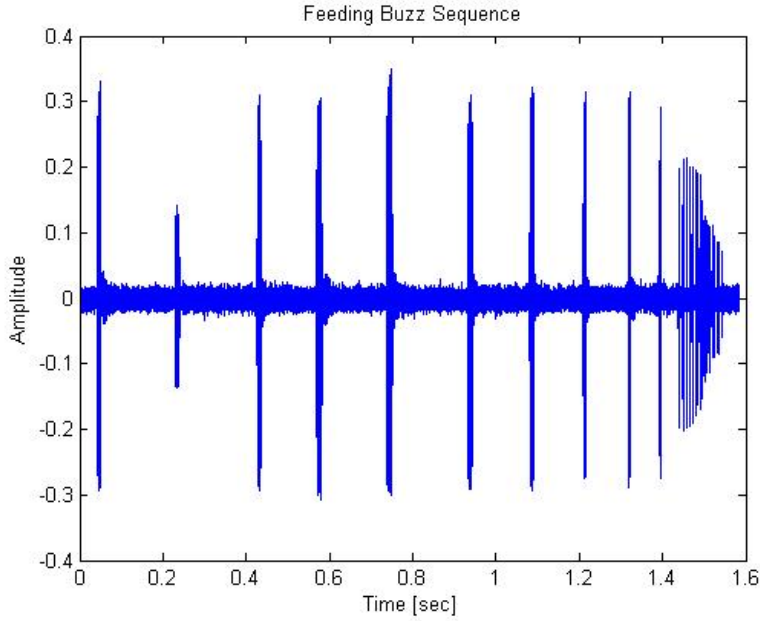
Figure 4.1: Feeding buzz by an *Epetesicus nilssoni* bat.

4.1 Description of the data

Figure 4.1 plots the feeding buzz sequence emitted by an *Epetesicus nilssoni* bat while first searching and then attacking a slow moving target. During data collection the bat was constantly changing its orientation, such that it viewed the target over a total angle range of approximately 270 degrees, and gradually getting closer and closer to the target. The signal was digitised using a sampling frequency of 220.5 kHz. Unfortunately, no further information is available on the experiment setup. From Figure 4.1 it is evident that the buzz sequence can be divided into two main phases. The first phase, called *searching phase*, corresponds to the initial part of the buzz in which it is believed the bat is looking for a possible target and performing classification. Ideally, this phase should include the task of target detection although,

for this particular experiment, not enough information on the experiment is available to decide whether the bat had already detected the target or not before the recording started. This phase is composed of echolocation calls characterised by amplitudes of about 0.3 V which are separated in time from each other by a PRI (Pulse Repetition Interval) of about 0.2 sec. The second phase, called *terminal phase*, is the last part of the buzz and corresponds to the time when the bat attacks the prey that has been selected. Pulses belonging to this phase of the buzz are separated by a much lower PRI (about 1 msec) and present amplitudes up to 5-6 times lower than those recorded in the searching phase. It is believed this is because in the terminal phase the bat is closer to the target and therefore can operate with lower power transmissions in order to save precious energy that can instead be used to transmit with a higher PRF to keep tracking the target before the final attack. Figure 4.2 and Figure 4.3 show the spectrogram and the normalised mean spectrum of the first pulse in the searching phase. The pulse is characterised by a time duration of about 9 msec and it is composed of three non-overlapping harmonics (in frequency) with peaks in power at about 30 kHz, 60 kHz and 90 kHz, respectively. Most of the energy is concentrated on the fundamental harmonic which can be fitted well to a hyperbolic function. The mean spectrum clearly shows the three non overlapping harmonics which present a non constant power/unit bandwidth that is typical of non-linearly modulated chirps. Figure 4.8 and Figure 4.9 show the ambiguity function for the same pulse together with its relative range and Doppler cuts. The range cut shows that the bat is operating with a range resolution of about 1.8 cm. The Doppler cut instead present a very narrow peak indicating that the bat is

trying to acquire fine Doppler information on the target. This is in very good agreement with the previous literature showing that Doppler information is critical for the task of classification and support the hypothesis that target classification takes place in the searching phase. Figure 4.4 and Figure 4.5 plot the spectrogram and the spectrum of the second pulse extracted from the same phase. Unlike all the other pulses in the searching phase this is composed of a fundamental hyperbolic modulated harmonic only that spans the frequencies between 60 kHz and 30 kHz. The mean spectrum shows the distribution of the mean power as a function of frequency. The peak is at about 30 kHz and again the mean power is not constant over the pulse bandwidth. Interestingly, the amplitude of this pulse is only about 1.2 V, i.e. half the amplitude of all the other pulses belonging to this part of the buzz. Unfortunately, it is impossible to determine whether the lack of the harmonics was deliberate by the bat or just the results of a lower output or redirected beam, as the recording of the signal at the microphones location may not necessarily reflect the output from the bat. The information on the location of both the microphone and the bat, the orientation of the microphone and its beam pattern, and the orientation of the bat at each call is unfortunately not available.

Figure 4.6 and Figure 4.7 give the same plots for a pulse in the final phase that is composed of two overlapping (in frequency) harmonics. The fundamental harmonic is well fitted to a linear chirp that spans frequencies between 75 kHz and 25 kHz, while the second harmonic decreases from about 90 kHz to 55 kHz. The pulse length is reduced to 4 msec, more than 50% with respect to the pulses described above, in order to conserve energy and avoid eclips-

ing. At the same time the degree of hyperbolic curvature increases to extend the bandwidth and improve range resolution. The plots of the wideband ambiguity functions for this pulse and its relative range and Doppler cuts are given in Figure 4.10 and Figure 4.11, respectively. As expected, the range cut of the ambiguity function is now much more narrow that the one associated to the pulse extracted from he searching and show that the bat now operates with a range resolution of about 8 mm. The Doppler cut instead has become much larger providing a poorer Doppler resolution. Overall, it is common to waveforms in the terminal phase to provide tolerance to any differential Doppler. This is likely to indicate that the bat at this stage has already gained the Doppler information for classification and is gathering the range information before the final attack.

Unfortunately, there is no direct knowledge of how the bat was changing its position and orientation with respect to the target during this specific recording. To show an example of a common bat-trajectory, Figure 4.12 plots the 3D position of a bat with respect to a static insect for a similar experiment that was carried out by the University of Maryland [68]. This was extracted by a video showing a feeding bat in a room foraging on an insect by echolocation. Each point in the plot corresponds to a position in which the bats emitted an echolocation call. From this sequence it is evident that, as in the previous experiment, the PRI (Pulse Repetition Interval) used by the bat tends to become shorter as the bat gets closer to the target and also shows that the bat tends to go around the target to acquire multi-perspective information before the actual attack [69]. As discussed in Chapter 2 it is known that multi-perspective information together with
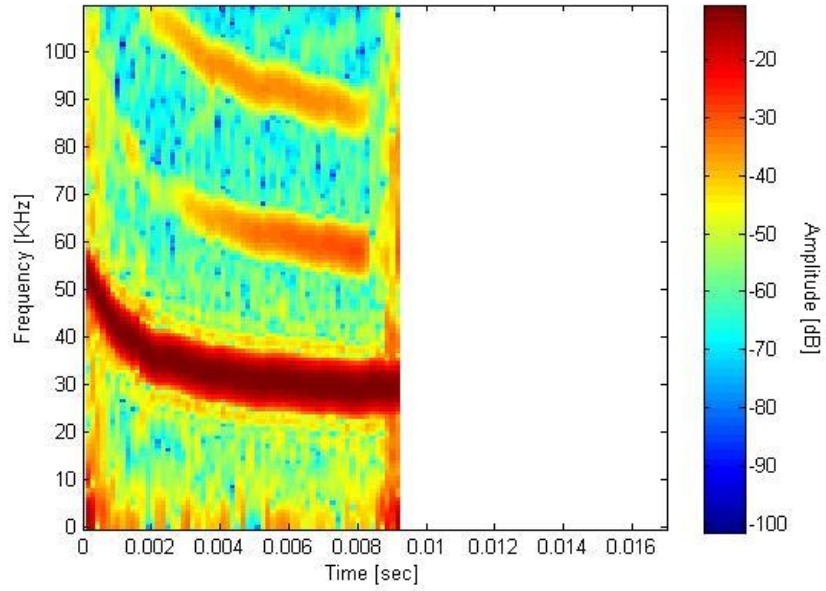
Figure 4.2: Normalised spectrogram of a pulse in the searching phase. The time axis limit corresponds to the duration of the longest pulse in the feeding buzz. It is kept constant in each plot to highlight how the duration of the calls is diversified throughout the sequence.
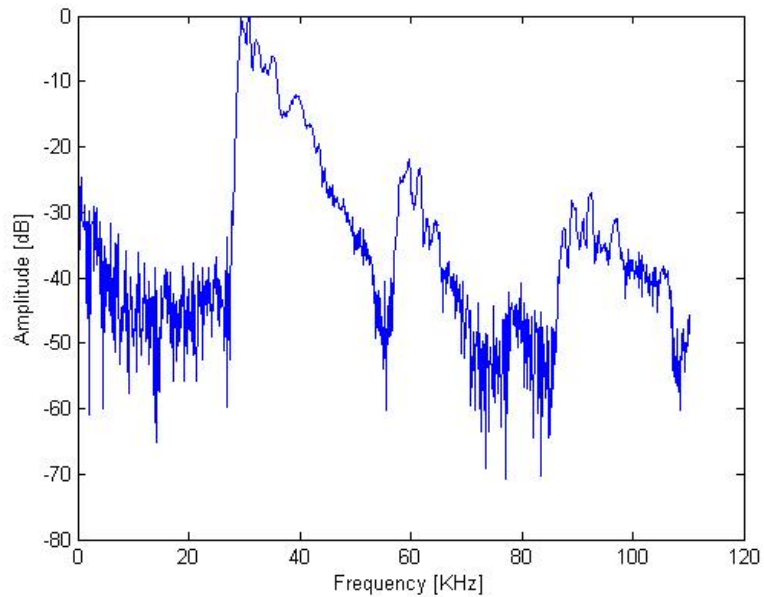
Figure 4.3: Normalised spectrum of a pulse in the searching phase.

89
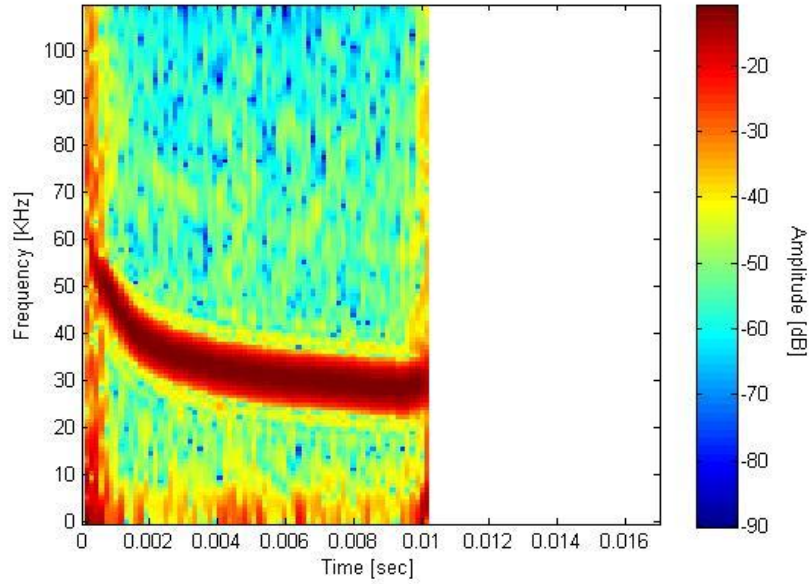
Figure 4.4: Normalised spectrogram of a pulse in the searching phase that is characterised by the fundamental harmonic only.
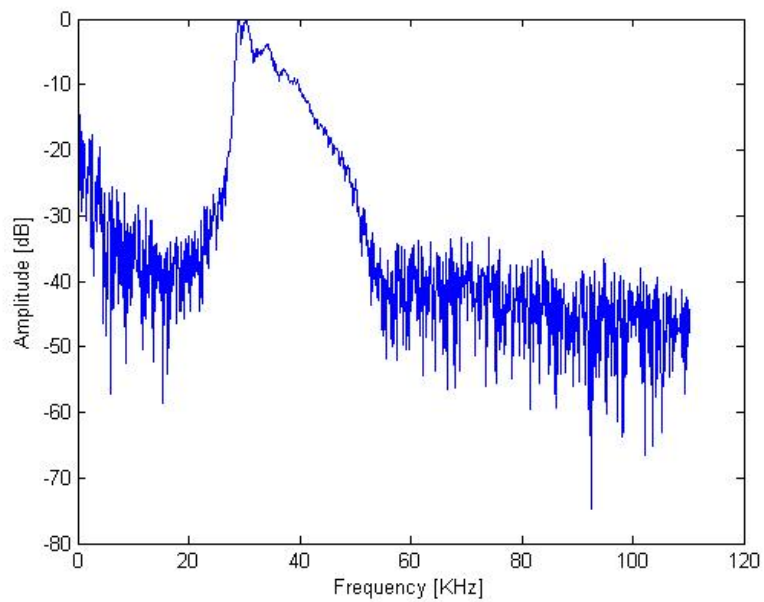
Figure 4.5: Normalised spectrum of a pulse in the searching phase that is characterised by the fundamental harmonic only.
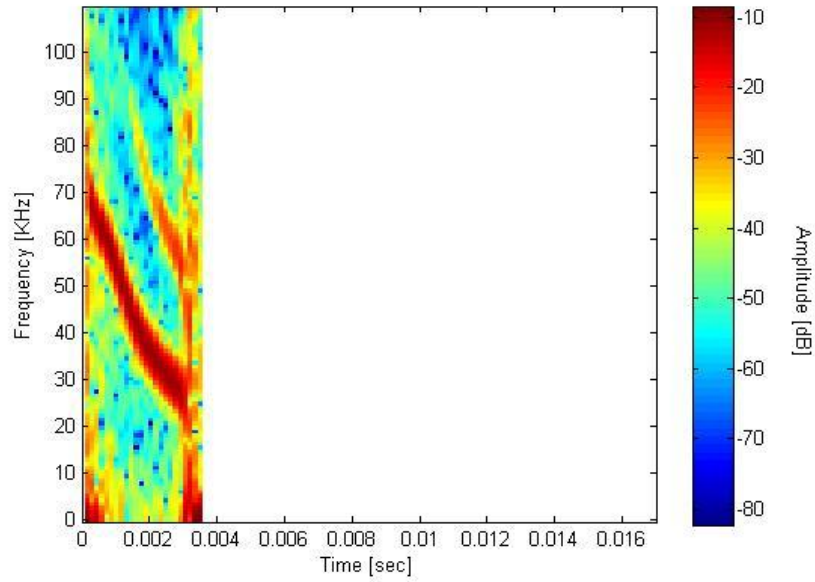
Figure 4.6: Normalised spectrogram of a pulse in the final phase.
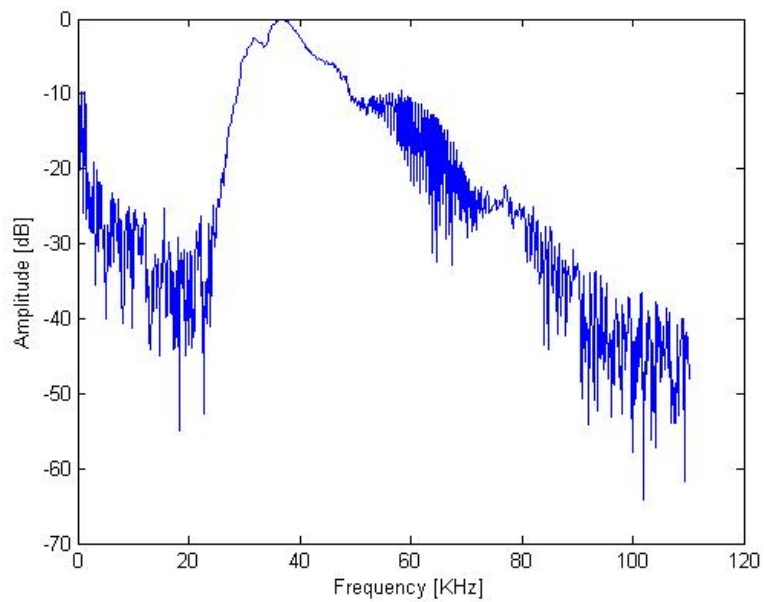
Figure 4.7: Normalised spectrum of a pulse in the final phase.

91
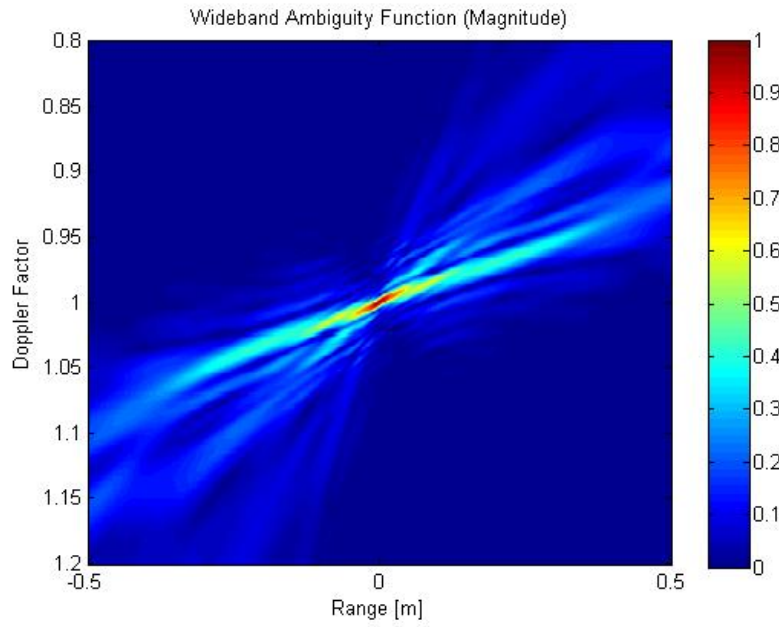
Figure 4.8: WAF of a pulse in the searching phase.
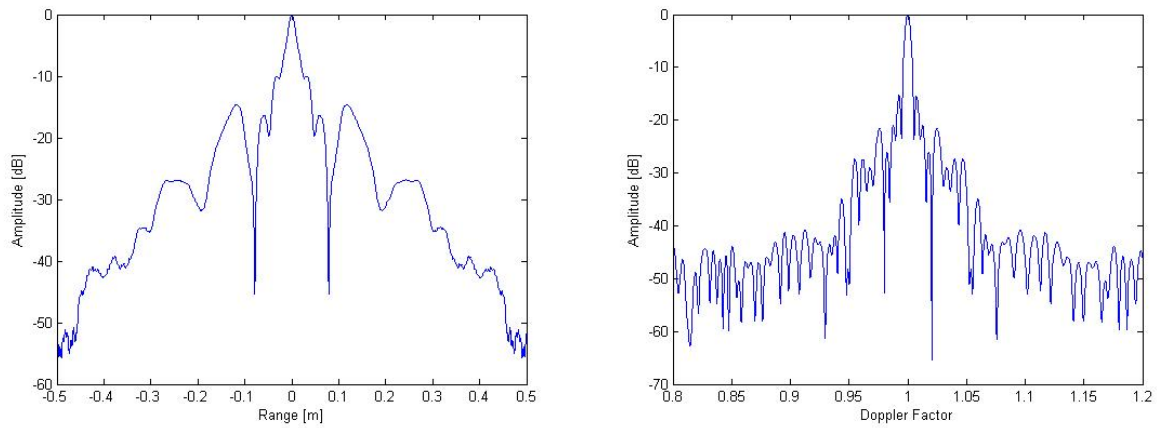
Figure 4.9: Range aand Doppler cuts of the WAF of a pulse in the searching phase.
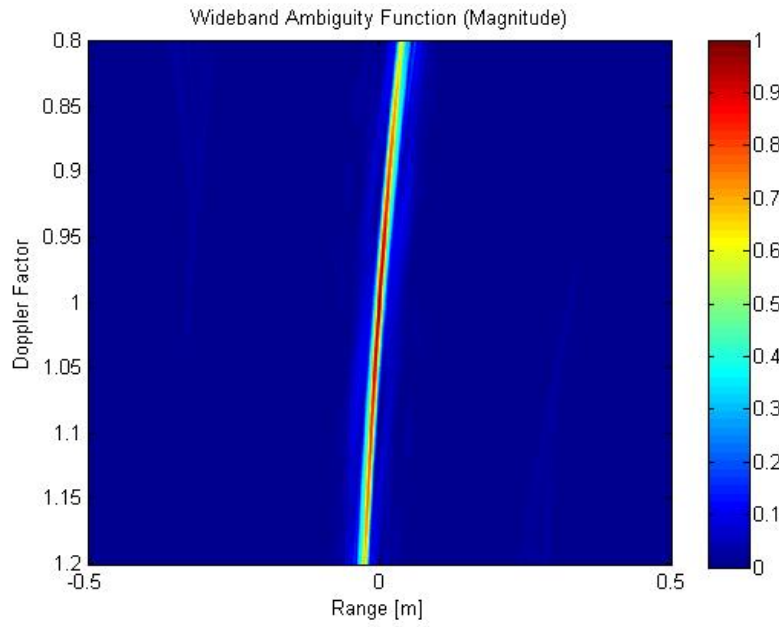
Figure 4.10: WAF of a pulse in the final phase.
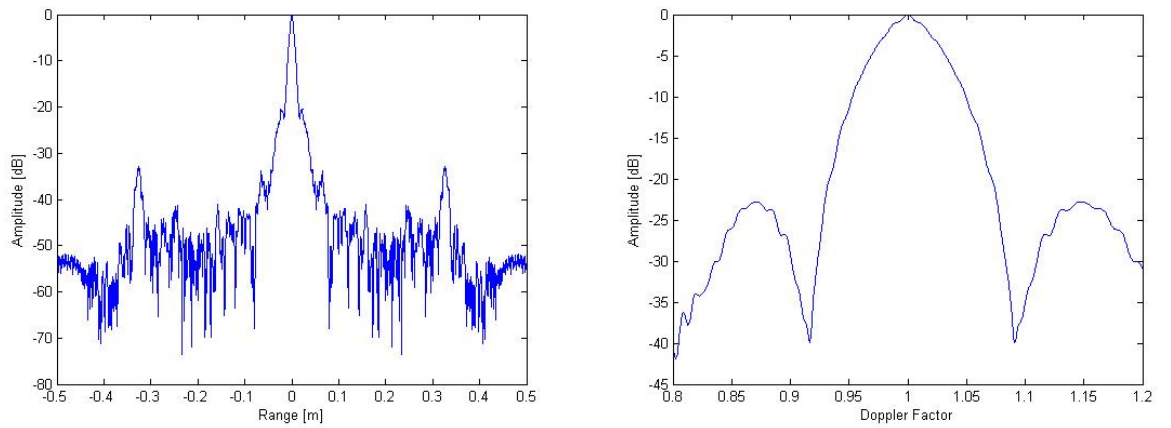
Figure 4.11: Range and Doppler cuts of the WAF of a pulse in the final
phase.

93
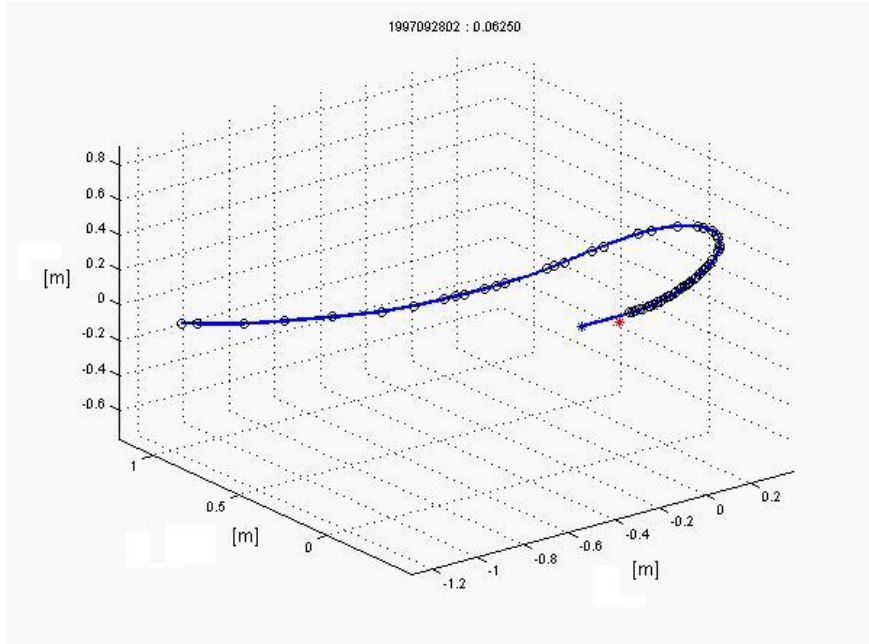
Figure 4.12: Trajectory of a bat (blue) with respect to a static insect (red) in a similar experiment performed at the University of Maryland [68].

Doppler information are likely to be key to target classification. The similarity of the two experiments suggests that these considerations are likely to be valid for our dataset as well.

In conclusion, results show that the bat sent very sophisticated waveforms which were intelligently diversified during the mission. Throughout the sequence the ambiguity function turns anti-clockwise through the sequence in order to achieve the appropriate range resolution and Doppler tolerance depending on the bat's final goal. The way the bat changes the waveform parameters is remarkable example of resource management which, it can be argued, to be much more sophisticated than what modern radar and sonar systems can do. These results show how the choice of a particular waveform and its parameters, such as bandwidth and duration, can be intelligently

94

diversified during a mission in order to achieve high level detection, localisation and classification performance. Indeed, it is self evident that this is an extraordinary example of waveform diversity and agility, which is the envy of modern radar and sonar systems [70]. The more demanding question that remains to be addressed is what are the appropriate adjustments that need to be made to maximise classification performance, and this would be an interesting and challenging topic for future research. As mentioned above the information on the relative position of the bat with respect to the insect was not available for this particular experiment but further research is necessary to address this problem.

4.2 Multi-component waveforms

Results show that bats tend to transmit waveforms composed of more than one harmonic. The function of these harmonics is as yet unclear. Figure 4.4, shows the spectrogram of a pulse composed of one fundamental harmonic only, suggests that *E. nilssoni* bats intentionally use harmonics and are able not to do so, although this type plot is not typical. They might do this in order to broaden the transmitted bandwidth and then obtain higher range resolutions when this is not possible with a single harmonic waveform because either it could be too challenging or they have pulse duration restrictions [71]. However, there is no proof yet of any physiological constraint that would impede transmission of a large bandwidth using the fundamental only. Indeed, another hypothesis is that harmonics could be used for different individuals to distinguish their calls in a multi-signal environment, i.e.

to give a distinctive 'voice' [53].

We believe that, if evolution has resulted in multi-harmonic waveforms and these are commonly used by bats during their tasks, it is likely that there can be advantages obtained by doing so. The fact that harmonics, or more in general multi-component waveforms, are not commonly used by radar and sonar systems suggests that investigating their effect on the ambiguity function of typical radar and sonar waveforms would be of interest. Here, multi-component linear chirps are simulated and the the properties of the range cut of their ambiguity functions are explored in order to exploit advantages and disadvantages for radar and sonar sytems.

4.2.1 Waveform analytic model

The analytic signal corresponding to a linear chirp characterised by a starting frequency f_0, a phase shift θ_0, and a chirp rate γ_0 can be written as

$$y_0 = e^{j2\pi(f_0 t + \gamma_0 t^2) + j\theta_0} \tag{4.1}$$

over a time interval $0 < t < T$ of duration T. Let us consider a waveform given by the sum of two linear chirps, y_0 and y_1, with y_1 described by the parameters f_1, γ_1, θ_1 as

$$y_1 = e^{j2\pi(f_1 t + \gamma_1 t^2) + j\theta_1}. \tag{4.2}$$

It can be easily shown that the analytic signal of the resulting waveform $y(t) = y_0(t) + y_1(t)$ can be written as

$$y_0 + y_1 = (1 + e^{j2\pi(f_d t + \gamma_d t^2) + j\theta_d}) e^{j2\pi(f_0 t + \gamma_0 t^2) + j\theta_0}, \tag{4.3}$$

with $f_D = f_1 - f_0$, $\gamma_D = \gamma_1 - \gamma_0$ and $\theta_D = \theta_1 - \theta_0$.

As discussed in Chapter 3, for wideband waveforms such as echolocation calls, the Doppler effect induces a time compression of the signal and the ambiguity function is defined in order to take this effect into account (Eq. 3.16). Here, the properties of the range cut of the ambiguity function of the signal $y(t)$ are exploited as a function of f_D and γ_D and are compared with the performance obtained by a single linear chirp spanning the same bandwidth. The two chirps y_0 and y_1 generating $y(t)$ were assumed to present the same signal levels and to be in phase, and therefore θ_D was set to zero ($\theta_0 = \theta_1$) for all the simulations. Because these assumption are not commonly satisfied by bat-signals, where the level of the secondary harmonics can be -20 dB weaker than the primary harmonic, the results of this analysis may not necessarily apply to the bat case. However, the main goal of this analysis is to assess advantages and disadvantages deriving by using multi-components waveforms for radar and sonar systems.

A set of waveforms $y(t)$ with $f_0 = 70$ kHz, $\gamma_0 = -5\text{x}10^6$ Hz/sec and $f_D = 10$ kHz were simulated for γ_D varying from $-4\text{x}10^6$ Hz/sec to 0 Hz/sec. The duration of the pulse was set to $T = 3$ msec. All the parameters were chosen in order to closely agree with those characterising real echolocation calls. The range cut of the WAF of $y(t)$ was calculated for all γ_D. Fig. 4.13 shows
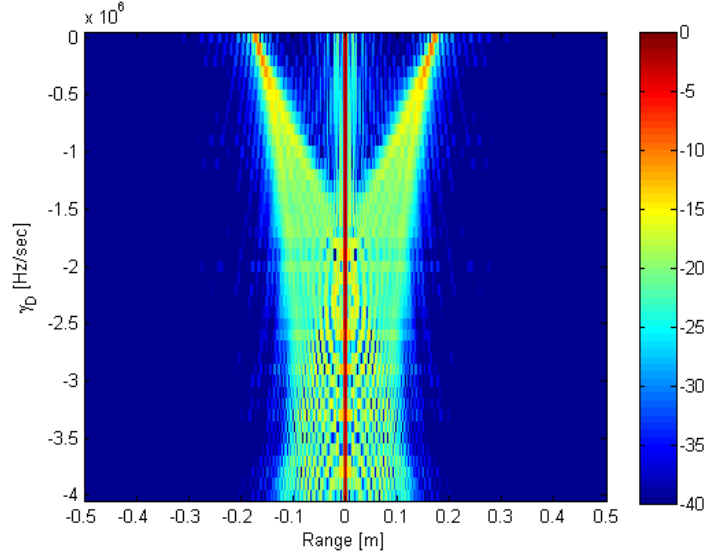
Figure 4.13: Range cuts of the wideband ambiguity function of a signal $y(t)$ with $f_0 = 70$ kHz, $\theta_0 = 0$ and $\gamma_0 = -5 \times 10^6$ Hz/sec as a function of γ_D ($f_D = 10$ kHz, $\theta_D = 0$).
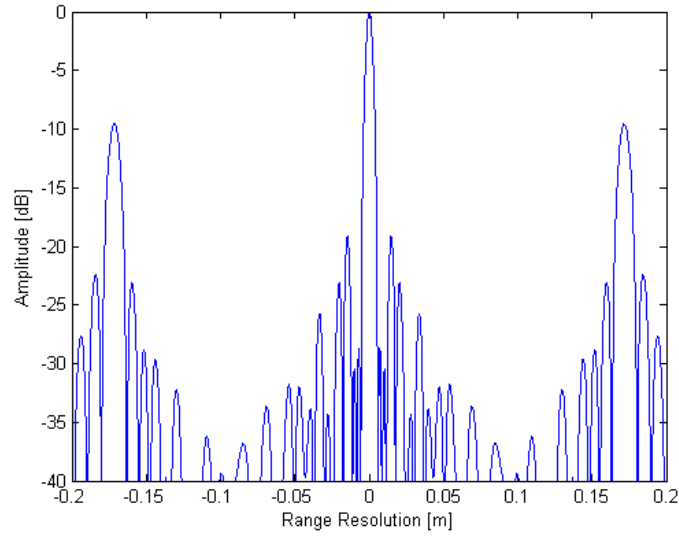
Figure 4.14: Range cut of the wideband ambiguity function of a signal $y(t)$ with $f_0 = 70$ kHz, $\theta_0 = 0$ and $\gamma_0 = -5 \times 10^6$ Hz/sec for $\gamma_D = 0$ Hz/sec ($f_D = 10$ kHz, $\theta_D = 0$).
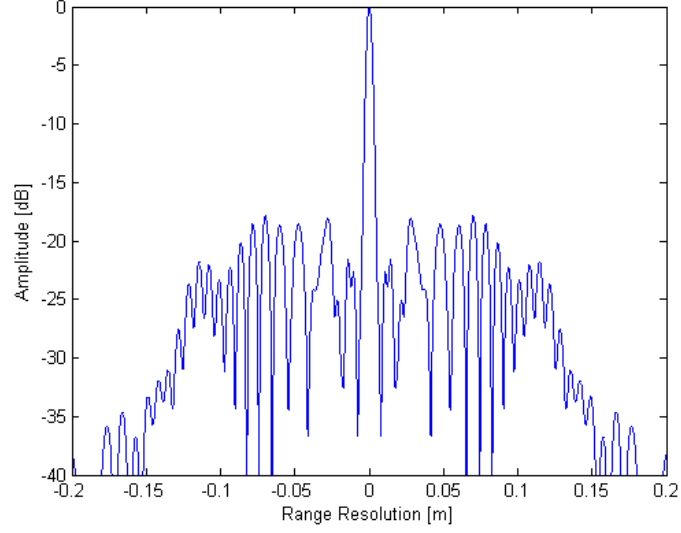
Figure 4.15: Range cut of the wideband ambiguity function of a signal $y(t)$ with $f_0 = 70$ kHz, $\theta_0 = 0$ and $\gamma_0 = -5\text{x}10^6$ Hz/sec for $\gamma_D = -4\text{x}10^6$ Hz/sec ($f_D = 10$ kHz, $\theta_D = 0$).
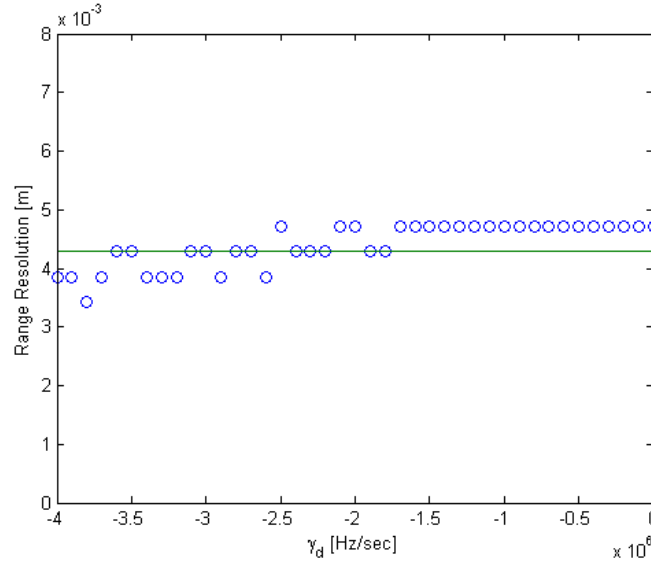
Figure 4.16: Estimated range resolution as a function of γ_D ($f_0 = 70$ kHz, $\theta_0 = 0$ and $\gamma_0 = -5\text{x}10^6$ Hz/sec, $f_D = 10$ kHz, $\theta_D = 0$). The green line represents the range resolution achieved by a single linear chirp with 40 kHz bandwidth.

the range cuts of the WAF as a function of γ_D and range. Results show that when γ_D assumes values from zero to about $-1.3x10^6$ the auto-correlation function of the resulting signal presents a main lobe at zero range and two additional -10 dB sidelobes located at about ± 18 cm. With the increase of γ_D these distant sidelobes gradually tend to move closer to the main lobe up to around $\gamma_D = -1.5x10^6$. For $\gamma_D < -1.5x10^6$ the energy spreads out in a greater number of sidelobes around the main lobe whose peaks reach a level of about -18 dB. A detailed view of the range cut for $\gamma_D = 0$ is given Fig. 4.14. In this case the resulting waveform $y(t)$ is composed of two parallel (in frequency) linear chirps spanning the frequencies between 70 kHz and 40 kHz and between 80 kHz to 50 kHz, respectively. Results show that the first sidelobes drop to about -30 dB. The highest sidelobes in the vicinity of the main lobe are at -20 dB and are located at about ± 1.5 cm from the main lobe itself. As previously discussed, the two main sidelobes at -10 dB are obvious and located 18 cm away from the main lobe. Fig. 4.15 shows the range cut for $\gamma_D = -4x10^6$. In this case the main sidelobes are all located in the vicinity of the main lobe and they reach levels of about -18 dB. Even in this case the very first sidelobes are about -22 dB lower than the main lobe. Considering that a typical linear chirp presents its highest sidelobes at -13 dB both the cases investigated above provide lower first sidelobes at the expense of having to deal with highest sidelobes away from the main lobe. To complete our first analysis the value of the range resolution was calculated as a function of γ_D. Results are given in Fig 4.16. As expected, because the waveform bandwidth remained the same for $\gamma_D \geq -1.66x10^6$ Hz/sec, differences in range resolution, calculated as the width of the main lobe at

−4 dB, are not such to justify significant improvements with respect to a typical chirp with 40 kHz bandwidth (green line in the plot), whose range resolution is theoretically equal to $c/2B = 0.43$ mm (where $c = 343$ m/sec is the speed of sound in air and $B = 40$ kHz is the chirp bandwidth).

The analysis of the range cut of the ambiguity function was repeated on a multi-component waveform with $f_0 = 70$ kHz, $\gamma_0 = -5\text{x}10^6$ Hz/sec and $\gamma_D = 0$ Hz/sec for f_D varying from 10 kHz to 70 kHz. The case corresponding to $f_D = 70kHz$ and therefore $f_1 = 140kHz$ is when the second component of the waveform is exactly a second harmonic of the signal. Fig. 4.17 shows the results for this analysis. It is evident how highest far-out sidelobes behave as a function of the frequency shift between the two components. In particular it is evident that these sidelobes assume high values between 10 kHz and 30 kHz. They then disappear from about 30 kHz onwards. Here the sidelobes closest to the main lobe start to rise significantly. Fig. 4.18 show the details of the range cut for $f_D = 70$ kHz. For this case the sidelobes show peaks that are higher than −4 dB, making this waveform useless for range analysis. Fig 4.19 plots the estimates of the range resolution achieved by $y(t)$ as a function of f_D. As expected, because the bandwidth of $y(t)$ increases as a direct function of f_D the range resolution improves when f_D increases. For high values of f_D range resolution improves with respect to a typical linear chirp (blue line), however, these correspond to the values of f_D that give the highest sidelobes.

The usual way of lowering sidelobes is by an amplitude taper or by waveform codes. Waveforms composed of extra portions of chirps with different slopes at the beginning and at the end of the main chirp have been used as

101
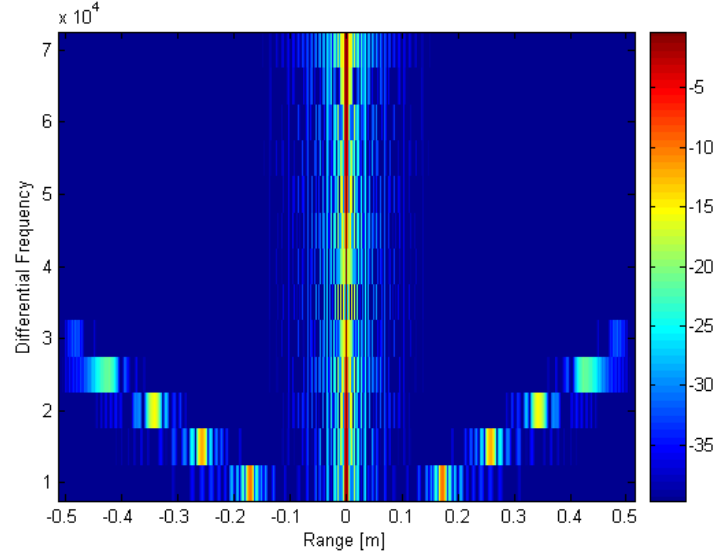
Figure 4.17: Range cuts of the wideband ambiguity function of a signal $y(t)$ with $f_0 = 70$ kHz, $\theta_0 = 0$ and $\gamma_0 = -5\mathrm{x}10^6$ Hz/sec as a function of f_D ($\gamma_D = 0$ Hz/sec, $\theta_D = 0$).
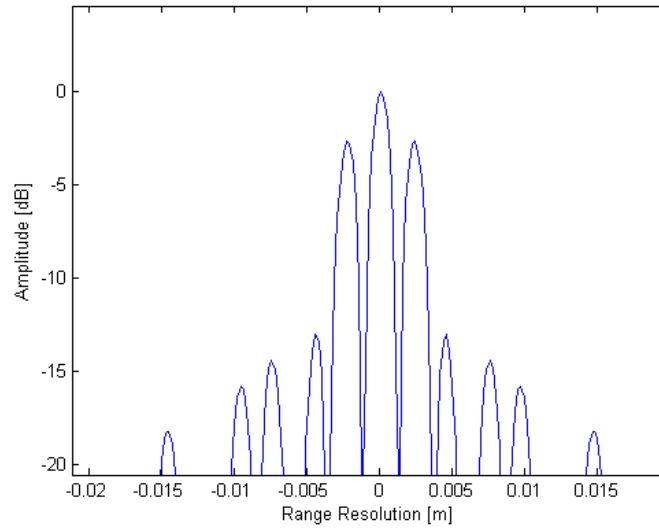
Figure 4.18: Range cut of the wideband ambiguity function of a signal $y(t)$ with $f_0 = 70$ kHz, $\theta_0 = 0$ and $\gamma_0 = -5\mathrm{x}10^6$ Hz/sec for $f_D = 70$ kHz ($\gamma_D = 0$ Hz/sec, $\theta_D = 0$).
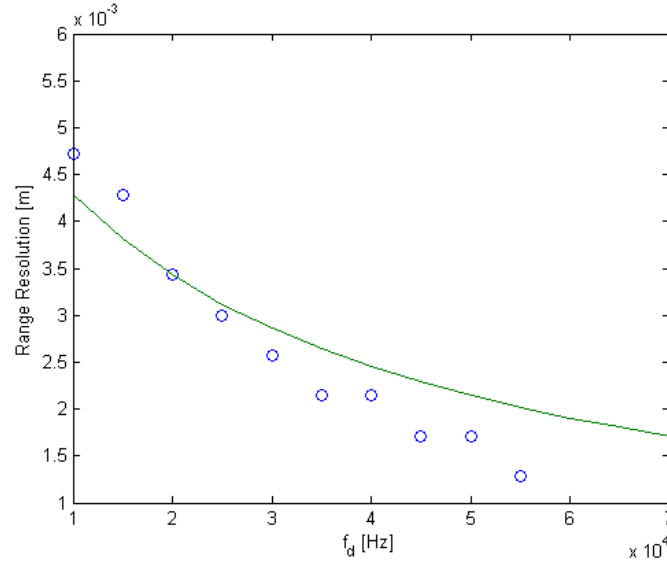
Figure 4.19: Estimated range resolution as a function of f_D ($f_0 = 70$ kHz, $\theta_0 = 0$, $\gamma_0 = -5\text{x}10^6$ Hz/sec, $\gamma_D = 0$ Hz/sec, $\theta_D = 0$). The green line represents the range resolution achieved by a single linear chirp with the same bandwidth (equal to $f_0 + f_D$) at each step.

well, in the past, to lower sidelobes [72]. Here, results show that an intelligent use of the harmonics might enhance some of the parameters characterising radar and sonar waveforms and this may offer an extra degree of freedom in waveform design. However, these are very recent results and, therefore, require further research aiming at corroborating these findings and at developing the necessary mathematical background.

Chapter 5

Analysis of floral echoes

In the previous chapter a sequence of echolocation calls transmitted by a feeding bat has been analysed in order to explore the ability of bats to change their waveform parameters in relation to the task they have to perform. This helped understanding the possible type of information the bat tries to exploit during detection, classification and selection of targets and how this information is prioritised during the task as well. It is clear though that the way bats adapt and the information available to them largely depends on specific target signatures, and therefore a study that looks at the characteristics of those targets which are attractive to bats is also of great interest. This last consideration becomes particularly interesting in the case of nectar-feeding bats, i.e. a class of bats which feed on nectar and by doing so play an important role in pollination of bat-pollinated plants. Although classification of flowers of bat-pollinated plants is a very challenging task, bats still obtain remarkable performance. The reason why they can do so is yet unclear and the hypothesis of a co-evolution between bats and bat-pollinated plant is be-

coming widely agreed. Most bat-pollinated flowers can be assigned to one of two different morphological types: flowers with long and numerous stamina, and bell-shaped flowers. Bell-shaped flowers may differ significantly in size. Large flowers allow the bat to land and typically are visited by a number of unspecialised bat species. Small flowers can instead be exploited by specialised bats only [2]. It is believed there might be some characteristics in the 'echo fingerprint' of flowers of bat-pollinated plant such that the information allows them to succeed in finding the nectarium, extract the nectar and thus pollinate the flower. Under this hypothesis, the aim of this work is to assess the type of information that is available to bats and which allows them to succeed so impressively in the task of flower recognition, with the goal to understand what are the methodologies deployed by bats to perform the task of classification of flowers and how this knowledge can be applied to radar and sonar systems. In order to address this problem a detailed exploitation of the characteristics of the echoes from these flowers with the goal to identify possible critical features in their shape that might allow correct classification is required.

5.1 Floral Echoes: Radar Comparisons

A first preliminary analysis of floral echoes was performed on a set of data provided by the School of Biological Sciences at the University of Bristol. These contained high range resolution profiles of four flower heads belonging to four different species: *Amphitecna latifolia, Markea neurantha, Crescentia cujete* and *Vriesea gladioliflora*. The flowers to be irradiated were impaled

by a long, very thin insect pin mounted at the top of a thin holder placed in the centre of a small turntable. Revolving the turntable allowed irradiation of the objects from all directions in one plane. The front view of the object was adjusted to 0 degrees. A custom-built condenser speaker and a microphone fixed at a distance of 20 cm from the target at the same height as the target object were used. The distance between the centre of the microphone and the loudspeaker was 18 mm. The microphone was placed parallel to the loudspeaker, approximately 45 degrees laterally above the horizontal with respect to the midpoint of the loudspeaker membrane. A picture of the experimental setup is given in Figure 5.1. Echoes were measured as impulse response functions of the flower heads by transmitting maximum length sequences (MLS), theoretically characterised by an unlimited bandwidth and a auto-correlation function which is equal to unity for perfect ovelapping and zero elsewhere. The received echo was sampled at 500 kHz and the impulse response functions of the flower heads were computed as the convolution between the transmitted and the received waveforms. The frequency response of the loudspeaker and microphone allowed measurements between 20 kHz and 140 kHz, covering the frequency range of the echolocation calls used by most flower-visiting bats, and leading to a theoretical range resolution of about 1.5 mm. Unfortunately, the actual range resolution was not verified at the time of the recordings. A more detailed description of the experiment and the data can be found in [2]. Before processing, the raw data were scaled so that in each image the maximum value of the amplitude was equal to unity. The Signal to Noise Ratio (SNR) was estimated in each image by selecting a noise only window and a signal plus noise window. The noise only windows

106
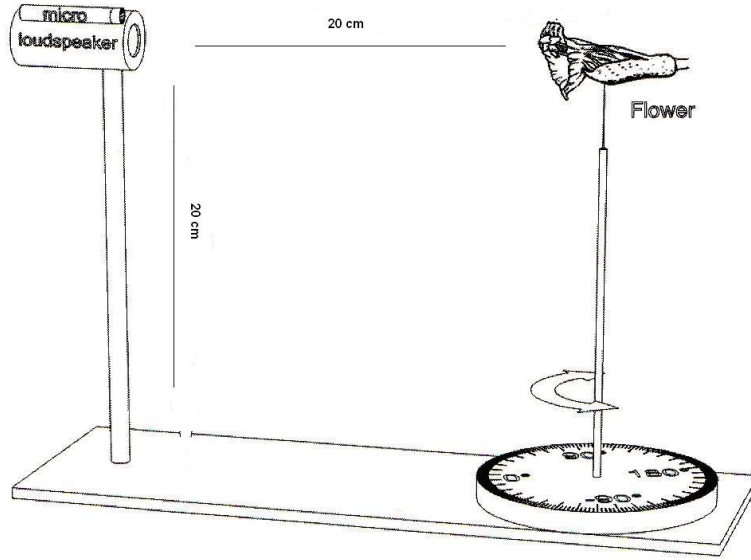
Figure 5.1: A sketch of the experimental setup. Taken from [2].

had to be taken in the region after the last arrival from the flowers because all echoes received before the flowers had been cut from the images that were provided. Both the windows were selected manually from the images of the flowers and therefore the regions that were used to estimate the SNR were different for each case. An example of selected windows is given in Figure 5.2.

An estimate of the power of the noise P_n and an estimate of the power of the signal plus noise P_{s+n} were computed as the root mean squared value of the squared samples of the respective window as

$$P = \frac{1}{N} \sum_{i=1}^{N} x_i^2, \tag{5.1}$$

where N is the total number of samples and x_i is the ith sample in the

107
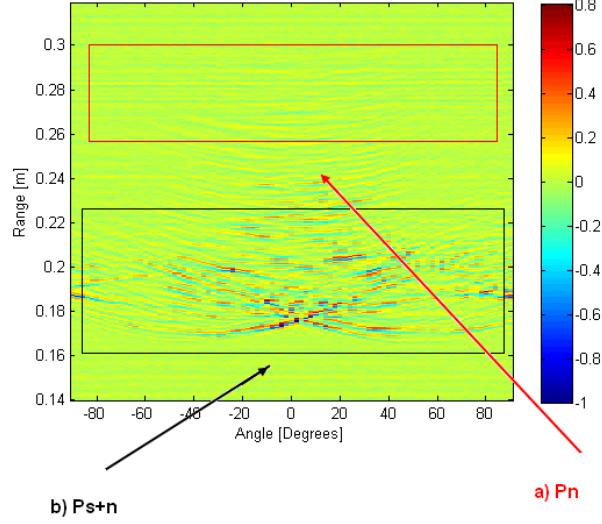
Figure 5.2: Window selection for SNR estimation. a) is the window that contains only noise and has been extracted to estimate P_n. b) is the window that contains signal plus noise and has been extracted to estimate P_{s+n}.

reference window, and the SNR was estimated as

$$SNR = \frac{P_{s+n}}{P_n} - 1. \tag{5.2}$$

The results are reported in Table 5.1 for each of the four flower heads. The variation in SNR is quite considerable and requires care to be taken in the interpretation of the results when applying a classifier. To examine multi-perspective classification performance a Knn classifier with $Knn = 3$ was implemented. A total of 16 range profiles, corresponding to 16 different angular perspective separated in angle by 5 degrees, were extracted from each dataset to train the classifier. These were selected to give the classifier full knowledge of the target over all angular negative perspectives using non-correlated range profiles. Because all the flowers visually presented a high

108

Table 5.1: SNR estimates for each image.

Flower Species	SNR (dB)
Amphitecna latifolia	22
Markea neurantha	9.5
Crescentia cujete	15
Vriesea gladioliflora	22

level of symmetry no training profiles were selected between the positive perspectives, i.e. those between 0 and +90 degrees. The training profiles were removed from the data to be classified, and all the remaining angular perspectives ($180 - 16 = 164$ test profiles) were used to form the test set on which performance was assessed. In both the training set and the test set the amplitude of all range profiles was scaled to lie between $[0, 1]$. For the single perspective classification, the decision was made by using only one test profile at the time. The amplitude of the test profile was compared with the amplitude of all 16 training profiles, by calculating their Euclidean distances. Among the resulting 16 distances only the smallest 3 ($Knn = 3$) were used to make the decision. No use was made of the known angle between the training profiles nor of the knowledge of the angle corresponding to the test profile itself. Each test profile was assigned to the class that owned the higher number of training profiles that generated the $Knn = 3$ lowest distances and all the ambiguous cases (i.e. draws) were not assigned to any class. For the multi-perspective analysis each decision was made by comparing jointly two or three test profiles, separation for each other of 10 degrees, with the training set. For each decisions, the $Knn = 3$ lowest distances were selected

between the resulting 32 (two perspectives case) or 48 (three perspectives case) distances. As in case of a single perspective, no use was made of the known angle between the training profiles nor of the knowledge of the angle corresponding to the test profiles. Figure 5.3 shows the output of the classifier when all the four classes were tested. White noise was simulated and added to the images in order to plot the performance as a function of signal to noise ratio. There are two clear conclusions that may be drawn. The first is that, as is the case for radar, for low SNRs there can be an increase in classification performance in going from one to two perspectives and there is a further, but lesser, improvement in going from two to three perspectives [8]. For high SNRs there is both an increase in classification performance in going from one to two perspectives and from two to three perspectives. Secondly, as the SNR increases the classification performance, as might be expected, also increases. As noise is added eventually there is a drop in performance, indicative of the loss of key information, possibly embedded in scatterers of smaller echo values. This may well be indicative of the mutually beneficial arrangement that nature has provided. Because classification performance was tested on a limited set of data it remains difficult to conclude on the actual significance of drops or increases in classification performance as there is not enough knowledge of the statistical fluctuation around the results.

As the image for *V. gladioliflora* presented a $SNR = 9$ dB the plot had to be stopped at 9 dB but the behaviour shows a clear tendency to increase further. In order to assess performance at higher SNRs the data related to the *V. gladioliflora* were removed from testing. Figure 5.4 shows the output of the classifier when only the three flowers that presented the highest signal

110

to noise ratios were tested. The behaviour in the plot is similar to that shown in Figure 5.3. Performance keeps on increasing after 9 dB as predicted although there is a change in the slope of the plot at around 8 dB. Below 8 dB performance falls off more rapidly. This may indicate that scatterers key to good classification are swamped by noise. Overall, as in the radar case the results do not appear to be very robust in either case. Small changes in processing such as the use of different range profiles to train the classifier or slightly different lengths of profile to be processed could lead to quite different results even when the images to be processed remained the same [11]. This could depend on the limited numbers of range profiles that were available to train the classifier though it might be the case that the classification approach is not robust itself. It is therefore not certain that the classifier performance can be improved by adding more training profiles. Further investigation is required to compare a greater number of images, possibly with higher signal to noise ratio, and to contrast and exploit the form of the four types of range profiles. In addition to this, it needs to be considered that here classification performance has been tested on data that were taken from the same set of measurements and that were gathered with the same system. Because of this, it remains impossible to exclude that the classifier has used some features in the return signals that were related to the specific background or to the collection system rather than features exclusively related to the flowers. In order to avoid any possible classification "bias", ideally, one should classify data collected in different scenarios by means of different systems. However, this work was aiming to relate images of flower heads to classic radar targets rather than quantify the performance of the classifier itself. In these terms
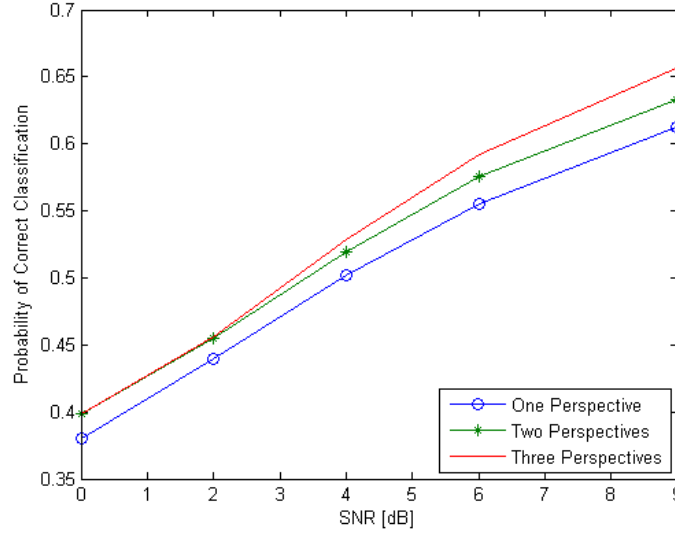
Figure 5.3: Output of the classifier when four classes are tested.

the obtained results are valuable and show close similarities to the radar case.

These results confirm the hypothesis of a close parallel between radar target classification and the task of classification by bats and, more specifically give evidence of close similarities between echoes from floral targets and those from classical radar targets.

Later on in this thesis an investigation of which features make these flowers so well recognizable by bats, and which role these features play in automatic target classification is presented together with results. Finding the right answers to these questions could give an important contribution to the way radar target classification is carried out nowadays.

The work described in this chapter present some limitations due to the way the data was collected. MLS sequences generate a waveform that is theoretically characterised by an ideal flat Fourier transform over an infinite band-
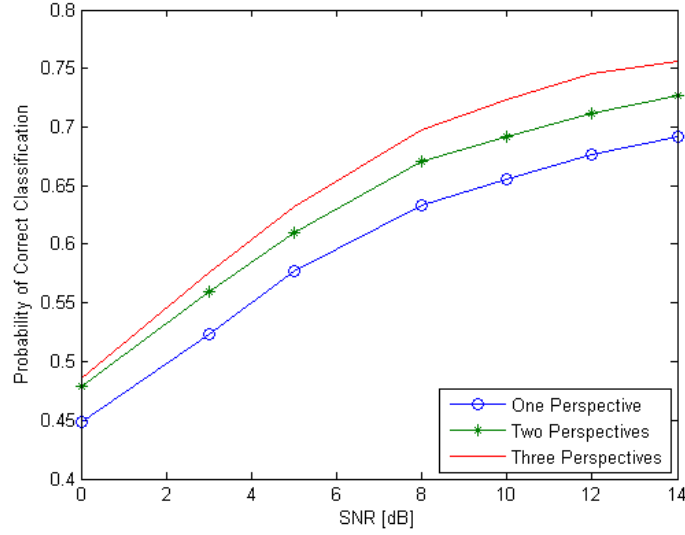
Figure 5.4: Output of the classifier when three classes are tested. Scales are different from the previous case.

width and an ideal autocorrelation function that is equal to 1 only when two replicas of the same sequence are perfectly overlapped and equal to zero otherwise. In real scenarios, because real systems are characterised by a limited bandwidth, MLS sequences are filtered before transmission and thus the ideal properties discussed above are altered. In addition to this, the impulse response of a real system is not flat over the entire system bandwidth and thus the properties of the signal obtained after cross-correlation between the signal recorded by the microphones and the transmitted MLS sequence do not match those of the theoretical case. There is also another effect to be taken into account. Because of the filtering of the system, the transmitted waveform, and thus the output from the cross-correlator, become bandpass signals and contain the carrier. If this is not removed the output after cross-correlation is likely to contain modulations due to the carrier that can have

a significant impact on the images of the targets and, in particular, these could show peaks that do not belong to real scattering from the target itself. For these reasons it is fundamental to assess the performance that can be achieved by a real system any time a measurement is done. This procedure commonly takes the name of *calibration* of the system. For this experiment, calibration results are not available and therefore it is now unknown what the performance of the system, such as range resolution and sidelobe levels, was.

To address these problems and to be able to carry out additional and independent experimentations, and thus collect a greater number of experimental data, an acoustic system capable of transmitting and receiving waveforms at the same frequencies deployed by bats has been implemented as part of this research work. This system, called an *acoustic radar* as it works as a radar that transmits ultrasound frequencies, is presented in the next section with a detailed description of the hardware together with an assessment of its performance.

5.2 Description of the acoustic radar

The acoustic radar used to collect data is composed of a transmitter and two receivers that represent respectively the mouth and the two ears of the bat. The transmission system is composed of a signal generator, an amplifier and a piezoelectric custom built loudspeaker (about 1.5 cm x 2 cm in size) capable of producing acoustic waveforms at the same range of frequencies deployed by echolocating bats ($\approx 20kHz- \approx 200kHz$). A detailed description

114

of the principal of operation of the loudspeaker is given in [73]. Table 5.2 reports the values of the loudspeaker beamwidths at 50 kHz, 100 kHz, 150 kHz and 200 kHz. For each frequency the level of the main lobe measured with respect to the maximum level achievable in the range of frequencies between 10 KHz and 220 kHz is also given [74]. The system is designed to produce a wide beam so that the whole flowers can be insonified as uniformly as possible. Indeed, bats show an excellent capability to adapt their beam pattern as well. They scan their beam around to detect the target and then modified its directionality once the target is on track [75] [76]. The signal generator is a National Instruments PCIe-6251 card capable of transmitting 500 kS/sec (16-bit resolution) on 16 channels simultaneously and thus 16 waveforms, each one characterised by a bandwidth of up to 250 kHz. The receiver is composed of two G.R.A.S. ultrasound microphones (type 40 BF) followed by one two-channel amplifier that is capable of amplifying each signal from the two microphones of an amplification factor equal to x40. Echoes recorded by the two ultrasound microphones are sampled at a rate of 500 kHz

Table 5.2: Beamwidth of the loudspeaker (calculated @-3dB) at 50 kHz, 100 kHz, 150 kHz and 200 kHz and the corresponding level of attenuation with respect to the maximum level obtained between 10 KHz and 220 kHz [74].

	Main lobe width [degrees]	Main lobe level
50 kHz	15	-7 dB
100 kHz	10	-7 dB
150 kHz	11	-2 dB
200 kHz	8	-20 dB
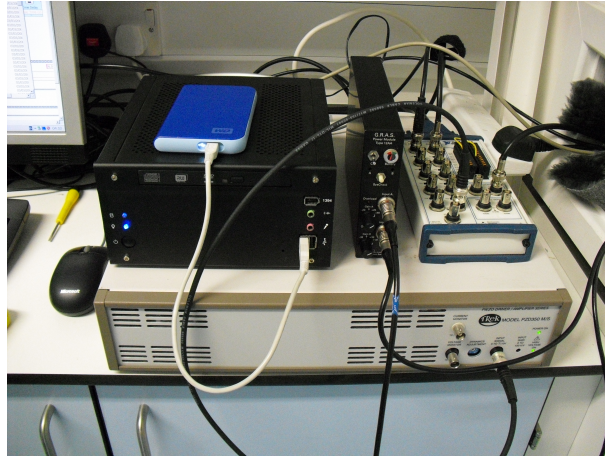
Figure 5.5: Photo of the instrumentation that controls the setup.

using the same National Instruments DAQ card (14-bit resolution) and then are matched filtered to the transmitted waveform using Matlab (v7.5 The Mathworks. Inc., Natick, USA). A picture of the ultrasound radar is given in Figure 5.5. For the purpose of this thesis, the acoustic radar was operated in a 6x2 meters ultrasound anechoic chamber at the School of Biological Sciences of the University of Bristol.

As discussed in the previous chapter, the goal of this thesis is to understand the methodologies deployed by echolocating bats when they perform classification of static targets. Because of this, in order for the results to be consistent, it is important to make sure that the information contained in the experimental data is as close as possible to the actual information that is available to a real bat that is echolocating. As this information critically depends on the spatial arrangements of all the sensors, the loudspeaker and the microphones were placed in an artificial bat head in order to reproduce the real spatial arrangements of a typical bat head. A picture of the artificial bat head is given in Figure 5.6.
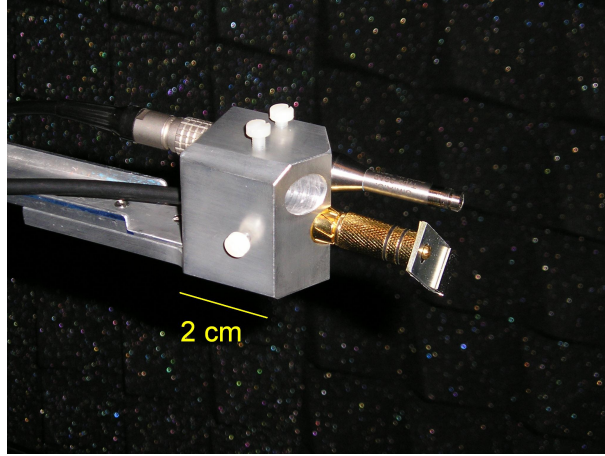
Figure 5.6: Artificial bat head with one loudspeaker and one microphone reproducing the spatial arrangements of a real bat head. The empty hole in the artificial head can host an additional microphone when binaural data are collected.

Because classification of static targets do not require any Doppler information, the performance of the system was assessed solely in terms of range resolution. This was estimated by sending a chirp towards a flat plate (45.4 x 41.1 cm), placed about 30 cm from the artificial bat-head and perpendicular to the signal direction, functioning as a mirror, and then matched filtering the echo to the transmitted signal. The matched filter was implemented in Matlab by cross-correlating the analytic signal of the received echo with the analytic signal of the transmitted waveform. The analytic signals were obtained by applying the Matlab Hilbert function to the original waveforms. Selecting the return from the mirror, in the plot of the amplitude of the matched filter output, and then looking at the width of its corresponding main lobe gives a good estimate of the range resolution that is achievable by the system. As previously discussed, this measure is of great importance because it takes into account any undesired effects from the hardware system.

117
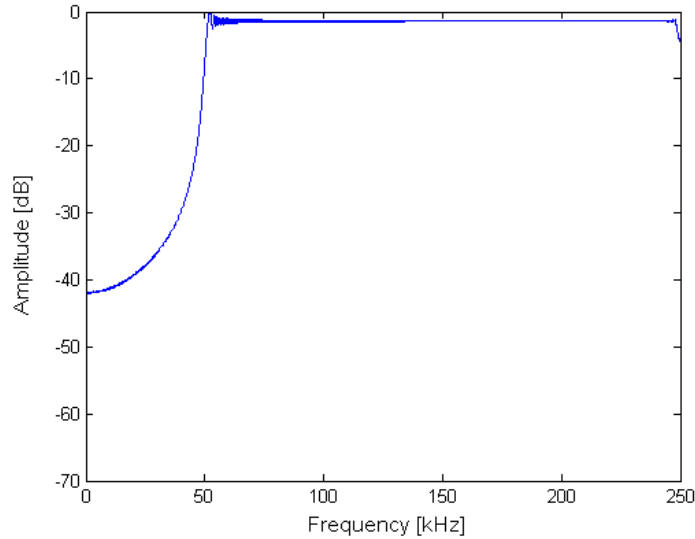
Figure 5.7: Fourier transform of the transmitted linear down-chirp spanning the frequencies between 250 kHz and 50 kHz.

The first measurement was performed by sending a linear down-chirp spanning the frequencies from 250 kHz to 50 kHz. The spectrum of the signal is given in Figure 5.7 and the spectrogram of the echo before being matched filtered to the transmitted chirp is given in Figure 5.8.

The spectrogram in Figure 5.8 shows the presence of a direct signal from the loudspeaker to the microphone. The echo from the mirror is well visible and shows that frequencies over 180 kHz are much more attenuated with respect to the lower ones. This is due to the effect of the acoustic propagation in air as well as to the attenuation due to the system hardware components. Distortions due to non-linearity in the system are clearly visible in the spectrogram in the form of harmonics after aliasing. These are introduced by the amplifier in transmission that had to be fed with a too high signal voltage in order to reach the right output voltage that was required by the loudspeaker.

118
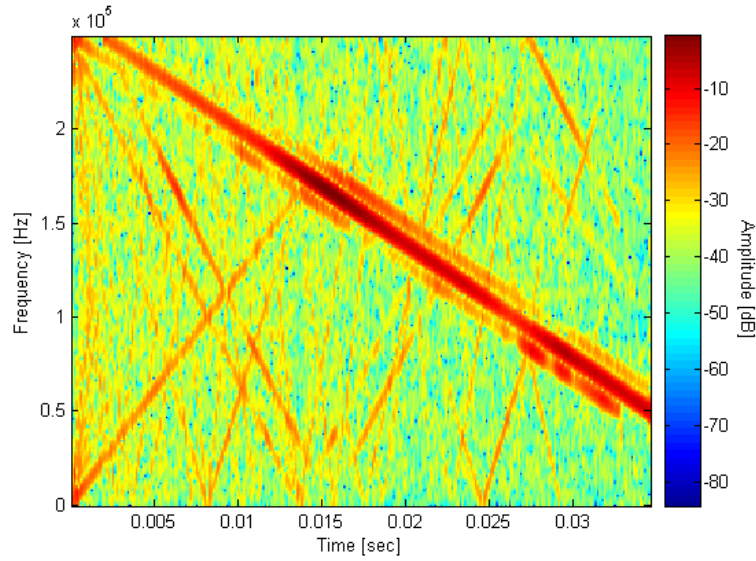
Figure 5.8: Spectrogram of the received waveform before the matched filter when a down-chirp from 250 kHz to 50 kHz was transmitted.

The impact of these unwanted effects, mainly due to the hardware, on the performance of the system in terms of range resolution are obvious in both Figure 5.9 and Figure 5.10. These show the amplitude of output signal from the matched filter and an expanded view of the return of interest from the flat plate.

As expected, the compressed pulse presents the return from the mirror at a distance of about 32 cm. The direct signal from the loudspeaker to the microphone, separated by just a few millimetres in the artificial bat head, and additional multiple reflections due to the artificial bat head are clearly visible as well. The width of the main lobe of the return from the mirror is the range resolution that is achievable by the system when this particular linear chirp is transmitted. Theoretically, the range resolution of such a chirp, characterised by a bandwidth $B = 200$ kHz, considering that the speed of

119
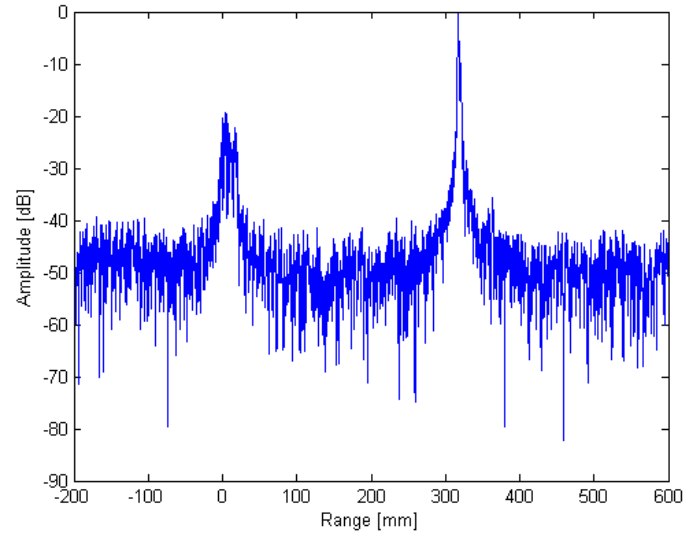
Figure 5.9: Magnitude of the output of the matched filter when a down-chirp from 250 kHz to 50 kHz was transmitted.
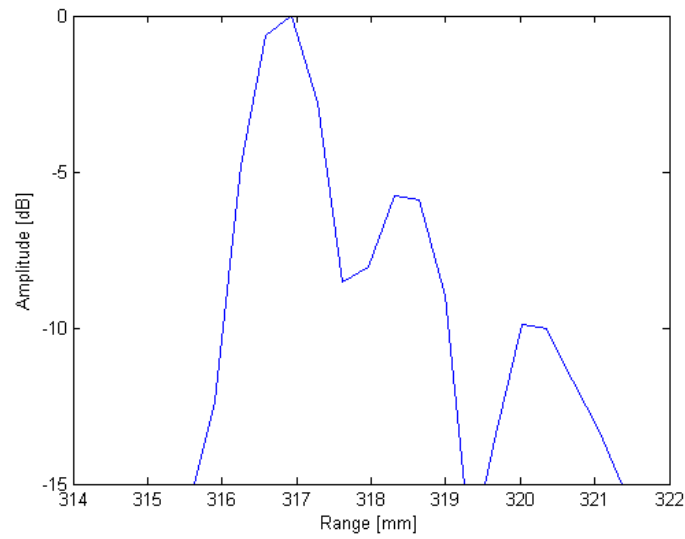
Figure 5.10: Expanded view of the return from the flat plate obtained from the magnitude of the output of the matched filter when a down-chirp from 250 kHz to 50 kHz was transmitted.

sound in air c is about 343 m/s, is equal to $c/2B = 0.85$ mm. Because the bandwidth of the system is not flat over the entire transmitted bandwidth and because of the effects of the non linearities in the amplifier, the width of the lobe and therefore the range resolution is slightly poorer than the theoretical one and equal to 1 mm. In addition to this, Figure 5.10 shows the main lobe belonging to the return from the flat plate is not as that of a linear chirp as described in the previous chapter. The lobe presents two peaks as if some multiple reflection was taking place at the time of the recordings, and further investigation was required to address this problem. Eventually it turned out that a grid placed on the end of the microphone in order to protect the membrane was the cause of these multiple reflections. Figure 5.11 shows the spectrogram of the received waveform before matched filtering when the same down-chirp from 250 kHz to 50 kHz was transmitted and received by the microphone with no protection grid. Again, for the reasons previously discussed, the higher frequencies are more attenuated with respect to the lower ones. Figure 5.12 and Figure 5.13 show the signal at the amplitude of the output of the matched filter. In this case the main lobe given by the return from the mirror presents, as expected, one peak only that is much more similar to a typical main lobe that characterises a linear chirp. Because the impulse response of the system and the non linearities are still diminishing the performance of the system, the width of the main lobe is still greater than the theoretical one and again the range resolution is about 1 mm.

The results described above clearly show how the impulse response of the system can significantly impact the performance of the acoustic radar and, in particular, diminish the range resolution. Because the frequency response
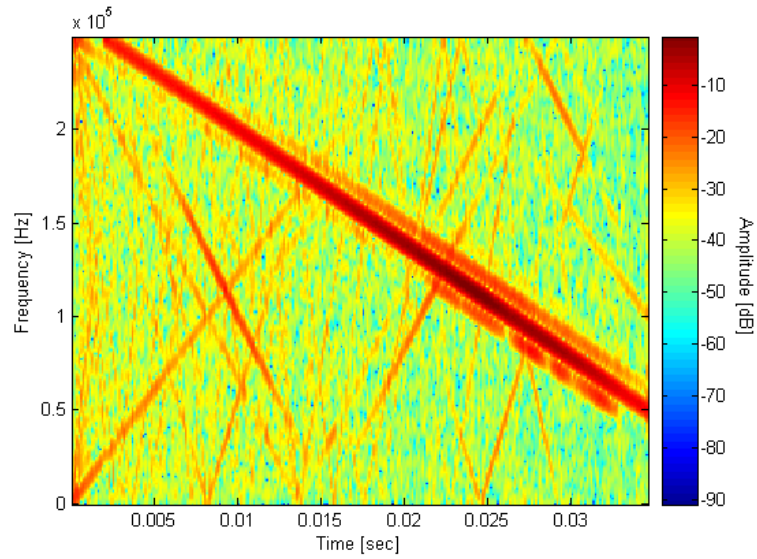
Figure 5.11: Spectrogram of the received waveform before the matched filter when a down-chirp from 250 kHz to 50 kHz was transmitted and the grid covering the microphone was removed.
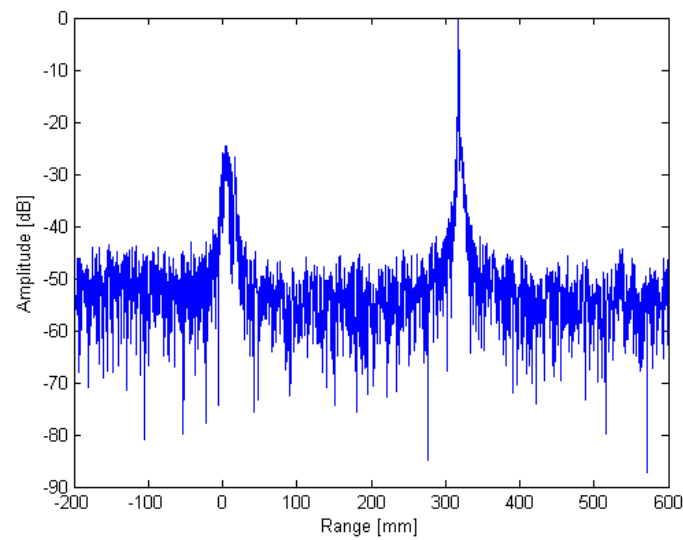
Figure 5.12: Magnitude of the output of the matched filter when a down-chirp from 250 kHz to 50 kHz was transmitted and the grid covering the microphone removed.
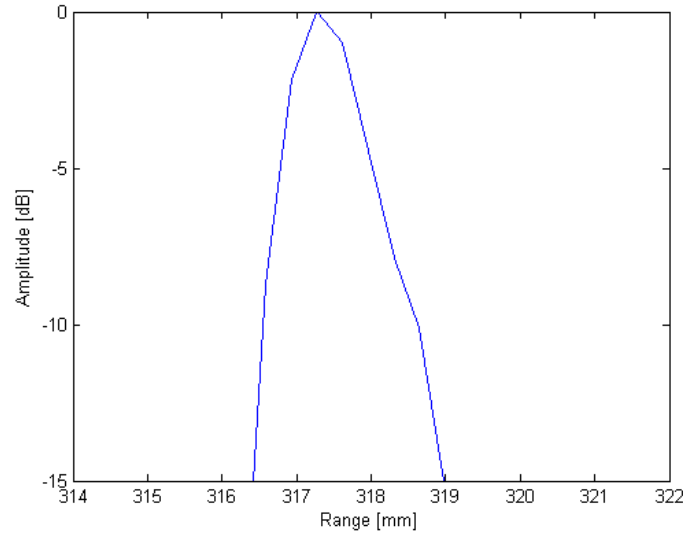
Figure 5.13: Expanded view of the magnitude of the output of the matched filter when a down-chirp from 250 kHz to 50 kHz was transmitted and the grid covering the microphone removed.

is not flat over a large bandwidth, it is interesting to explore how the system performs when lower bandwidth and thus lower frequencies are transmitted.

The same type of analysis described above was then repeated transmitting another linear down-chirp characterised by a bandwidth $B = 100$ kHz spanning the frequencies between 150 kHz and 50 kHz. Figure 5.15 shows the spectrogram of the echo before the matched filter. Both the direct signal from the loudspeaker and the reflection from the mirror are well visible. In this case higher frequencies are not much more attenuated with respect to lower ones, indicating that the impulse response of the system is much more flat at these range of frequencies. This also depends on the attenuation in air due to the propagation of sound waves. For the same reasons discussed above, as expected, non linearities due to the amplifier in transmission are

123
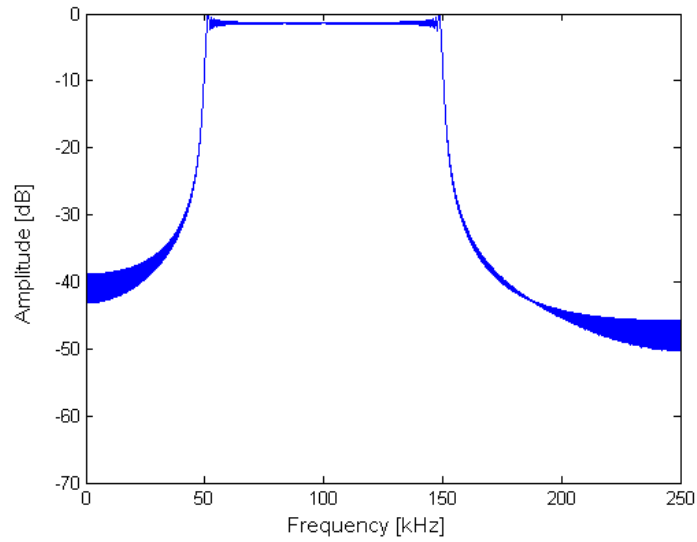
Figure 5.14: Fourier transform of the transmitted linear down-chirp spanning the frequencies between 150 kHz and 50 kHz.
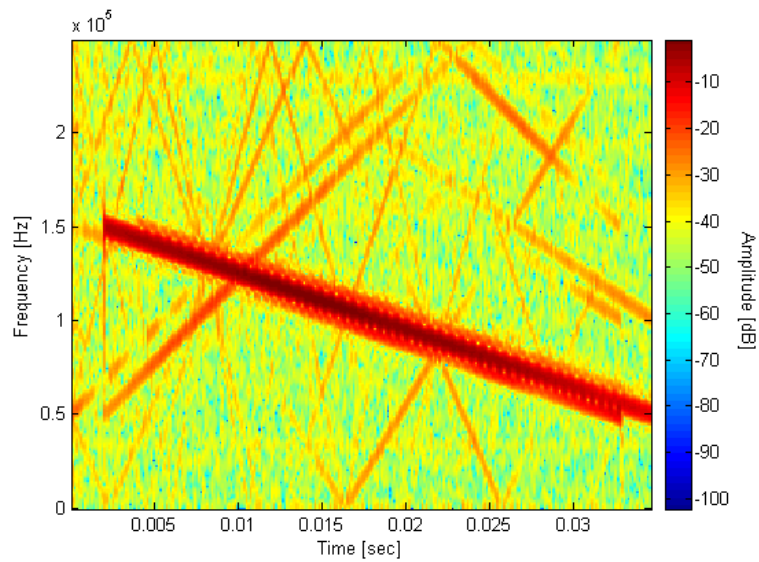
Figure 5.15: Spectrogram of the received waveform before the matched filter when a down-chirp from 150 kHz to 50 kHz was transmitted and the grid covering the microphone was removed.

still present because the amplitude of the voltage input in the amplifier in transmission was the same.

How the system performs when lower frequencies are transmitted is clearly visible in both Figure 5.16 and 5.17 where the amplitude of the output from the matched filter is given together with an expanded view of the main lobe due to the reflection from the mirror. In this case, in fact, the shape of the reflection from the mirror at about 32 cm is much more similar to the theoretical one presenting sidelobes that decayed as expected with the first sidelobe at about -13dB. In this case the measured range resolution is about 1.7 mm and therefore close to identical to that expected in theory (343m/sec over 200kHz equal to 1.7mm). This result confirms the scaling effect of changing the bandwidth of the transmitted waveform. The experiments described above were obtained without applying any sort weighting to the data. Weighting the data before match-filtering would certainly help reducing the sidelobes at expense of the range resolution.

5.2.1   3D data collection

In the previous section the acoustic radar has been described together with an assessment of its performance. This allows transmission of waveforms towards a target and reception of their echoes that, depending on the type of waveform that was transmitted, contain different information on the target. In particular, processing of the echo allows to distinguish scatterers in the target separated by a distance greater than the range resolution. It is self evident, though, that the information from the target varies depending
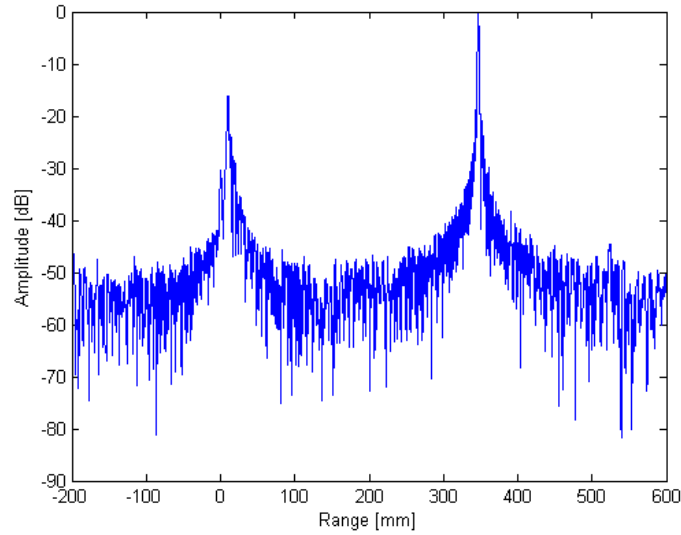
Figure 5.16: Magnitude of the output of the matched filter when a down-chirp from 150 kHz to 50 kHz was transmitted and the grid covering the microphone removed.

on the angle that the sensors forms with the target, commonly called *look angle* or *look direction*. As it is in the interest of this research to exploit the type of information that can be extracted from a multi perspective analysis a setup that allowed collection of three dimensional multi perspective target data was built and a picture of this setup is given in Fig. 5.18. The setup is composed of two LinearX System precision turntables, model LT360, capable of rotating with a step angle of 0.1 degrees. These can be controlled by sending digital pulses into a *pulse step* input that is available on each turntable. The digital pulses that trigger the turntables are generated by the same LabView program that controls the acoustic radar so that the setup can be synchronised with the acoustic radar in order to guarantee that any measurement is taken when the target is not moving. The target is placed

126
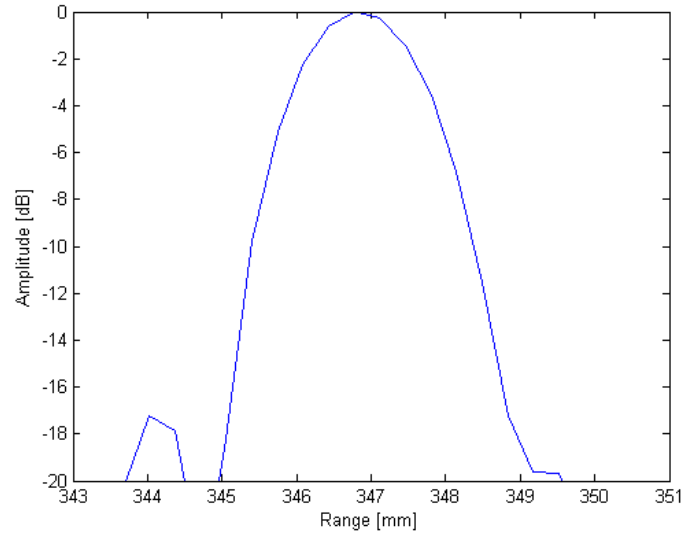
Figure 5.17: Expanded view of the magnitude of the output of the matched filter when a down-chirp from 150 kHz to 50 kHz was transmitted and the grid covering the microphone removed.

on the horizontal turntable at a height of about 20 cm by means of a thin pin. High range resolution profiles are measured by transmitting a waveform and receiving its echo at each step of the turntable. By doing so 2D high range resolution profiles of the target can be taken over 360 degrees. An arm carrying the artificial bat head that contains the loudspeaker and the microphones is connected to the vertical turntable. Rotating the arm allows collection of the data at different vertical angles as well leading to collection of 3D data set.

5.2.2   Summary

In this chapter a first analysis of floral echoes of a dataset collected at University of Bristol has been carried out and a discussion of similarities and

Figure 5.18: Photo of the setup that was used for data collection in the ultrasound anechoic chamber at University of Bristol.

differences with radar/sonar target echoes has been presented. The *acoustic radar* system that has been developed to collect the data that will be analysed later in this thesis has been described, and its performance in terms of range resolution assessed. Results have shown that a range resolution of better than 2 mm can be achieved and have been used to describe what the impact of the deployment of high bandwidth, and thus high frequencies, can be on this type of systems. Finally, a description of the setup that allows collection of 3D data has been given as well.

Chapter 6

Floral echoes from a single individual

The acoustic radar described in the previous chapter represents a fundamental achievement of this research. As previously discussed, it is the aim of this work to investigate what type of information is made available to bats by floral echoes and to exploit how this changes as a function of physical flower features, stage and age of the flowers. Because bats successfully detect and select flowers of bat-pollinated plants, under the hypothesis of co-evolution, it is expected that there is a lot of information in floral echoes. In particular, because bats have to distinguish between good flowers, wilting flower and buds, characteristics in the echo fingerprint in floral echoes between these different cases are expected to be such to allow high level performance. From this perspective the dataset described in the previous chapter contained a lot of limitations and was just not enough to carry out this type of analysis. Firstly, the dataset consisted of only one image for each species of flower.

Secondly, all of the images were taken by ensonifing flowers that were suitable for pollination. In addition to this, as discussed earlier, calibration results were not available for these measurements, so that it remained impossible to conclude on parameters such as the achieved range resolution. The acoustic radar provides us with the flexibility and the full system control that is needed to carry out the experiments that will follow.

In this chapter an analysis of floral echoes from flowers of two bat-pollinated plants, the *Rhytidophyllum auriculatum* and the *Cobaea scandens* is carried out. The way the information contained in floral echoes can change as function of specific parts of the flower, such as anthers and petals (see Figure 6.1), and as a function of their stage is investigated by processing a dataset consisting of HRRPs that was collected with the ultrasound radar.

6.1   *Rhytidophyllum auriculatum*

The plant *Rhytidophyllum auriculatum* hook is a bat-pollinated plant which grows in the Caribbean region and produces small flowers whose nectar is very attractive to bats. A photo of a typical *R. auriculatum* flower is given in Figure 6.2. In order to exploit the contribution associated with specific physical part of the *R. auriculatum* flower and determine how these change as a function of the age and stage of maturity of the flower itself, two datasets containing HRRPs of *R. auriculatum* flowers are analysed. In particular, here, the contribution associated to the distal parts of the petals of the corolla and the anthers is investigated by examining high range resolution profiles (see Figure 6.1). This data was collected at the School of Biological Sciences at

130
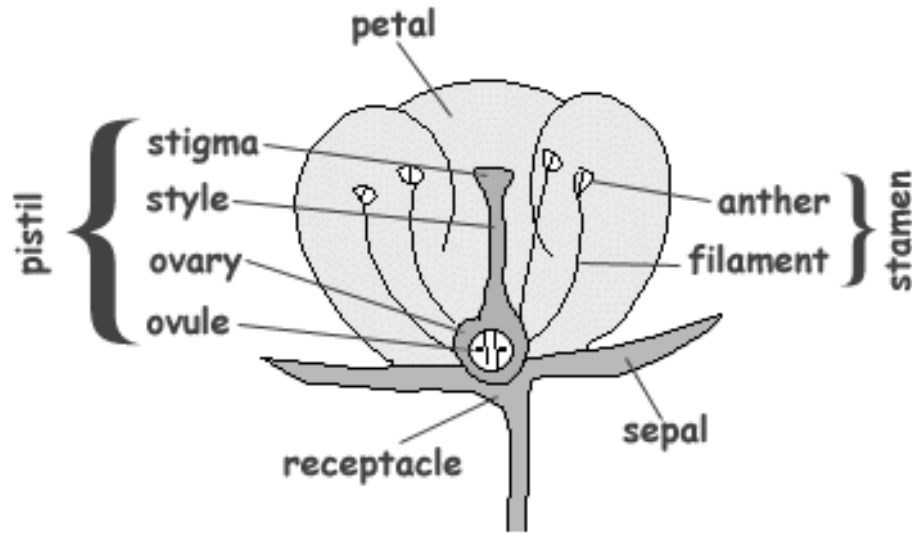
Figure 6.1: Sketch representing the structure and indicating the main physical parts of a flower.

the University of Bristol where one *R. auriculatum* plant is currently grown and perennially produces flowers that therefore are available for experiments at any time of the year. The first dataset, collected in October 2008, consists of HRRPs of an open flower and two modified flowers obtained by manually removing the distal part of the petals and the anthers from an open one. The second dataset, collected in June 2009, consists of HRRPs of an additional open flower and a bud taken from the same plant. Because the *Rhytidophyllum auriculatum* is successfully pollinated by bats, it is likely that co-evolution has shaped its flowers in order to display critical information to bats. The goal of this section is to investigate what are the physical parts of the flower which add such information to the flower echo fingerprint. Because of its bell shape, scattering from the inside of the corolla might be expected to be stronger than the scattering associated with other parts of the flower.

131
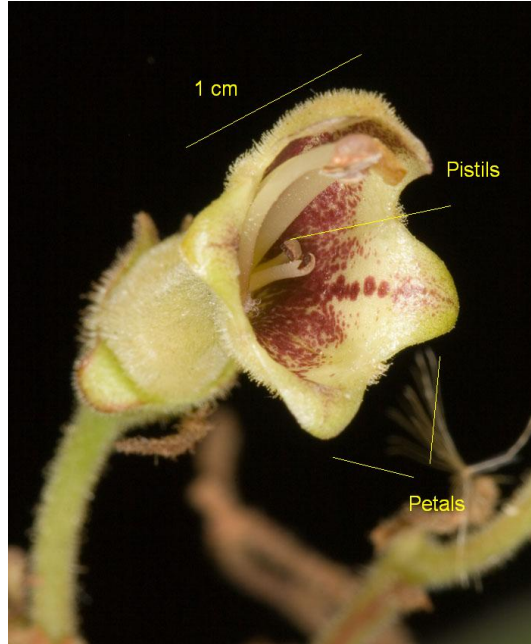
Figure 6.2: Photo of a *Rhytidophyllum auriculatum* open flower. During the experiments the loudspeaker and the microphones were placed at the same height as the flower and arranged in order to look straight into the corolla when the perspective was 0 degrees.

As it is part of the classification task to distinguish open flowers from closed buds, the HRRPs fingerprint of the bud is expected to be significantly different from that associated with the open flower. Finally, buds are closed and smaller than open flowers and so it is likely that the amount of energy they can reflect is considerably lower than that of open flowers.

The data was collected as described in the previous chapter. The flowers were impaled on a thin metallic pin (1.5 mm of diameter) placed at the centre of the horizontal turntable (Figure 5.18), set to rotate over 90 degrees (between -45 degrees to +45 degrees) with an angular resolution of 1 degree, and were ensonified using the same custom-built loudspeaker fed with a linear chirp spanning the frequencies between 50 kHz and 250 kHz (1 mm range

132

resolution). The echoes were recorded with the ultrasound microphone and sampled at a rate of 500 kHz. Unfortunately, only one microphone was available at the time of this experiment and thus, for this dataset, binaural information is not available. A measure of the background was taken before gathering data with the flowers. However, in this experiment, subtracting the background from the data was not enough to cancel the imperfections introduced by the amplifier, which was then replaced and this was not a problem in the following experiments. Collection of the second dataset was performed as for the previous one but the data was measured by rotating the horizontal turntable over a wider angular window in order to collect 180 perspectives spaced by 1 degree. Because another microphone became available before the time of the experiment, two microphones were placed into the artificial bat head and thus binaural data is available for this dataset. Unfortunately, a measure of the background is not available for this dataset. Figure 6.3 shows the image representing HRRPs of the open flower in the first dataset. Scattering from the inner part of the bell-shaped corolla, including additional multiple reflections, is visible between 25 cm and 26 cm. The maximum amplitude is at 0 degrees, i.e. when the artificial bat-head was directly facing the flower. Petals are visible between 25 cm and 25.5 cm and cover the entire angular window between -45 degrees and +45 degrees. The scattering beyond the petals at -30 degrees and at a distance of about 26 cm may be due to the sepals covering the back of the corolla. Results show that, on average, the scattering originating from the inside of the corolla is comparable to that originating from the petals, although at 0 degrees the scattering from the inside of the corolla is about 5 dB higher than that

133
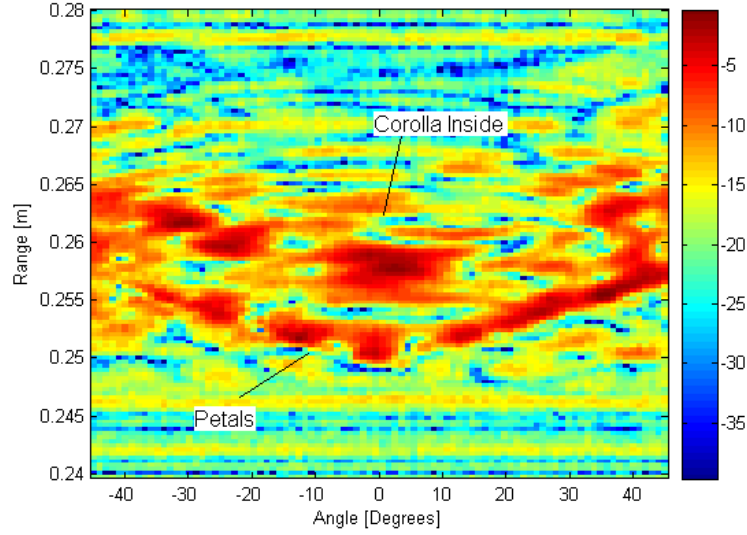
Figure 6.3: Magnitude of the HRRPs of a *Rhytidophyllum auriculatum* open flower. Colour scale is in [dB].

originated from the petals.

Figure 6.4 shows the HRRPs fingerprint of the flower after the anthers were manually removed from the corolla. The image shows that in this case, at 0 degrees the scattering from the inside of the corolla is much stronger than that originating from the petals with respect to the previous case, in which the anthers were partly obstructing/filling the opening of the flower. The overall structure of the echo has not changed. The distal parts of petals were manually removed from the corolla as well and results for this case are given in Figure 6.5. As expected, the scattering associated with the petals between 25 cm and 25.5 cm disappears and the HRRP fingerprint loses complexity. Also, removal of the petals results in a less directional scattering from the nectarium (i.e. the inside of the corolla that contains the nectar).

Figure 6.6 shows HRRPs of another open *Rhytidophyllum auriculatum*
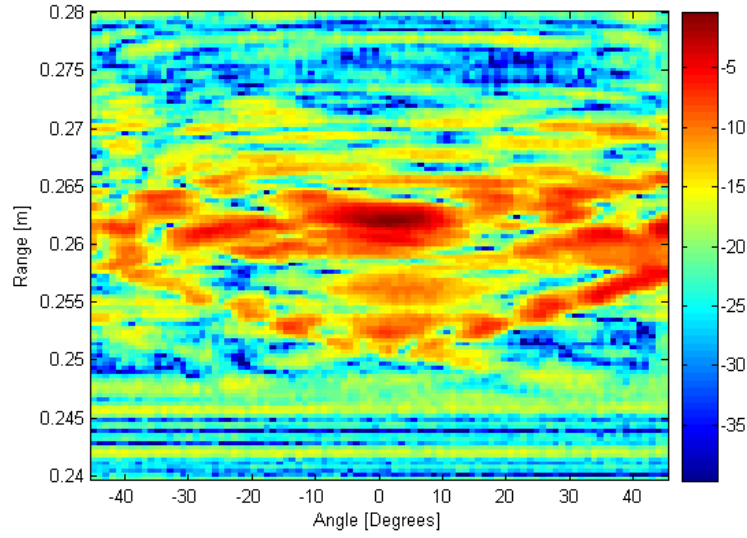
Figure 6.4: Magnitude of the HRRPs of a *Rhytidophyllum auriculatum* open flower after the anthers were manually removed from the corolla. Colour scale is in [dB].
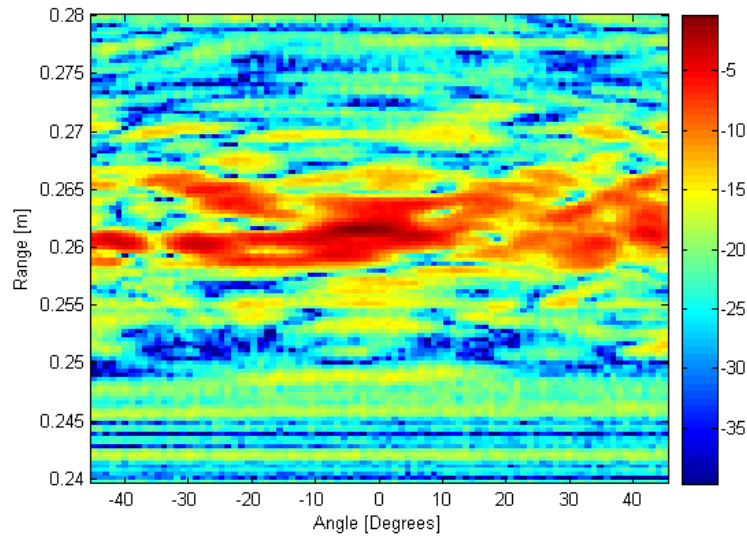
Figure 6.5: Magnitude of the HRRPs of a *Rhytidophyllum auriculatum* open flower after the anthers and the distal parts of the petals were manually removed from the corolla. Colour scale is in [dB].

flower taken from the dastaset collected in 2009. This dataset was collected by means of another amplifier (Piezo Driver/Amplifier Series, Treck, PZD 350 M/S) and by transmitting a linear chirp from 200 kHz to 50 kHz. The range resolution was slightly poorer and equal to 1.4 mm. As with the previous dataset the structure of the scattering from the corolla, visible from -60 degrees to +60 degrees, remains complex. The petals significantly contribute to the amount of energy that is reflected and, as expected, are visible over a wide angular window that goes between -90 degrees and +90 degrees. The structure of the open flower appears different with respect to that shown in Figure 6.3 and this is most likely due to the position of the anthers growing out from the corolla. Results obtained when the bud was ensonified are given in Figure 6.7. The structure of the echo in this case is very different from that associated with the open flower. The scattering is present over all angles but does not present the same complex structure. The image indeed is very similar to the typical sinogram that is obtained when an ideal point-target is ensonified. At zero degrees, i.e. when the bat head was facing the bud, the scattering is weaker with respect to other look angles because the surface that is ensonified is smaller with respect to any other angle. The scattering originated by the sepals that cover the back of the corolla is also visible at around 21.5 cm over all angles between -90 and +90 degrees.

Results confirm that, as expected, there is a relative relevance of specific parts of the flower in displaying information to bats. In particular, anthers and petals may add components to the HRRP fingerprint that might contain the information bats use to decide to visit specific individuals flower. Results show that, on the average over all perspectives, in the unmodified flower the

136
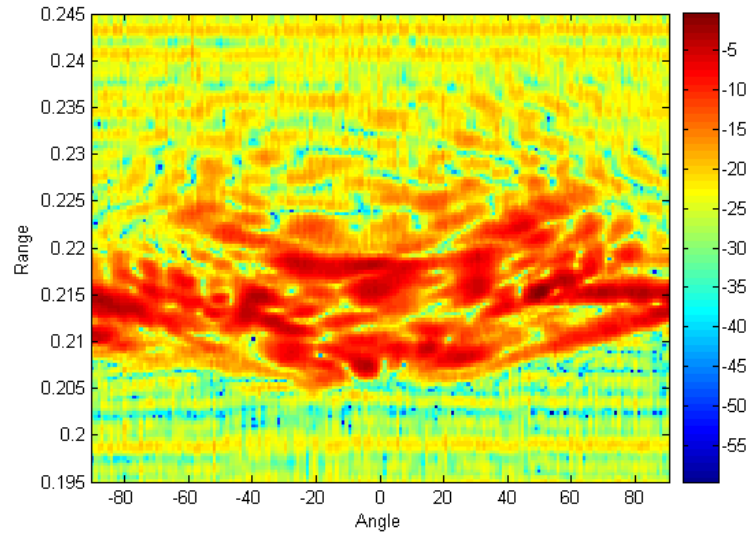
Figure 6.6: Magnitude of the HRRPs of a *Rhytidophyllum auriculatum* open flower. Colour scale is in [dB].
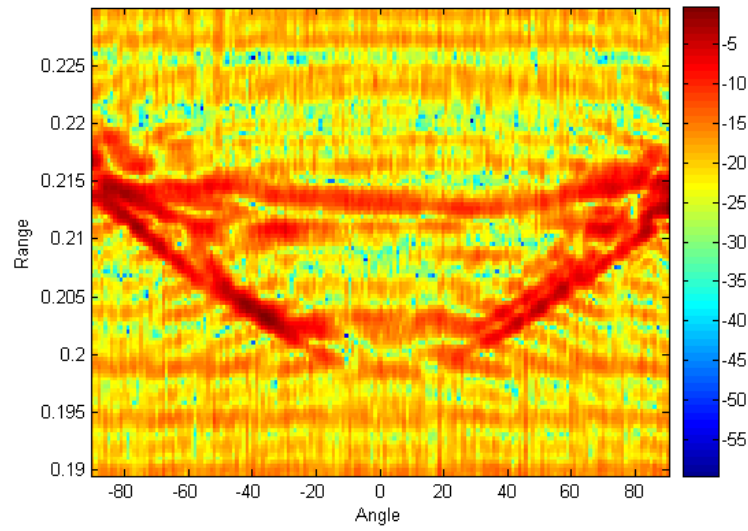
Figure 6.7: Magnitude of the HRRPs of a *Rhytidophyllum auriculatum* bud. Colour scale is in [dB].

amount of scattering originating from the inside of the corolla is comparable to that originating from the petals. This might be due to the protruding anthers that obstruct the opening of the corolla and hence attenuate the signal. From a frontal view though, scattering from the inside of the corolla is about +5 dB stronger than that from the petals. This information might be used by the bat as a directional cue to orientate and find the nectarium. The echo fingerprint of the flower changes significantly after the distal parts of the petals is removed. It is evident that, on the other hand, a further investigation looking at how it is likely that bats actually explore the same characteristics or features by adaptive flight and echolocation behaviour is required and these topics will be covered later in this chapter. As expected, results show that the HRRPs fingerprint of the closed bud present characteristics that are very different from those of the open flower. Also, differences in the dynamic range confirm the hypothesis that scattering from the open flower is much higher than that of the closed bud.

6.2   *Cobaea scandens*

The plant *Cobaea scandens* Cav. (Cup-and-Saucer Vine) is a bat-pollinated plant that grows in tropical America and produces flowers that are about 5 cm large (about 4-5 times bigger than the *Rhytidophyllum auriculatum*). A photo of a *C. scandens* flower is given in Figure 6.8. Here, a similar analysis to that which was carried out in the previous section on the *R. auriculatum* flower is repeated on *C.scandens* flowers. Because these flowers are larger than the *Rhytidophyllum auriculatum* results are expected to show a better

138

detail when the same range resolution is achieved. In particular, in this section the aim is at assessing how the information available to the bat changes when going from an open flower, suitable for pollination, to a wilting flower that has started to lose the interest of the bat. Exploiting how the shape of the corolla can change as the flower wilts, i.e. stops producing nectar hence losing attractiveness to bats, could contribute to understand which features in the flowers are responsible for high level recognition by bats. This will be done by comparing three different horizontal images, each one representing HRRP fingerprints of a *C. scandens* flower in three different cases: (i) a flower in ideal condition for pollination, (ii) a desiccated flower, (iii) and a flower whose distal part of the petals were removed by hand. The flowers were provided by the Botanic Gardens of the University of Bristol and the data was collected at the School of Biological Sciences of the same university in October 2008.

Under the hypothesis of co-evolution, because bats can detect and identify the flowers that are suitable for pollination between a number of individuals of different age and stage, HRRPs of the wilting flower are expected to differ significantly with respect to those of the flower suitable for pollination which is under full turgor. In particular, the energy reflected by a wilting flower is expected to be lower because the loss of turgor reduces the reflectivity of the flower which is related to the acoustic impedance (which is proportional to the difference between the density of the air and the density of the reflecting surface). The details of the HRRPs fingerprint are also expected to change as the flower's general shape changes in the wilting process.

An image containing HRRP of an individual of *C. scandens* that is ready

139

Figure 6.8: Photo of the wilted *Cobaea scandens* flower used for the measurement. This is characterised by protruding anthers, a bell-shaped corolla of largely merged petals whose unmerged petal ends fold back, and a ring of partly merged sepals at its base.

for pollination is shown in Figure 6.9. The image contains HRRPs over look angles ranging between -90 and +90 degrees, where the 0 degree line corresponds to the case when the flower was facing the microphone and the loudspeaker. As expected, there is a huge increase in detail in the HRRRPs and the SNR is higher with respect to the case of the *Rhytidophyllum auriculatum* flower. The figure shows strong reflections at a distance of between 21 cm and 23 cm from the microphone that are originating from the distal parts of the petals of the corolla. The weaker reflections between 20 cm and 21 cm are from the anthers protruding from the corolla (see Figure 6.8). An overall weaker scattering originates from the bell-shaped inner part of the flower's corolla between 25 cm and 27 cm. This is the part of the corolla that contains nectar and from which the pistil grows. Weaker scattering due
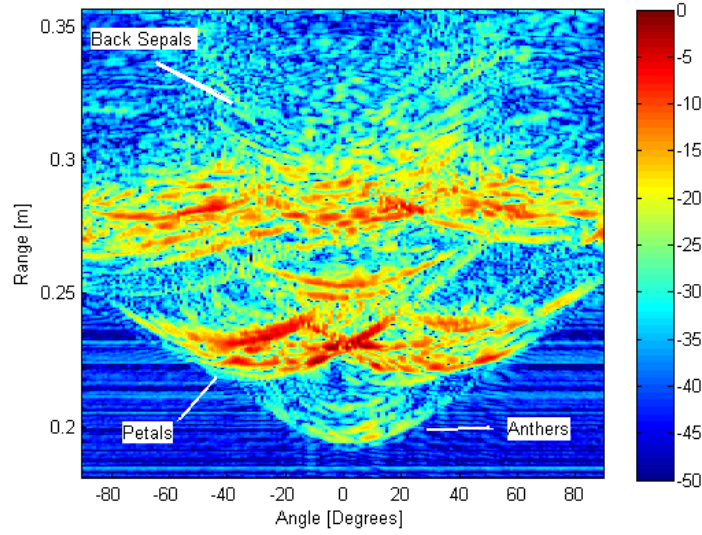
Figure 6.9: Magnitude of the HRRPs over 180 degrees of a *C. scandens* ready for pollination. 0 degrees is to the front of the flower as shown in Figure 6.10. HRRPs direction is horizontal, i.e. from left to right with respect to the flower's bell-shaped corolla. Colour scale is in [dB].

to the echo generated by the ring of sepals that cover the external back side of the flower is also visible from about 28.5 cm to 29.5 cm. It is interesting to observe how the petals can scatter a considerable amount of power over a wide range of angles that goes between -60 degrees and +60 degrees. This could be important to allow flower classification and selection from a wide angle range and could be helpful also in terms of multi-perspective information. The image is normalized to its maximum value located at about 22 cm when the corolla faced the microphone (0 degrees). HRRPs of another individual of *C. scandens* that had started to wilt due to an overnight frost are displayed in Figure 6.11. The figure shows that the scattering due to the petals between 21 cm and 23 cm is less complex with respect to that in Figure 6.9. A wide scattering that goes between -60 degrees and 0 degrees is
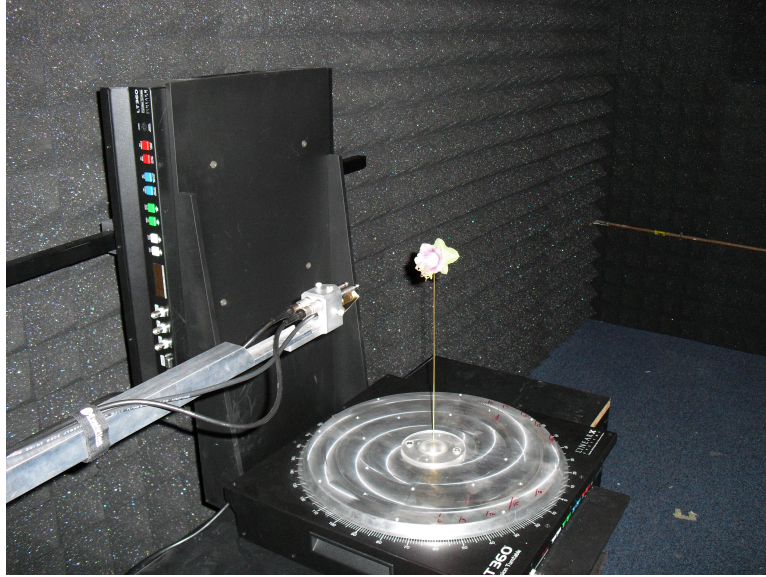
Figure 6.10: Acoustic radar gathering the 0 degree perspective of a *Cobaea scandens* (the flower in the photo is not the same flower related to the results of this thesis). The -90 degrees perspective corresponds to the flower's opened corolla facing the vertical turntable on the left of the photo.
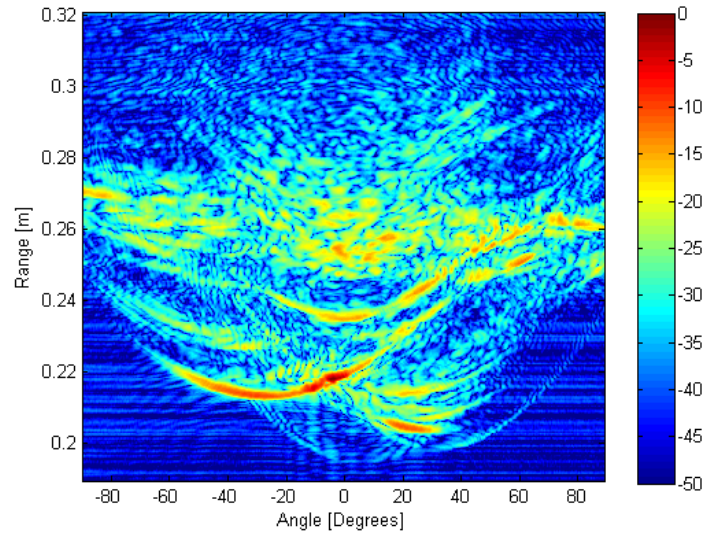
Figure 6.11: Magnitude of the HRRPs over 180 degrees of a desiccated flower of *C. scandens*. Colour scale is in [dB].
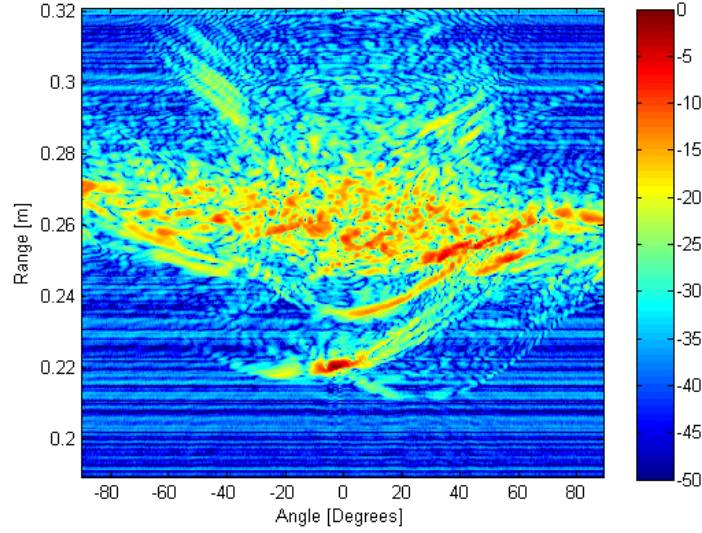
Figure 6.12: Magnitude of the HRRPs over 180 degrees of a modified desiccated *C. scandens*; the petals and the pollen sacs were removed by hand from the flower. Colour scale is in [dB].

still present at about 22 cm and probably due to one petal that was still in good shape at the time of recording. However, most of the scattering from the petals is no longer visible, leading to a marked loss of information. The scattering from inside the corolla does not show any loss of complexity but it is weaker than before after normalisation with respect to the maximum value of the image. To investigate what the image of the flower would be without petals at the corolla, the front ends of the petals from the same individual were removed manually using a pair of scissors. Figure 6.12 shows the HRRPs fingerprint obtained from this modified flower. The scattering from the petals disappears over all angles. A fraction of power is still scattered at 0 degrees probably originated by some residuals of petals that might have not been removed properly or simply by the line delimiting the aperture of

143

the corolla. Scattering from the inside of the flower is now more visible than in Figure 6.11, but no relevant change in the complexity of the echo is observed. This is for effect of the data normalisation because after removal of the petals the dynamic range of the image is reduced.

Results confirm that, as expected, there are significant differences between the HRRPs fingerprint of an open flower suitable for pollination and that of the flowers that started to wilt. In particular, results show that the scattering from the petals tends to disappear when the flowers start to wilt. This might be because the petals tend to fold back during the wilting process resulting in a lower sonar cross section than that associated to the petals being in the upright position. The fact that the HRRPs fingerprint of the modified flower is very similar to the one obtained from the wilting flower further proves that the scattering from the petals tends to disappear when the flower is no longer suitable for pollination. It is evident that a greater number of data from flowers must be analysed in order to corroborate these findings and in particular to relate differences in the echo fingerprints to the wilting process of the flower. As, previously discussed, the loss in turgor might also negatively affect reflective properties of the plant tissue resulting in a diminishment of the reflected power. The acoustic impedance, that determines the reflectivity of a layer and that is proportional to the difference between the density of the propagation mean (the air) and the flower, is in fact expected to be higher when the flower is moist and lower when the flower is dry. This is not evident in the results reported above and it is going to be further investigated in the next section. Overall, I believe that the fact that scattering from petals tend to disappear with the wilting process

might be a key info towards classification and selection performance and this is something that will have to be addressed in future work, with an experiment aiming to quantify differences in selection performance of bats when presented with open flowers and desiccated ones.

6.2.1 Power reflection as a potential cue

One cue available to bats is the overall power of the echo. In order to investigate differences in the received power and assess if these might be useful to distinguish between suitable and less suitable flowers for pollination, the mean scattered power in each of the three cases was estimated. This was achieved by selecting a window that covered all the angular perspectives and which contained only the return from the flowers (plus background noise). The background noise, that was the same in all the three images, was not removed from the results. This did not affect the calculation of the relative differences in the received power. The window was selected manually from the images and remained the same in the three cases. Indeed, a more quantitative way to select the window could be to use a threshold over the noise level and then calculate the power associated with the pixels over the threshold only. Selecting a rectangular window to estimate the power of the flower, for example, did not allow repetition of this analysis on the *Rhytidophyllum auriculatum* because either the background noise level was too high (and not always stochastic because of the unwanted effects introduced by the system) and therefore comparable with the flower return, or it was impossible (like in the case of the bud) to choose a rectangular window containing the target

Table 6.1: Mean power scatterred by flowers.

	Full Flower	Desiccated	Modified
Cobaea scandens	62 dB	59 dB	57 dB

return only.

The mean power was calculated in each window as

$$P = \frac{1}{N_i N_j} \sum_{i=1}^{N_i} \sum_{i=1}^{N_k} |x(i,j)|^2, \tag{6.1}$$

where N_i and N_j are the number of rows and columns respectively, and $x(i,j)$ is the received complex sample in the (i,j) position of the window. The results are reported in Table 6.1 and show a maximum difference in the power of 4 dB between each of the three cases. Figure 6.13 plots the mean power of the echo for each look angle calculated as

$$P(j) = \frac{1}{N_i} \sum_{i=1}^{N_i} |x(i,j)|^2 \quad with j = 1, 2, ..., N_j. \tag{6.2}$$

As expected, in the case of the full flower the mean power of the echo presents higher values over a larger angular view due to the presence of the petals. There are differences in the power depending on the perspective that might be used by bats as a clue for classification [17], although this information is not available over at all angles.
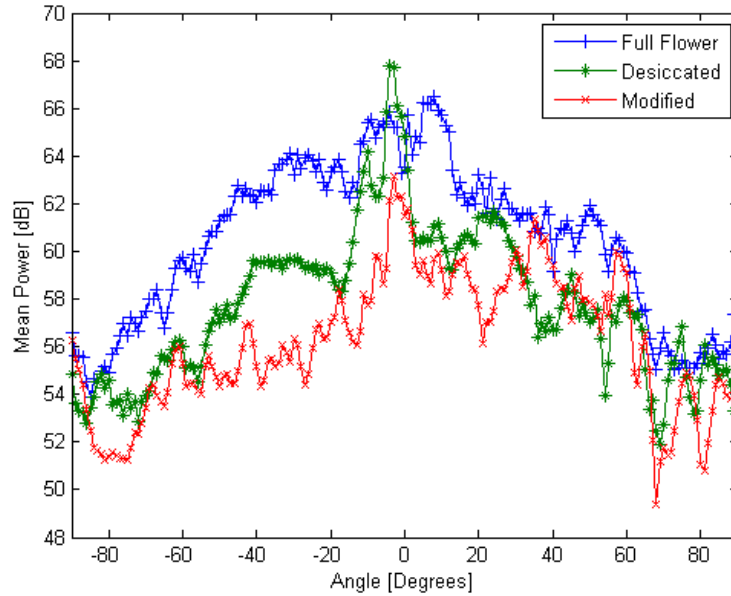
Figure 6.13: Mean power received at each look angle. Estimated as in Eq. 6.2.

6.3 Bat Behaviour

The results presented in the previous section clearly show how the information that the flowers display to bats can change depending on the flowers' suitability to be pollinated. However, it is of great importance to exploit how the bats relates to this type of information and thus a further analysis that looks at assessing the behaviour of the bat is also required. Here, a typical bat trajectory is exploited in order to assess if it is possible that bats may try to acquire the information on the same flower's features by moving around the flower.

Figure 6.14 shows the horizontal and vertical projection of a typical trajectory of a nectar feeding bat approaching an artificial feeder that contains nectar from a distance of about 2.5 m. This data was collected during be-

havioral experiments carried out in Germany in 2006 and kindly provided to us by A. Volz [77]. The reported results are computed assuming that the feeder was placed at the origin of the XYZ plane corresponding to the coordinates (0,0,0). Figure 6.15 shows the horizontal and vertical angular position of the bats with respect to the feeder at each call. The figures shows that the bat emits about 10 calls before directing towards the feeder following a straight line at a constant angle of about -40 degrees below the horizontal plane. Within these ten calls the bat has already exploited an angular view range of about 40 degrees on the vertical plane and about 15 degrees on the horizontal plane. After this first exploration the bat keeps emitting calls at a higher pulse repetition frequency (PRF) and gathers a further angular information on the horizontal plane. At the end of the approach the bat has gained an overall angular information collected over about 40 degrees on both the horizontal and vertical plane. The bat takes almost a straight line on the XY axes and hence exploited a wider angle on the vertical plane. This might be due to the orientation of the feeder and the dimension of the flight tunnel for this particular experiment.

It is very interesting to observe that the angular range used during this approach flight is in agreement with the angular window in which the scattering from petals is very obvious in *C. scandens* and it might be the case that a bat needs the same angular view because it has to gather the right information before making the final decision on whether the flower is worth being visited or not. However, this result has to be treated with caution as in the experiments the bat was presented with artificial feeders containing nectar instead of the actual flower. Also, because of the short distance from
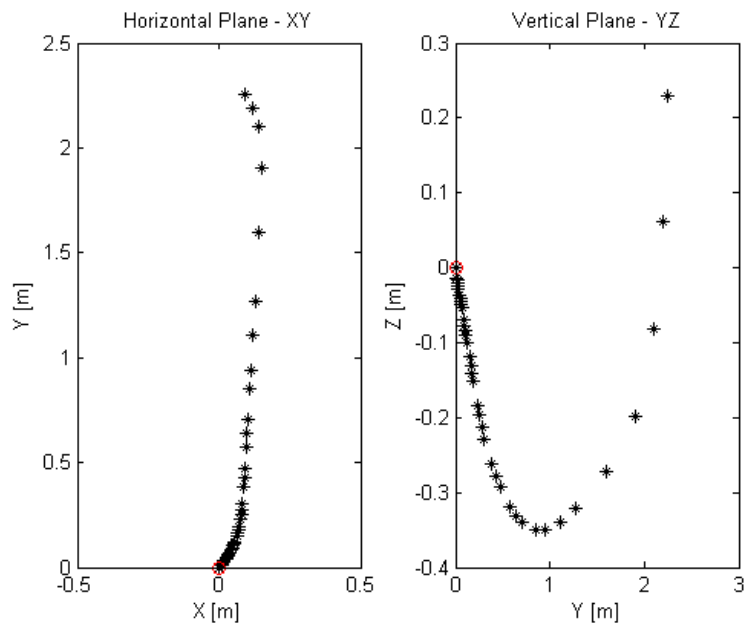
Figure 6.14: Trajectory taken by a nectar feeding bat that is approaching a feeder with nectar. Each localisation corresponds to the position the bat has produced an echolocation call. Trajectory from the bat species *Choeronycteris mexicana*. Data provided by [77].
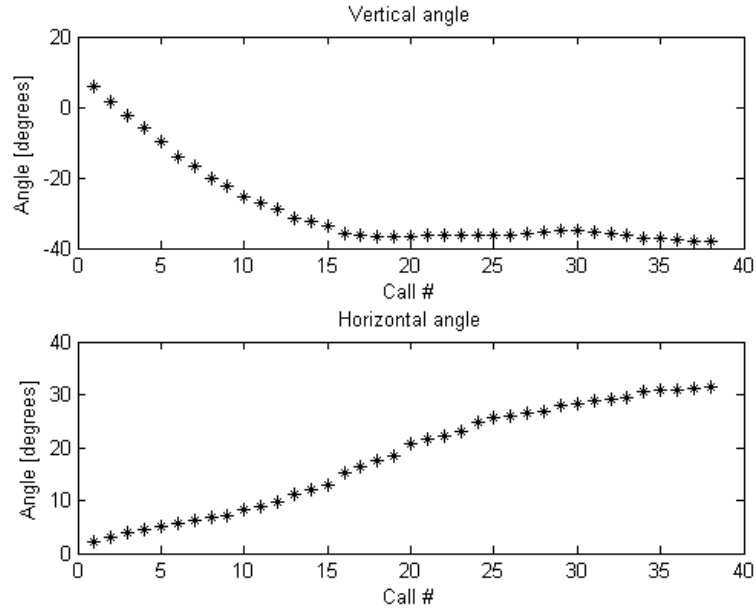
Figure 6.15: Angular position of the bat in the horizontal and vertical plane with respect to the feeder.

the target it might be argued that at that stage the bat had already classified the feeder and made the decision to visit it. In this case the bat would be using the information from echoes rather to orientate itself to feed in the correct way. Also, it is assumed that the bat is looking straight towards the flower at each call although there is a small probability that the bat's head might have a different orientation. These two last points are important and then require further investigations in future works. If there was a match between angular sampling by bats and the directional information content in different flowers, different approach strategies should be taken depending on the flower type and orientation.

6.4 Summary

Results show that floral echoes are a very important means for bat pollinated plants to display information to bats in order to support high recognition performance [61]. The scattering from the petals and the way this changes as a function of the state of the flower could be a way of letting bats know which flower is most suitable for pollination, i.e. holds a nectar reward, and hence plays an important role for recognition and selection of the flowers. Results show that HRRPs differences between flowers of different age and stage of maturity are also obvious. On the other hand the results also show that a type discrimination that looks at the backscattered energy is also possible although may be restricted to certain looking angles. If co-evolution has shaped flowers to ease recognition by bats, then radar and sonar systems could be modelled accordingly in order to allow a better classification of specific targets. The analysis of a trajectory has shown that the bat gathers multi perspective information on the target on both the horizontal and vertical axis prior and during the final approach into the flowers. The angular perspectives that are exploited are in agreement with the angular window in which features, such as petals, are present in real flowers' echoes. Nature suggests that classification is not only about knowing the actual geometrical characteristics of the target and that performance can probably be enhanced by the use of intelligent feature extraction algorithms and by taking into account the target behavior, such as spatial changes in echo structure as experienced during exploration flights, for classification. This study also suggests that having a good strategy is the key to high level classification performance.

The lesson that can be learnt from these results is that radar and sonar systems could possibly deploy a better way of performing target classification than just comparing a great number of measured data with look up tables. Future work must look into relating these findings to other adaptive aspects of the behaviour of the bat, such as the signals that these bats transmit and the initial trajectories that they take before detecting and deciding to visit the flowers from greater distances. Unfortunately, having access to this kind of information requires more behavioural experimentation.

In the next chapter the information available to the bat within a plant inflorescence is exploited. As bat pollinated plants can be densely populated with flowers, it is important to investigate what kind of information is contained in the sum of the echoes of a large number of individual flowers.

Chapter 7

Inflorescence

An inflorescence is a group or cluster of flowers arranged on a stem that is composed of a main branch or a complicated arrangement of branches. In a real scenario, the bat often has to detect an individual flower on a plant or even within an inflorescence composed of many individuals flowers/buds of different age and status. The bat has to be able to process a complex echo by the inflorescence to gather the right information for the success of the mission [59]. In these terms it seems likely that the in-flight trajectory that the bat takes before approaching the flower is, in a first stage, of great importance to extract useful information for the detection of the open flowers. On the other hand, because it is in the interest of the plant too that pollination takes place successfully it is likely that the spatial and shape arrangements between individual flowers, buds and flowers without corolla (*Calyx*) are such to give the bat all the necessary information to succeed in the task of flower recognition. The aim of this chapter is to exploit the information available to a bat in 3D space by measuring HRRPs of an inflorescence from points in

the space that are likely to belong to a typical bat trajectory.

In the previous chapter results have shown that flowers of different age, status, and closed buds present significantly different HRRP fingerprints when they are ensonified individually. On this same line, there is a high expectation that differences between buds, flowers without the corolla (*Calyx*) and open flowers are also obvious within an inflorescence to allow the bat to detect the right target (the open flower). In particular, because flowers of bat-pollinated plants are commonly bell-shaped, they are expected to scatter more energy and to be more directional than closed buds and Calyxes. If open flowers within the inflorescence are visible only over limited angular windows, on both the vertical and the horizontal plane, it is likely that the bat uses the information deriving from their directionality to plan its approaching trajectory into the nectarium. Also, because the bat must be physically facilitated and thus have enough space to approach open flowers, it is common sense to make the hypothesis that these must be arranged where they are easily reachable by bats and protruding from the rest of the plant. In addition to this, it is also expected that this spatial arrangement is such to enable high level detection performance against background clutter. In order to exploit this, a real dataset containing high range resolution profiles of a bat-pollinated plant inflorescence from different vertical angular perspectives is analysed and results are discussed and related to the case of radar and sonar systems.

The data analysed in this chapter consists of HRRPs of one inflorescence of *Rhytidophyllum auriculatum* composed of an open flower, three buds, and three dead branches with Calyx whose spatial arrangement is given in the sketch of Figure 7.1 and in the photos of Figure 7.2 and Figure 7.3. The

154
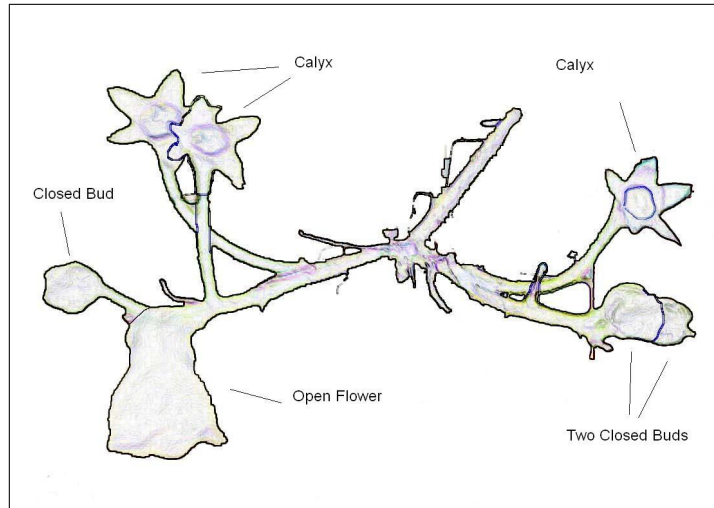
Figure 7.1: Sketch of the spatial arrangements of the portion of *R.auriculatum* plant composed of an open flower, three buds, and three flowers without corolla (*Calyx*).

Figure 7.2: Frontal photo of the inflorescence. The pin is fixed at the centre of rotation.

Figure 7.3: Photo of the inflorescence from the vertical direction. The pin is fixed at the centre of rotation.

data was collected at the School of Biological Sciences of the University of Bristol in July 2009. The inflorescence to be ensonified was impaled on a thin metallic pin (1.5 mm diameter) that was placed at the centre of the horizontal turntable set up to rotate with an angular resolution of 1 degree. A linear down chirp spanning the frequencies between 50 kHz and 200 kHz was transmitted towards the plant with the custom-built loudspeaker. The echo, recorded with the ultrasound microphone (G.R.A.S. type 40 BF), was sampled at a rate of 500 kHz using the National Instruments PCIe-6251 DAQ card and matched filtered to the transmitted waveform using Matlab (v7.5 The Mathworks. Inc., Natick, USA). During these experiments, both the loudspeaker and the microphone were placed into the artificial bat-head and thus binaural data is available for this entire dataset. Rotating the vertical turntable, connected to the arm containing the artificial bat-head, allowed data collection of HRRPs of the plant from different vertical angles and heights as shown in Figure 7.4. The initial calibration procedure showed
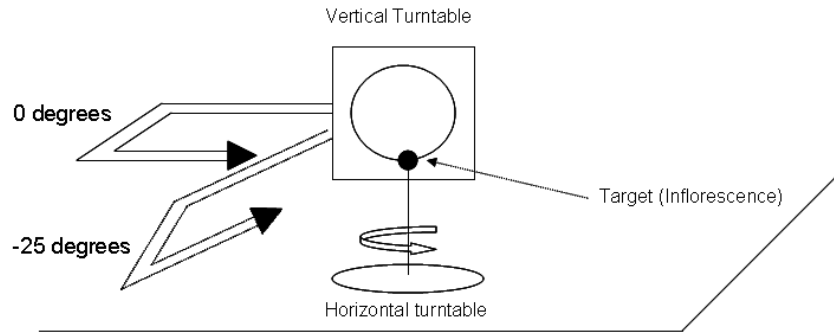
Figure 7.4: Sketch of the experiments setup. Revolving the vertical turnable allowed measurements from various vertical perspectives.

that measurements were taken with a range resolution of less than 2 mm. Figure 7.5 shows the horizontal angular HRRPs obtained when the bat-head was facing the plant inflorescence from a vertical angle of 0 degrees, i.e. when the metallic arm was parallel to the floor plane (Figure 7.4). In the figure, the y-axis represents the distance in metres between the artificial bat-head and the centre of rotation of the horizontal turntable located at about 20 cm, and the x-axis represents the angle that the horizontal turntable formed with the bat-head at each step. The 0 degree line corresponds to the case when the bat-head was facing the plant. The image is normalised to its maximum value. The scattering from the two buds, which are located on the right of the open flower from a frontal view, is clearly visible at a distance between 16 cm and 18 cm and is present over a large angular window that goes between -80 degrees and 0 degrees. The scattering from the bud located on the same side as the open flower superimposed with echoes from the dead branches is visible between -30 degrees up to +80 degrees at a distance from 16 cm to about 19 cm. This component on the average is 20 dB weaker than the

157
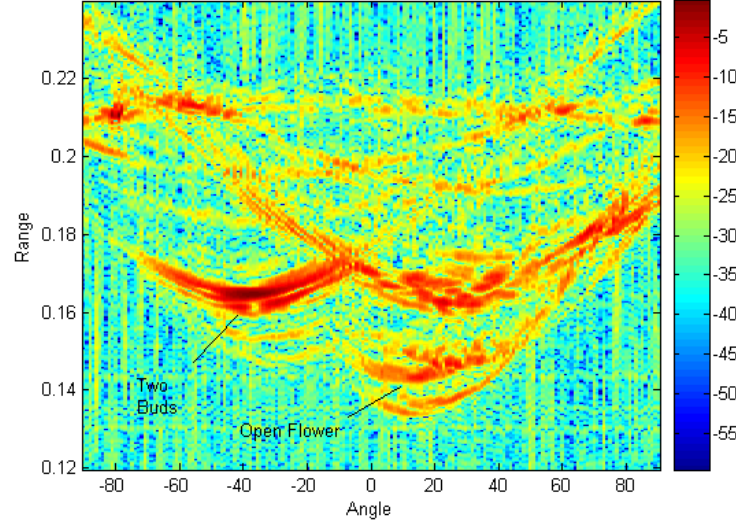
Figure 7.5: Inflorescence of a *R.auriculatum* plant composed of an open flower and three buds measured from a vertical angle of 0 degrees. Colour scale is in [dB].

scattering produced by the two frontal bud on the other side, most likely, due to the their vertical orientation. The open flower is protruding maximally from the inflorescence and hence is visible at a range of about 14 cm and, as expected, its reflections are more directional than those associated with the buds. This is interpreted as a cue to separate open flowers from closed buds and give the bat information on the best approach direction. Figure 7.6 shows the image obtained when the bat-head was ensonifing the plant from a vertical angle of -25 degrees, i.e. from below the target. From this vertical perspective the scattering associated with the two buds that were dominating the previous image is weaker than the scattering due to the bud located next to the open flower. This is well visible over an angular window that goes from +10 to +80 degrees with its highest value at about 40 degrees
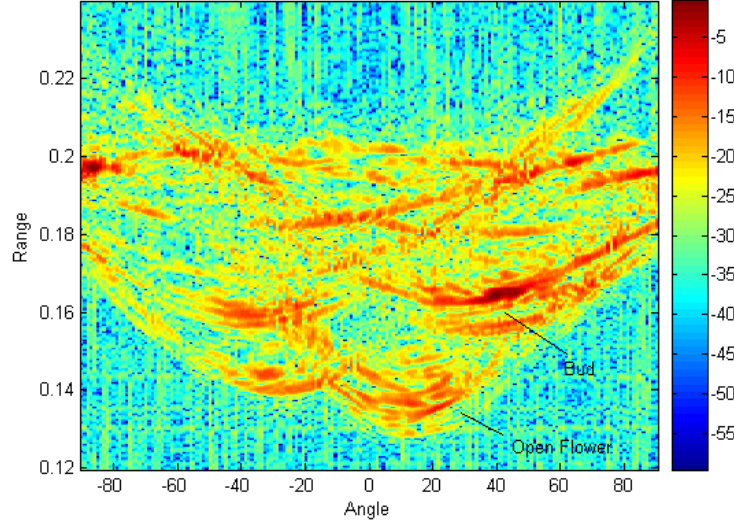
Figure 7.6: Inflorescence of a *R. auriculatum* plant composed of an open flower and three buds measured from a vertical angle of -25 degrees. Colour scale is in [dB].

and 16.3 cm. As in the previous case the open flower is visible around 14 cm and over a smaller angular window that goes between -10 degrees and + 20 degrees. In this case reflections from the open flower are visible between -10 degrees to about 30 degrees and cover a range of 1 cm corresponding to the typical length of an open individual. The interjection between two scatterers belonging to the flower (probably two anther lines) at about 10 degrees at 14 cm from the bat-head, also bring information on the center of flower itself. This is the point from where the bat has to extract the nectar. This significant increase in the amount of information on the flower is likely to be related to the downward deflection of the flower, meaning that ensonifying the flower from an optimal angle might results in an improvement in the quality of information. The fact that the corolla was pointing downwards
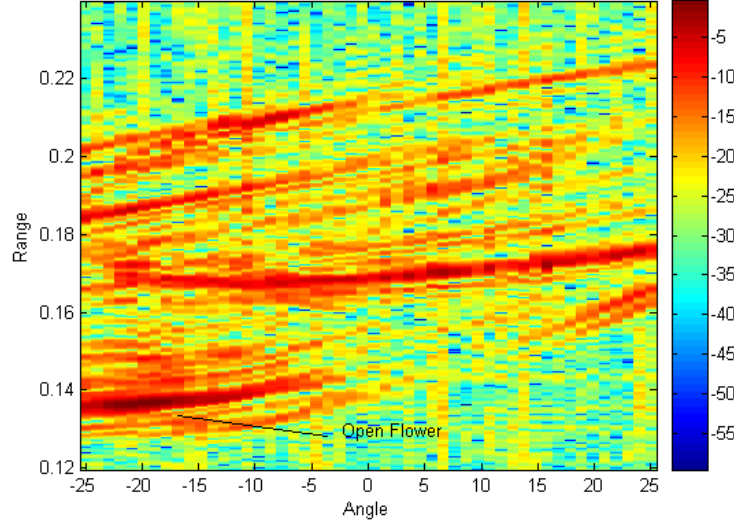
Figure 7.7: Inflorescence of a *R. auriculatum* plant composed of an open flower and three buds measured on a vertical plane when the horizontal angle was 0 degrees. Colour scale is in [dB].

means the bat-head looked more straightly into the opening of the corolla which resulted in a longer and more structured echo. Unfortunately, at the time of the experiment, it remained impossible to characterise in any quantitative way such deflection. Because both the images of Figure 7.5 and Figure 7.6 were normalised to their mean power, calculated over all available angles, the power associated to the open flower seems to be weaker than that associated to the buds. Under the hypothesis that the reflected power represent an important cue, what is really important to the bat though is the total acoustic energy reflected by the open flower compared to that from a single bud at the angles where the flower is actually visible. This will be exploited better in the next experiment.

In order to investigate what information is available to the bat on the vertical

plane HRRPs were collected rotating the vertical turntable from -25 degrees (below the flower) to +25 degrees (above the flower) as well. In this case the horizontal angle was kept at a constant angle of 0 degrees (i.e. frontal) corresponding to one of the angles where the open flower was visible. Results relative to this experiments are given in Figure 7.6 and show that scattering from the buds and the dead branches with Calyx are visible from a distance of 16 cm and are present over almost all perspectives. The open flower is visible at a range of 14 cm and over a smaller angular window that goes between -25 degrees and around -10 degrees. This further corroborates the comparatively higher directionality of floral echoes also in the vertical plane and shows and the bat is provided with critical information to decide the best vertical approaching angle into the nectarium. Finally, Figure 7.6 confirms that, as expected, the scattering from the open flower at the angles where this is visible is stronger than that from the buds.

Results corroborate the hypothesis of high directionality of open flowers on both the horizontal and the vertical plane with respect to closed buds and Calyxes. There is no doubt that nectar-feeding bats must have a remarkable ability to process the information gained by exploring a number of vertical and horizontal perspectives, and then decide for the best approaching angle into the corolla. Results confirm that, in this case, the open flower was protruding maximally from the inflorescence and thus, as expected, was easily separable, in the range domain, from buds, Calyxes, and even from the background clutter. Finally, results corroborate the hypothesis that scattering from open flowers at the angle of interest is much higher than that originated by buds and Calyxes. Future work will have to exploit differences at

the two ears of the bat as binaural disparities are likely to provide important information for object localisation and recognition as well. This is a very interesting and fundamental topic and will form the centre of future research. From an engineering perspective, the results presented in this chapter show that the information that is available to the bat during the pollination task highly depends on the in-flight trajectory that the bat takes around the plant. This suggests there is another close parallel between nature and the radar and sonar case, where the target detection and classification performance significantly depends on the location of the sensors as well. Results support the commonly accepted idea that, as in nature, radar and sonar systems should operate adaptively with the target in space and time.

Chapter 8

Bio-Inspired Target Classification

In this thesis introduction it has been argued that classification of bat-pollinated flowers by bats might provide important clues to exploit the process of recognition of targets in synthetic sensors such as radar and sonar. The results presented in the previous chapters represent a contribution that fuels the commonly shared thought that bats might adjust position and flight speed, together with sensor signal parameters such as bandwidth and waveform design, in order to gain the best possible information on the target and hence maximise recognition. Also, results have shown that although they transmit a limited number of calls and exploit the targets over a limited angular window, they still obtain high recognition performance. The analysis of floral echoes and bat trajectories suggests that bats might change their trajectories as a function of the position of the main features of a target. An investigation that aims at relating trajectories to features is therefore

necessary as this could lead to a different approach to the task of radar and sonar target classification and enhance classification performance. This could also yield advantages in terms of efficiency. A good strategy, in fact, might allow high performance target classification by deploying only a small number of appropriately designed calls together with a small number of carefully selected angular perspectives. This might be particularly important in congested environments, i.e. when a number of sensors are present simultaneously (although bats do so even when they are left alone [77]).

Here, a bat inspired approach to radar and sonar target classification is discussed and then tested on real data. In particular there is an attempt to take into account the fact that classification by bats presents a number of challenging constraints that are likely to occur in the case of radar or sonar systems as well. It is, in fact, common sense to accept the idea that radar and sonar systems have not always the freedom to move around a target over wide angles and to transmit as many pulses as desired. It is interesting to exploit how classification performance varies as a function of the degree of freedom of these two parameters and relate the results to the features of targets.

8.1 Description of scenario and classification approach

Let us suppose to be in the situation described in Figure 8.1 where a remote sensor has to perform classification of a target and at the same time

follow some operational requirements. In particular it is assumed that the sensor is only allowed to transmit a limited number of calls N_{calls} around a main looking direction α_0 and, at the same time is restricted to exploiting the target over a limited window of angular perspectives α. Under these circumstances, the step angle between two successive calls is assumed to be uniformly distributed over look angle during the task, and is therefore given by the expression $\frac{\alpha}{N_{calls}}$. This assumption is in close agreement with the functionality of the turntables that were used to collect experimental data, which were capable to rotate with a constant step angle only. No restriction is made on the look direction α_0 of the sensor with respect to the target so that the sensor system is able to choose to perform classification from any desired angle. It seems evident that under these restrictions the direction α_0 from which the sensor chooses to look at the target is a critical parameter for the task of classification and can widely affect the success of the mission. Here, classification performance is exploited as a function of the look direction by testing the same dataset, discussed in Chapter 6, containing HRRPs of *C.scandens*, and the results are related to the features of the flower that were identified in the previous section. In particular classification performance is measured when only two of the three classes, represented by the desiccated flower and the modified one, are tested. The fact that the modified flower was obtained by removing petals from the desiccated individual, guaranteed that the only differences between the two classes were due to the removed features. The aim here is not to develop a new classifier or a new mathematical algorithm to perform target classification, but it is to investigate whether a more intelligent use of even simple and well known classifiers, such as the

165

Knn, can lead to higher performance. As described in the previous chapter, each of the two images of *Cobaea scandens* was composed of 180 HRRPs corresponding to the angular perspectives going from -90 degrees and +89 degrees and collected with an angular step of 1 degree. In both images, all HRRPs were normalised to mean value equal to zero and mean power equal to unity before classification. 6 HRRPs were extracted from each image to train the classifier leading to a total $N_p = 12$ HRRPs training profiles. These corresponded to the 6 angular perspectives that starting with the one gathered at -90 degrees were then separated of 30 degrees. Classification was performed by means of a *Knn* classifier characterised by a parameter K_n with $n = 3$. The test set was formed by selecting, in both the images, the profile corresponding to the perspective at α_0 degrees plus the $(N_{calls} - 1)/2$ profiles collected soon before and soon after it, for a total of $2 * N_{calls}$ test profiles. The separation angle between the test profiles determined the size of the angular window α around the main looking direction α_0. Each test profile was compared with the training set by calculating the maximum value of the magnitude of its cross-correlation function with each training profile as

$$C^j(k) = \frac{1}{N} \sum_i x_{test}(i) x^j_{train}(k - i) \ \ i = 1, .., 2N - 1 \ \ j = 1, .., N_p. \quad (8.1)$$

In the equation, x_{test} is the range profile under test, carrying both the amplitude and the phase information (complex number), that is compared with the jth training profile x^j_{train}. N is the length in number of samples of the range profiles. For each test profile, between all the $N_p = 12$ maximum values

of all the cross-correlation functions, only the $n = 3$ highest values were used to make the decision. Each test profile was assigned to the class that owned the highest number of training profiles between those generating the selected n values. The probability of correct classification was estimated, for each looking angle α_0, as the ratio between the number of correct decisions and the total number of test profiles. This analysis was then repeated for each looking angle α_0. It is worthwhile to highlight that although the training set remained the same for each α_0 the test set did not, and for this reason this approach is clearly different from the one used in Chapter 5.

8.2   Results

Figure 8.2 shows classification performance when N_{calls} was limited to 11 and the angular step angle between two successive calls was set to 2 degrees, leading to a maximum angular view of the target α of only 20 degrees. These parameters are in very good agreement with the ones chosen by the bat in the experiment described above and reported in Figure 6.15. Figure 8.2 shows that classification performance presents its maximum values at around -25 degrees and +25 degrees. As $\alpha = 20$, this corresponds to the case when the target is observed over the angular windows that go between -35 degrees and -15 degrees, and between +15 degrees and +35 degrees, respectively. As expected, these are the two angular windows in which the features that were removed from the desiccated individual of the *C. scandens* were very clearly visible before removal (Figure 6.11 and Figure 6.12). These parts of the flowers seem to be key determinants to establishing good classification

167

performance. The drop in performance at 0 degrees might be due to the scattering from petals that disappears at these angles. Scattering from the pollen sacs, which were also removed from the desiccated flower, was not strong enough to support high recognition between these two classes using this classifier. Anthers scattering was very clearly visible at around 0 degrees and 18 cm range in Figure 6.11. Classification performance drops to 0.5 between -80 and -60 degrees and between 50 and 80 degrees i.e. in correspondence of the parts of the flowers that were not modified. As expected, 0.5 is the probability of randomly choosing either classes assuming that they are characterised by the same probability of occurring equal to 0.5. Results reveal an oscillation around the mean line that is due to the fact that the estimation of the probability of correct classification has been averaged over a small number of calls. Figure 8.3 shows the behaviour in classification performance when the number calls is $N_{calls} = 7$ and the step angle is equal to 2 degrees, meaning that the target could be observed over a maximum angular window $\alpha = 12$ degrees. Even in this case classification performance is maximised when the classifier has the information on the features that were removed available. In order to investigate classification performance when the angular window was enlarged the case with $N_{calls} = 21$ and a step angle equal to 2 degrees was performed on the two classes from the same dataset. In this case the parameter led to an angular view range of 40 degrees on the target. Results are reported in Figure 8.4. As expected classification performance as a function of looking angle is much smoother and more or less constant at a level equal to 0.8 over a wide range of looking angles between -40 and 40 degrees. This is because when the angular window is large the

168
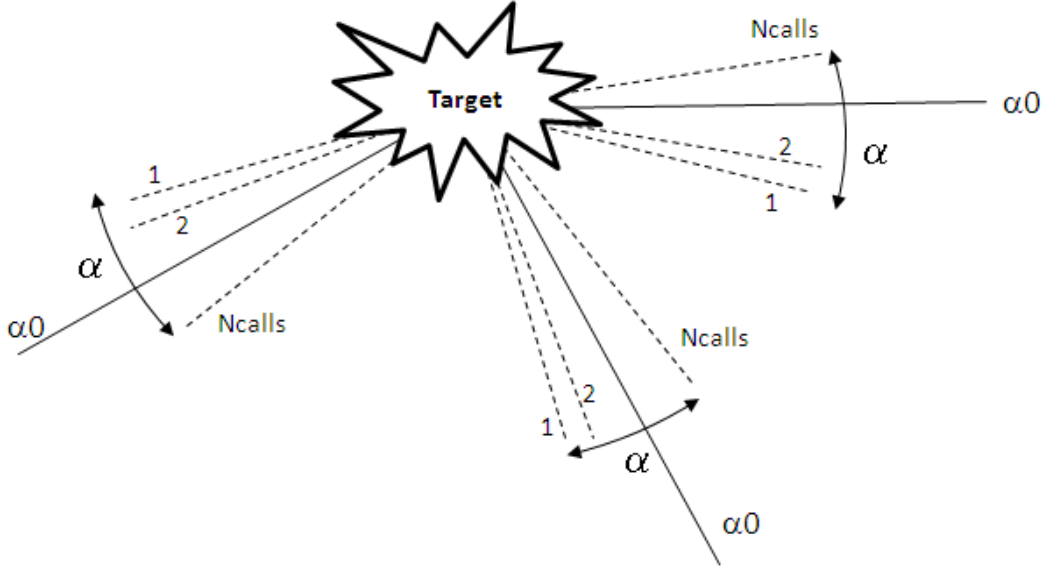
Figure 8.1: Schematic drawing of a sensor that has to accomplish classification of a target by sending a limited number of pulses $Ncalls$ and is restricted to move around the target over a limited angular window α.

information available at each step de-correlates more slowly. As the classifier does not use any *a priori* information on the position of the features, classification with large windows is performed on profiles that either do or do not carry feature information. This results in lowering the probability of correct classification at each step.

8.3 Summary

In this chapter classification performance of a classifier that is allowed to transmit only a limited number of pulses and exploit the target from a limited angular window have been reported. Results show that the classifier performs better when it is exploiting those frontal angular windows that contain the information on the main features of the target, i.e. in our case
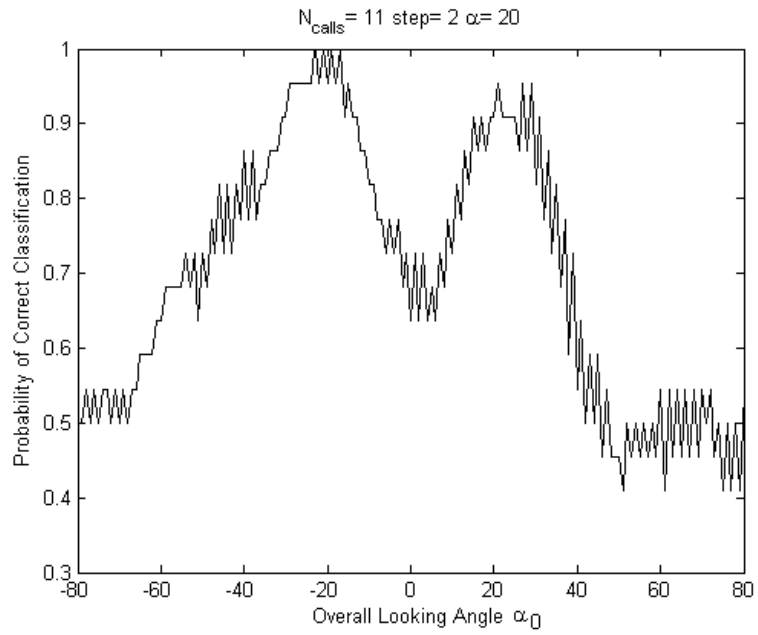
Figure 8.2: Classification performance as a function of look direction angle of a Knn classifier ($Ncalls = 11$, $\alpha = 20$ degrees).
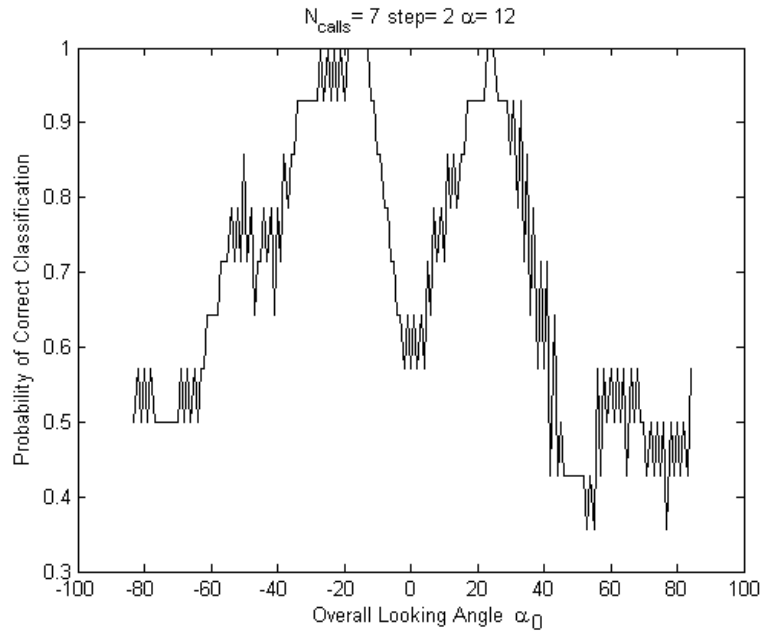
Figure 8.3: Classification performance as a function of look direction angle of a Knn classifier ($Ncalls = 7$, $\alpha = 12$ degrees).
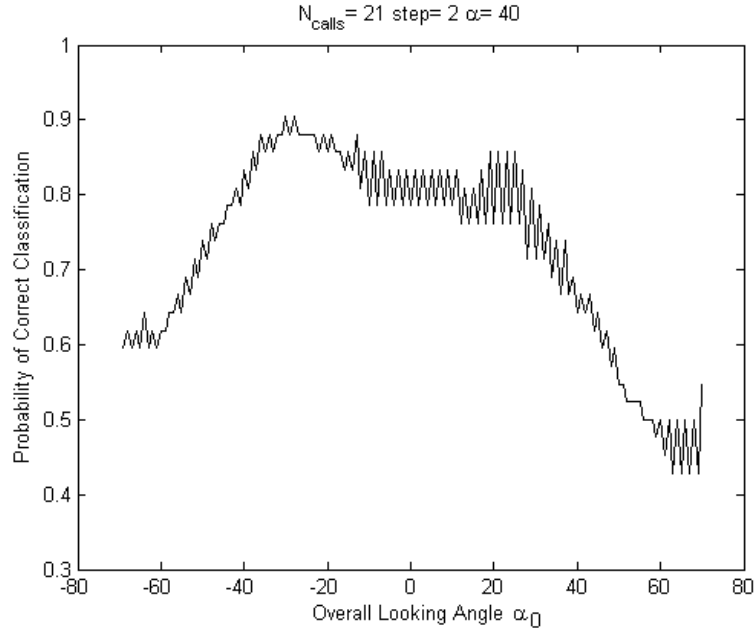
Figure 8.4: Classification performance as a function of look direction angle of a Knn classifier ($Ncalls = 21$, $\alpha = 40$ degrees).

the petals of the flower, as might be expected.

Overall, these results suggest that target recognition could be widely improved via a general knowledge of what the main features that distinguish particular targets from one another are. Knowing under which angular windows these features are available is of great importance in order to adjust the look angle of the sensor with respect to the target under test. This might require changing the position of the radar or sonar itself to collect data from perspectives where these main features are available. Multi perspective data would help to accomplish imaging of the target as well as to track the spatial changes of these characteristic features. Tracks can be compared with prior knowledge of the behaviour of the features of interest in order to make sure that classification is based on the most relevant features. It seems that this

171

approach is worth being exploited towards typical radar and sonar targets as this could lead to high performance target classification as well as to a reduction of the overall complexity of current target recognition algorithms.

Chapter 9

Bio-inspired ultrasound tomography

Results showing the performance of the acoustic radar, and those obtained from the analysis of floral echoes and their relation to the bat behavior, generate a few further considerations. Firstly, the fact that the acoustic radar can achieve very high range resolutions suggests that similar setups might be potentially used to help detect and classify small objects in real scenarios to allow detailed surveillance. Secondly, the way the bat moves around the target collecting multi perspective information and, in particular, the frequency (step) of the angular sampling (irregular of a few degrees) suggests the bat might be trying to perform some sort of imaging on the target itself. Although there is no real evidence of bats performing imaging of targets, a further investigation on this topic at this range of ultrasound frequencies in air would be of interest. In this chapter the ability of the acoustic radar to achieve very high range resolution is reviewed against a dataset obtained by

Figure 9.1: Picture of the 1:400 metallic scale model Boeing 737-500 used for the experiment.

ensonifying real scaled targets. Bio-inspired ultrasound tomographies in air are also exploited from the same dataset and related to the bat trajectory presented in Chapter 6. Results are given together with a discussion on how the acoustic radar and airborne ultrasound tomographic imaging might be used to exploit and enhance radar and sonar target classification performance.

9.1   HRRPs of a scale model Boeing 737

In this section the performance of the acoustic radar when a scaled radar target is ensonified is exploited, with the goal to assess what level of detail can be extracted from small objects in the acoustic regime using ultrasound frequencies. In order to do this, data from a metallic scaled model Boeing 737-550 was collected using the acoustic radar in May 2009.

This data consists of high range resolution profiles (HRRP) of a 1:400 scaled Boeing 737-500 (Figure 9.1) collected as described in Chapter 5. The techni-

174
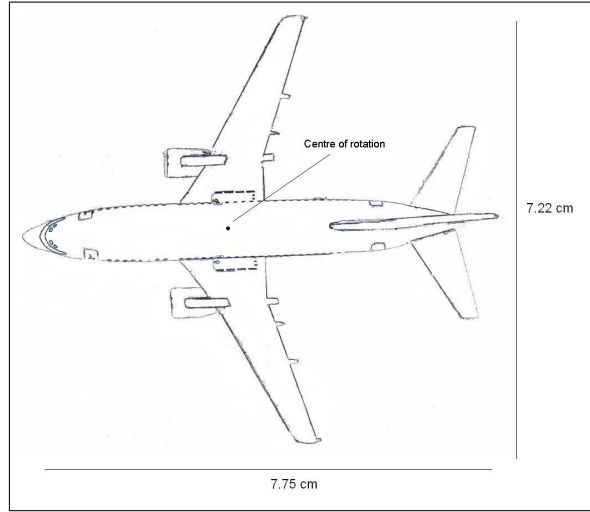
Figure 9.2: Sketch of the 1:400 scale model Boeing 737-500 used for the experiment. During the experiment the scaled aircraft was impaled on a thin pin at the same height as the microphone and the loudspeaker at a distance of about 21 cm from the artificial bat head. The centre of rotation of the target was between the two wings as indicated. The target was insonified uniformly.

cal specifications of the aircraft are summarised in both Table 9.1 and Figure 9.2. The scaled aircraft was impaled on a thin pin (at the same height as the microphone and the loudspeaker) that was placed at the centre of the horizontal turntable set to rotate with an angular step of 1 degree, at a distance of about 21 cm from the artificial bat head. A linear down chirp spanning the frequencies between 50 kHz and 200 kHz was transmitted towards the object with the custom-built loudspeaker and the echo was recorded with the ultrasound microphone (G.R.A.S. type 40 BF) and sampled at a rate of 500 kHz. This was then matched filtered to the transmitted waveform using Matlab. The loudspeaker and the two microphones were placed into the custom built artificial bat-head providing binaural data for this entire dataset. The setup allowed measurements with a range resolution of less than 2 mm. Data was

175

Table 9.1: Specifications of the Boeing 737-500 and its 1:400 scaled version. Information taken from www.geminijets.com.

	Boeing 737-500	Boeing 737-500 (metric)	Scaled Aircraft
Lenght	101ft. 9 in.	31.01 m	7.75 cm
Wingspan	94ft. 9 in.	28.87 m	7.25 cm
Height	36ft. 6 in.	11.13 m	2.78 cm

acquired for three different cases: (i) the original unmodified aircraft, (ii) the aircraft with one engine only, (iii) engines and wings only. A measure of the background was removed from the raw data. Figure 9.3 shows HRRPs of the unmodified scaled aircraft taken over angles from -90 degrees to 90 degrees (where the 0 degree line corresponds to the bat head facing the nose of target) with an angular step resolution of 1 degree. The front of the aircraft is clearly visible for all perspectives and its signature follows a cosine-like fluctuation that varies from 17 cm and 20 cm presenting its minimum value at 0 degrees. The tail is visible over the same angles between 21 cm and 24 cm and its scattering follows the same behaviour, characterised by a phase shift of the sinogram equal to 180 degrees with respect to the scattering associated with the front of the aircraft. As expected, at 0 degrees, reflections from the tails are much weaker than elsewhere both because of the attenuation due to the propagation of acoustic waveforms in air and because this is the configuration where the sonar cross section of the tail assumes the lowest values. Scattering due to the engines is visible between 20 cm and about 21 cm. It is interesting to observe how the engines can generate strong returns. This is likely to be due to their convex cowling that makes them perform like small

176
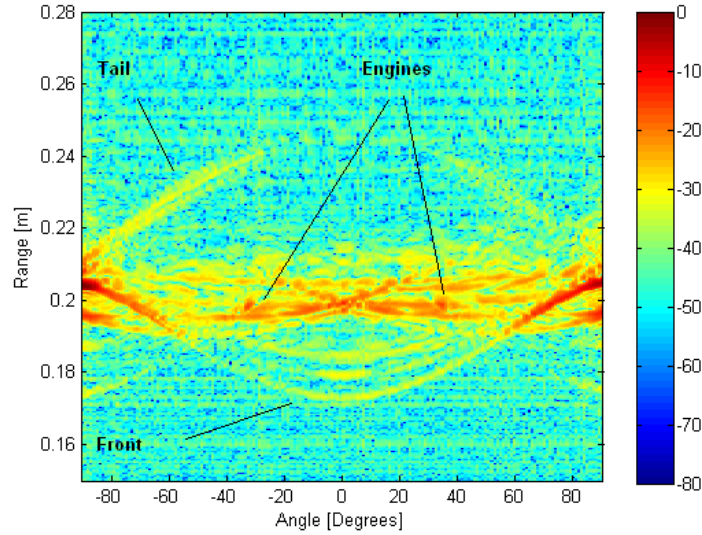
Figure 9.3: HRRPs over 180 degrees of a scaled Boeing 737. Colour scale is in [dB].

reflectors and enhance reflectivity. Their signature is clearly visible and their corresponding sinograms cross at 0 degrees. Analysis of floral echoes and the assessment of classification performance as a function of the look angle carried out in Chapter 8 have shown that finding the right target features is one of the keys to high level target classification and thus, here, the same analysis that was performed on the flowers is repeated for the scale target. This is done with the main aim to assess if the acoustic radar is capable to characterise the contribution of features, needed for good classification, in small targets, and to identify the main features of the target under test (the scaled aircraft). If this is possible the acoustic radar can become an important tool to support detection and classification of small object in a number applications including surveillance.

Figure 9.4 shows HRRPs of the scaled aircraft when the left engine was

manually removed from the wing. All scattering at about 20 cm covering the angular window between -40 degrees and 0 degrees almost disappears except for some reflections due the pin that allows connection between the engine and the wings that could not be removed.

Such changes in a target might significantly affect classification performance and thus lead to different results at the output of a typical classifier. A way to quantify the impact of these changes in the target is to calculate the cross-correlation function between corresponding HRRPs taken from the unmodified scaled aircraft and the modified one, and then investigate the properties of the resulting cross-correlation matrix. For the case of the scaled aircraft, this is displayed in Figure 9.5. In the image the y-axis corresponds to the range shift between profiles in range, and the x-axis indicates the angular perspective from which the two profiles to be cross-correlated were gathered. In other words, each pixel $C_{i,j}$ has been calculated as

$$C_{i,j} = |\sum_{k=1}^{2N-1} x_{k,j} y_{i+k,j}^*|, \tag{9.1}$$

where $x_{i,j}$ and $y_{i,j}$ indicate the i,j pixel of Figure 9.3 and Figure 9.4 respectively. Results show that the cross-correlation function drops off by at least 8 dB at the angles where the scattering from the removed engine is obvious in Figure 9.3. As expected, elsewhere HRRPs are highly correlated. It is clear that, if classification is performed by using the cross-correlation function as a measure of distance between training profiles and test profiles, classification should drop significantly when such changes in the target occur. This type of information is significant as it allows us to better understand the impor-
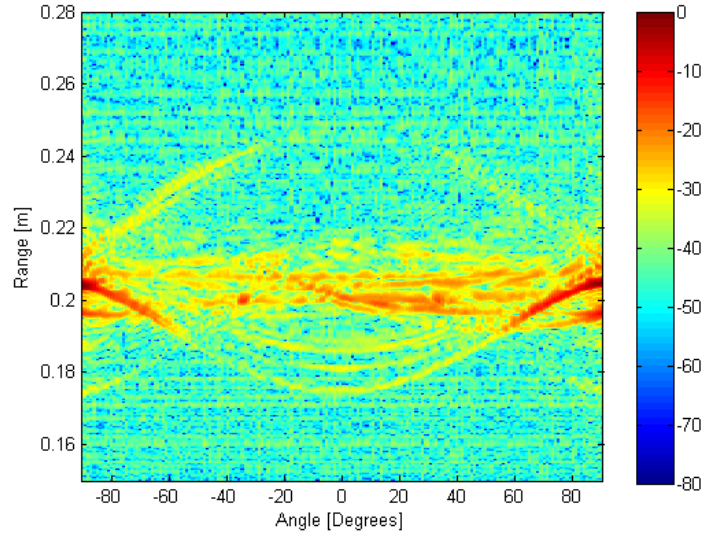
Figure 9.4: HRRPs over 180 degrees of a scaled Boeing 737 when one of the two engines was manually removed from the fuselage. Colour scale is in [dB].

tance and the role of the engines as a feature for target recognition. Figure 9.6 shows the results when both the engines and the wings were detached from the aircraft fuselage and separately ensonified. Because all the images are normalised to their maximum values, that corresponded in most case to the fuselage being orientated at -90 degrees and +90 degrees with respect to arm containing the bat head, here scattering from the engines appears to be stronger and then better visible. The inside of the engines is clearly visible as in the previous images while part of the remaining scattering is due to the two pins that connect the wings to the fuselage. The cross-correlation matrix between the full scaled aircraft and the wings with engines only is given in Figure 9.7. As expected, the angular window between -35 degrees and +35 degrees present most of the highest values of the cross-correlation function, and this corresponds to the angular perspectives where the engines are visi-
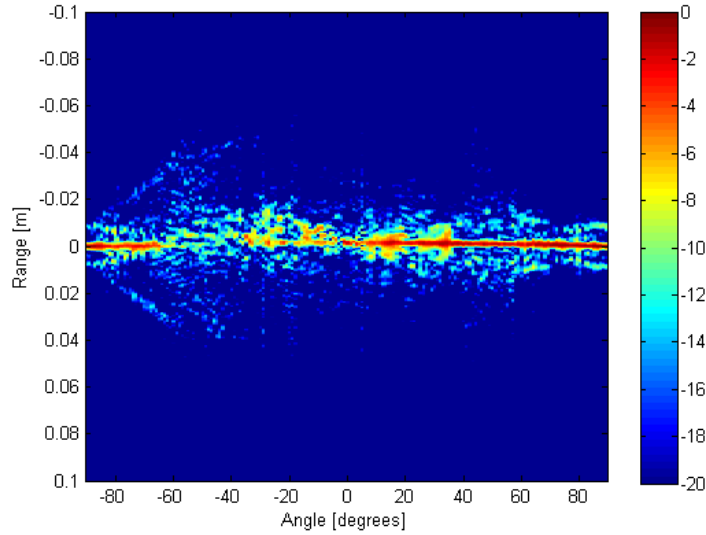
Figure 9.5: Cross-correlation function between the unmodified scaled aircraft and its counter part without an engine. Profiles taken from the same angular perspectives were cross-correlated. Colour scale in [dB].

ble in both the images. Results obtained from the stand alone fuselage are given in Figure 9.8. The front of the fuselage is clearly visible starting from 21 cm at -90 degrees and then getting closer to the bat-head reaching the closest point at 0 degrees. The tail is also visible between 22 cm and 15 cm and its contribution does not differ to that of Figure 9.3. Scattering from the front wheel that was left open is also visible in the frontal view between - 40 degrees and +40 degrees. The line at an almost constant range must be due to the pin and the scattering around it to the discontinuity caused by the hole left from the point of attachment to the wings. The image of the cross-correlation matrix, given in Figure 9.9, now presents its highest values between -90 degrees and -60 degrees, and between 60 degrees and 90 degrees. As expected the window between -60 degrees and +60 degrees, do
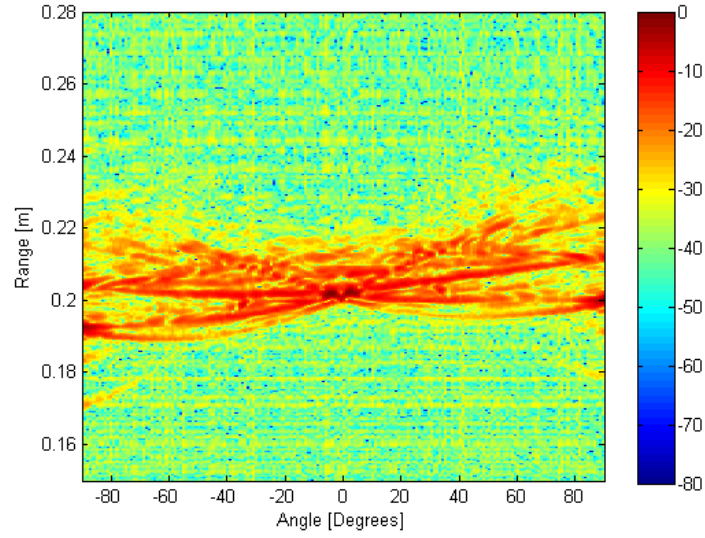
Figure 9.6: HRRPs over 180 degrees of the part containing the two engines and the wings that was manually removed from the scaled Boeing 737. Colour scale is in [dB].
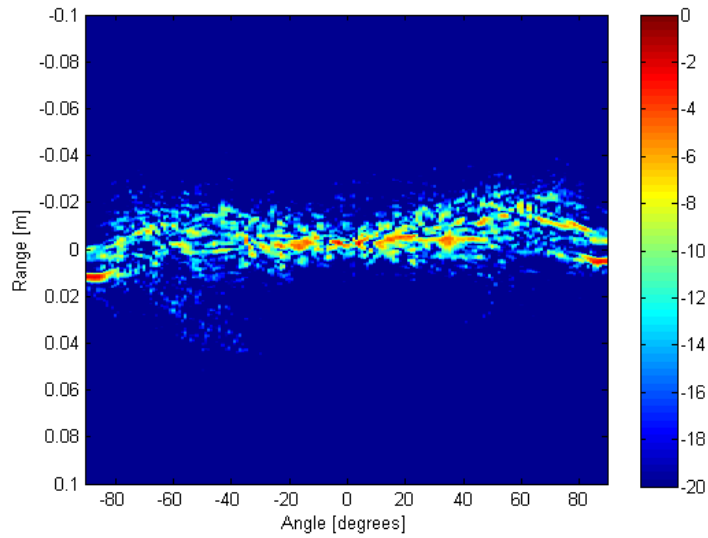
Figure 9.7: Cross-correlation function between the unmodified scaled aircraft and its counter part with engines only. Profiles taken from the same angular perspectives were cross-correlated. Colour scale in [dB].
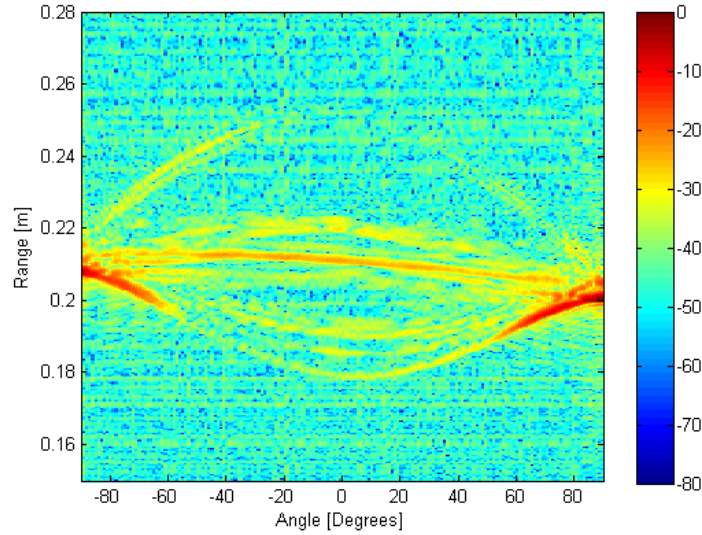
Figure 9.8: HRRPs over 180 degrees of the fuselage that was manually removed from the scaled Boeing 737. Colour scale is in [dB].

not present high values in the cross-correlation for the obvious effect of the removal of the engines from the fuselage.

Overall, the results presented in this section show that a very high level of details can be achieved by using sound waves at ultrasound frequencies and, more importantly, show that it is possible to detect small changes in targets that can be used to assess the robustness of classification performance of specific targets.

As previously discussed, the way the bat moves around the target collecting multi perspective information suggests it might try to perform some sort of imaging on the target itself. As it is shown in Chapter 6 the bat tends to move around the target to collect information from a number of angular perspectives that are commonly separated by 3 or 4 degrees. This means that even for small targets, such as flowers, migration of scatterers through

182
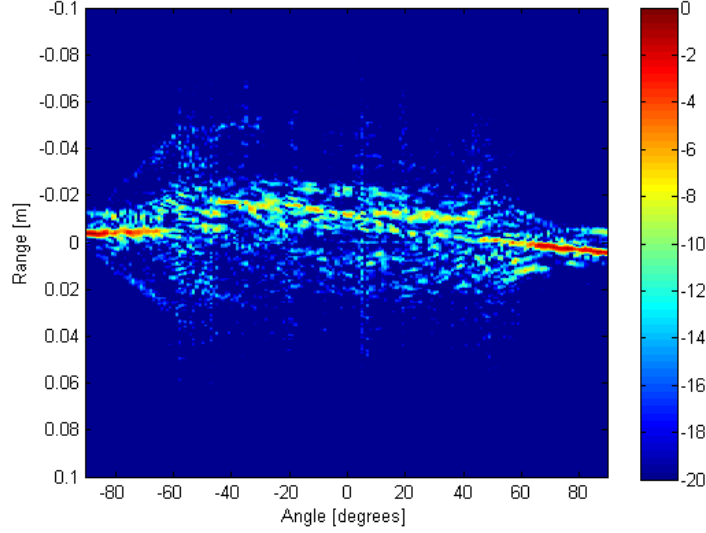
Figure 9.9: Cross-correlation function between the unmodified scaled aircraft and its counter with fuselage only. Profiles taken from the same angular perspectives were cross-correlated. Colour scale in [dB].

range cells is likely to occur after a short number of calls, i.e. the range cell containing the scatterer changes due the movement of the bat. Figure 9.10 displays a sketch describing range migration of a scatterer within a target. In the figure, it is assumed that the source (transmitter and receiver) is stationary in a point $(-L, 0)$ along the y axis, with L much greater than the dimension of the target r. The target is rotated on a turntable centered in $(0, 0)$, corresponding to the origin of the xy plane. Under these assumptions, the iso-range points from the source are circumferences characterised by a radius that is much greater than the target, and therefore can be approximated with lines parallel to the x axis. The range shift of a scatterer due to an angular rotation Δ_ϑ can be approximated with the shift Δ_y on the y-axis only. Table 9.2 reports typical values of range shifts (Δ_y) for two

Table 9.2: Analysis of range migration for a scaled target whose longer dimension is r ($\Delta_\vartheta = 3$ degrees).

r	$\vartheta_0 = 90^o$	$\vartheta_0 = 45^o$	$\vartheta_0 = 0^o$
4 cm	0.06 mm	1.4 mm	2.1 mm
5 cm	0.07 mm	1.8 mm	2.6 mm

targets whose longest dimensions are $2r = 8$ cm and $2r = 10$ cm assuming an angular separation between perspectives of $\Delta_\vartheta = 3$ degrees. The values of these parameters have been chosen to closely reproduce a real scenario where bats operate. The range shifts were calculated following the expression $\Delta_y = |rsin(\vartheta_0 + \Delta_\vartheta) - rsin((\vartheta_0)|$. Results show that the scatterers that are located at $\vartheta_0 = 0$ degrees and those located at $\vartheta_0 = 45$ degrees present range shifts that are comparable with the value of the range resolution $R_r = 2$ mm, meaning that their range migration occurs after the first call. These results suggest that, under the hypothesis that bats use classic target imaging, SAR, SAS or ISAR imaging would be too challenging to perform, as this would require the bat to compensate for range migrations [78] [79]. The frequency of the angular sampling, instead, is typical of tomographic imaging techniques and suggests a further investigation of tomography at this range of ultrasound frequencies in air would be of interest.

To exploit tomographic imaging at ultrasound frequencies in air the backprojection algorithm was applied to the data to generate the tomographic images of the scaled aircraft. In order to do so, the inverse Radon transform was applied, for each target, to the matrix composed of all the measured HRRPs arranged in order of collection one next to each other, with each col-
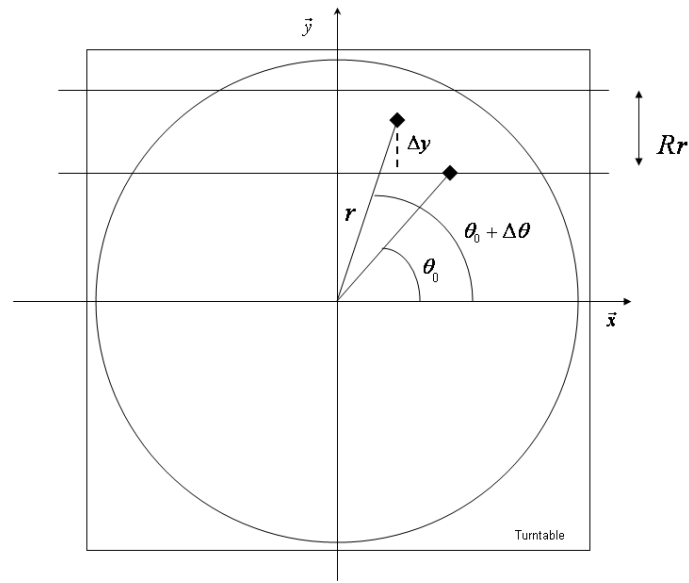
Figure 9.10: Range migration for a scatterer within a scaled target. The source (transmitter and receiver) is stationary in a point $(-L, 0)$ along the y axis, with L much greater than the dimension of the target r. The target is rotating on a turntable centered in $(0, 0)$, corresponding to the origin of the xy plane. The range shift of a scatterer due to an angular rotation Δ_ϑ can be approximated with the shift Δ_y on the y-axis only.

umn of the matrix therefore corresponding to one angular perspective. Each HRRP was obtained by matched filtering the analytic signal of the echo, for each angular perspective, with the analytic signal of the transmitted signal. The analytic signals were obtained through a Hilbert transform with Matlab. The Matlab code used to generated the images can be found in Appendix A. In the matrix formed by all the perspectives, the mean value of each row was set to zero to get rid of the non variable unwanted clutter. The inverse Radon transform was applied to the data with the iradon.m Matlab standard toolbox function. Because, this Matlab function assumes that the centre of rotation of the target (the centre of our horizontal turntable at about 20 cm) is exactly at half the number of rows making the matrix, zero padding was necessary at the bottom of the images to adjust the centre of rotation. A wrong choice of the centre of rotation results in a badly focuses image. This analysis was firstly performed on the data by using both the amplitude and phase information of the HRRPs (coherent analysis), and was then repeated by using the amplitude information only (non-coherent analysis).

Figure 9.11 shows the image that was obtained when the back-projection algorithm was applied to the measured HRRPs of the unmodified scaled aircraft. It was generated using a frontal view of the target made up of 180 profiles. This corresponds to the angular window that covered the angles between -90 degrees and +90 degrees, with the 0 degree profile corresponding to the range profile acquired when the aircraft was facing the microphone and the loudspeaker. The image shows a high level of detail. The front of the fuselage is clearly visible and well focused, as well as the two engines that are very well distinguishable. The dimensions of the image are close to those

186

of the real scaled target. As expected, the scattering from the two wings is very weak in comparison to that from the engines and the fuselage. This is because during the measurements the object was placed on the same horizontal plane with the microphone and the loudspeaker. This is the configuration where the cross section of the two wings is expected to be small. As range profiles over 180 degrees were used, the back of the target is not visible and not focused. Results obtained from the non-coherent processing of the same data are given in Figure 9.12. The shape of the nose of the aircraft plus the two engines is still visible although there is an evident drop in the quality of the image that qualitatively appears much more noisy. The two wings are not visible in the image, probably due to the fact that their contribution falls below the noise level.

Figure 9.13 shows the image of the scaled aircraft obtained when the left engine was removed from the fuselage. As in the previous case the level of detail remains high. The front of the fuselage is still visible and focused. The shape of the unmodified engine remains the same and, as expected, the scattering from the engine that was removed disappears from the image although some residual reflections, due to the pin that allows the junction between the wing and the engine, is still visible.

In order to exploit whether the level of detail that was achieved can allow a further investigation of the feature of the targets, the engines and the wings were taken off the fuselage and range profiles were acquired. For this case HRRPs over 360 degrees were gathered. Figure 9.15 shows the tomographic image that was obtained by processing the range profiles recorded from the removed parts. The two engines are very well distinguishable and impres-
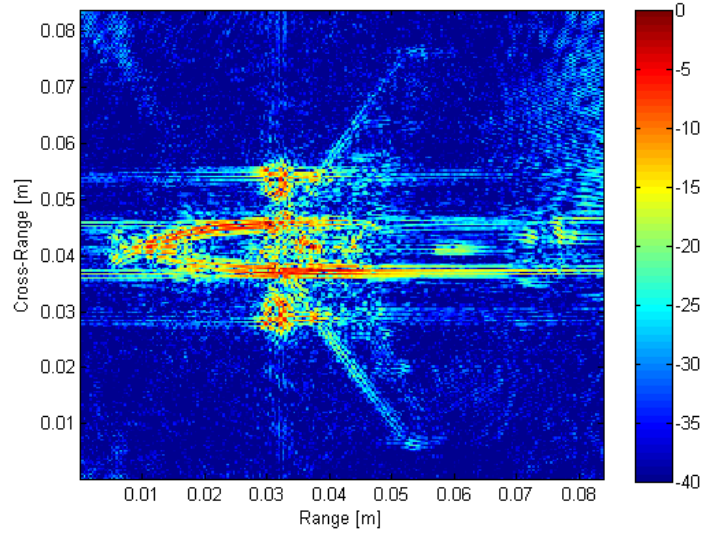
Figure 9.11: Tomographic image of the scaled aircraft obtained by using a frontal view of 180 profiles obtained from coherent data.

sively the two tiny pins that connect the fuselage to the wings plus engines are very well visible and very well focused too. As in the previous cases the wing are visible but very weak for the reasons already discussed. Figure 9.14, Figure 9.16 and Figure 9.18 show the results obtained from the non-coherent processing in the last three cases. Overall, the same considerations resulting from the non-coherent analysis of the unmodified aircraft remain valid. Non-coherent processing results, on the average, in a drop in the quality of the image although the structure and shape of the objects remains visible in all cases. Only the parts that present a weaker contribution in the coherent images, such as the wings or the small connecting pins, disappears after falling under the noise level.

Although, as previously stressed, there is no real scientific proof that bats perform any sort of target imaging, it remains interesting to assess what

188
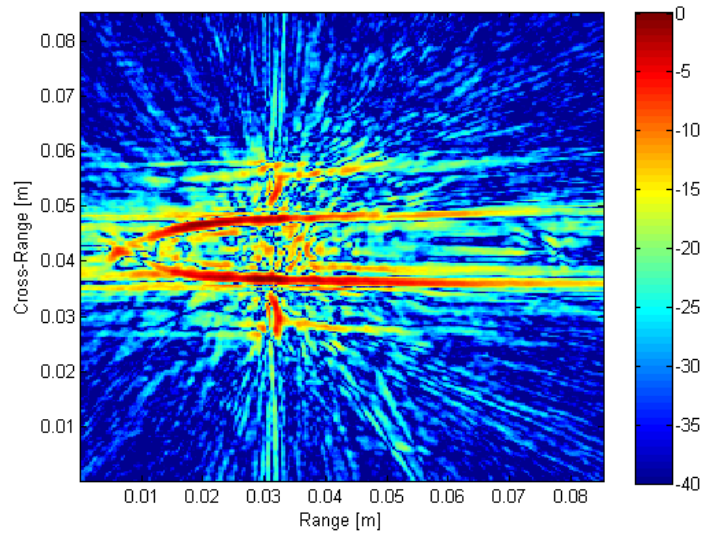
Figure 9.12: Tomographic image of the scaled aircraft obtained by using a frontal view of 180 profiles obtained from non-coherent data.
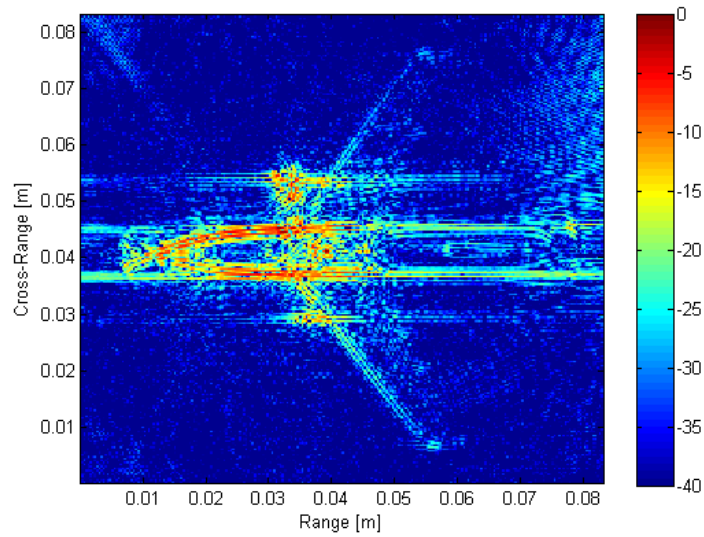
Figure 9.13: Tomographic image of the scaled aircraft without an engine over a frontal view of 180 profiles obtained from coherent data.
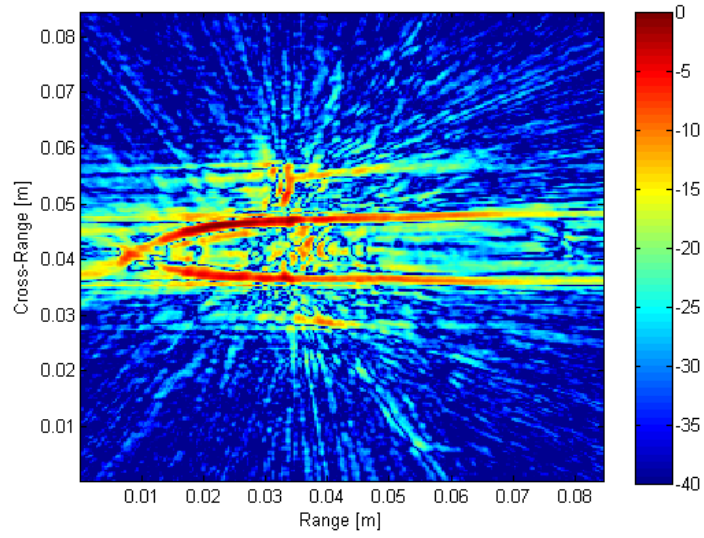
Figure 9.14: Tomographic image of the scaled aircraft without an engine over a frontal view of 180 profiles obtained from non-coherent data.
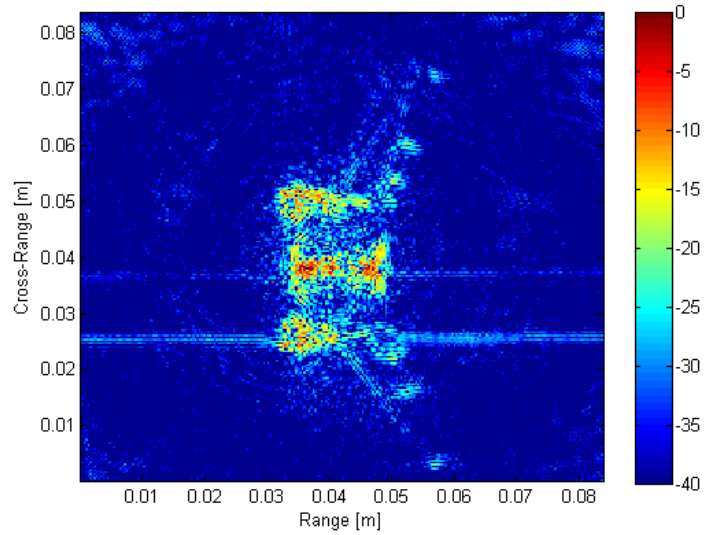
Figure 9.15: Tomographic image of the engines and wings of the scaled aircraft obtained from coherent data over a complete view of 360 profiles.
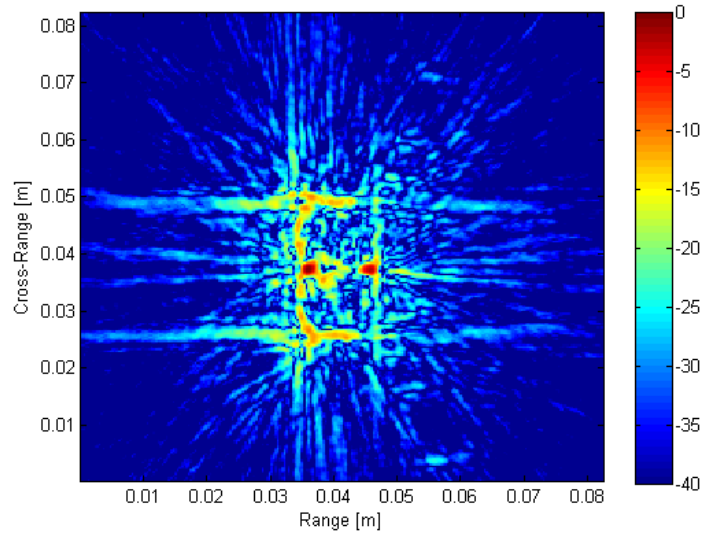
Figure 9.16: Tomographic image of the engines and wings of the scaled aircraft obtained from non-coherent data over a complete view of 360 profiles..
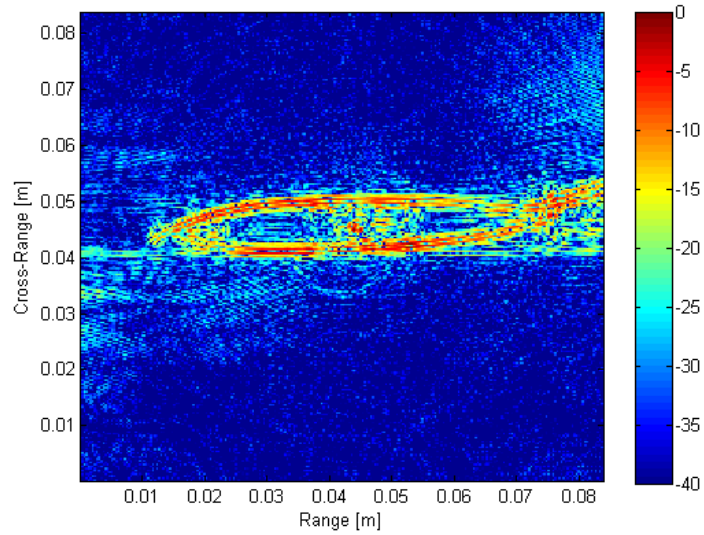
Figure 9.17: Tomographic image of the fuselage of the scaled aircraft obtained from coherent data over a complete view of 360 profiles.
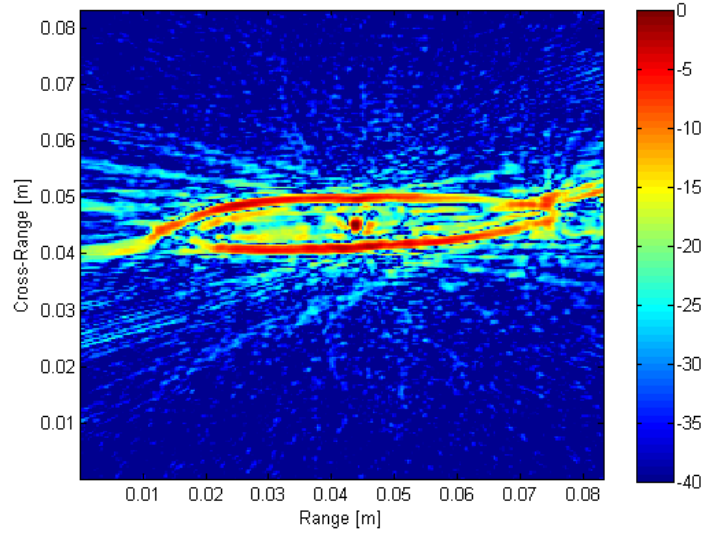
Figure 9.18: Tomographic image of the fuselage of the scaled aircraft obtained from non-coherent data over a complete view of 360 profiles.

type of information would be available under the hypothesis that they do so. The results presented earlier have been obtained by processing HRRPs of the target gathered by collecting perspectives around the target with a constant angular step over a wide angular window of at least 180 degrees. The bat trajectory presented in Chapter 6 clearly shows that firstly bats do not send pulses from angular perspectives which are separated by a constant angle and, secondly that they only use a small number of angular perspectives before approaching the target. This considerations suggest that to really exploit the information that would be available to a bat, in the case it performed tomographic imaging, it is important to repeat the results of the above analysis by processing only the echoes that were measured from the angular perspectives that were really exploited by the bat in the available trajectory dataset. Results from this analysis are given in Figure 9.19. As expected because only
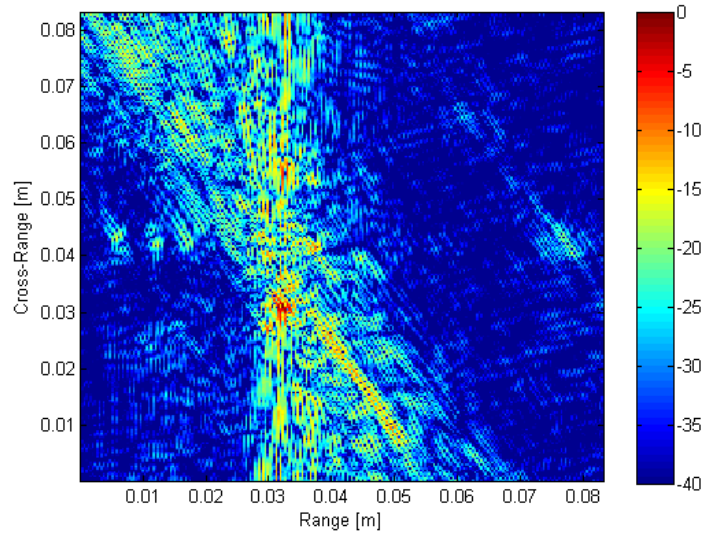
Figure 9.19: Tomographic image of the unmodified scaled aircraft obtained by processing only the angular perspectives that were exploited by the bats in the available trajectory data.

17 HRRPs were used to create the image the quality of the image degrades significantly. These correspond to only 10% of the data that were used to build the previous images. The image shows that although target outline information may not be available to the bat, there remain information corresponding to the features that were visible at the angular perspectives that were actually exploited. In this particular case information on the left engine is available.

Results show that the acoustic radar is capable of capturing detailed information of small static targets and in particular allow detection of differences due to small changes in their shape. They also show that ultrasound tomographic imaging in air is possible and can lead to good imaging of small static targets. Because the results presented in this chapter were obtained

193

by processing data gathered in an ultrasound chamber further investigations aiming at assessing the impact of multipath (if and when multipath overlaps in time with the return from the target) and clutter on these results are an imperative and will be at the centre of future research works. Finally, results suggests that ultrasound systems, such as the acoustic radar, might potentially be used in real scenarios to allow detection and classification of very small objects. Because the speed of sound in air at this range of frequencies, typically used by echolocating bats, is only about 343 m/sec the acoustic radar allows a very high range resolution that cannot be easily achieved by other sensors. This could be also used as support to other sensors, such as typical radar systems, to enable a better and more efficient surveillance of areas of interest, such as ports, airports or stations.

Another point to note is that the size of the target to range resolution ratio in the ultrasound case is comparable to that of air surveillance radar systems and air targets. This suggests that the acoustic radar could be deployed to gather data of scaled targets in order to carry out a preliminary analysis of classification performance and produce predictions for real radar scenarios. These could be validated when data collected by actual radar systems becomes available.

It is evident that this required an analysis aiming at proving that ultrasound data and real RF data are sufficiently similar, i.e. present the same characteristics, with respect to the task of classification and a preliminary analysis on this topic is going to be presented in the next chapter.

Chapter 10

Radar Comparisons

The results presented in the previous chapter have shown that the acoustic radar can sense fine object details and detect differences in the scattering due to small target components. Understanding how target classification performance varies as a function of these parts/features of real targets is of great interest to the radar and sonar community. The work presented in this thesis suggests that it is likely that this analysis can be carried out by testing data gathered from scaled targets with the acoustic radar, so to obtain a set of preliminary results that then can be validated with data collected by an actual radar or sonar system. If it can be proved that ultrasound data and real RF data are similar 'enough', i.e. present the same characteristics, with respect to the task of target classification, the acoustic radar might become an important tool to ease data collection for the study and the development of radar and sonar target classification. This has a number of advantages. Firstly, the acoustic radar allows very high range resolution at a much lower cost than a real radar or sonar system and secondly exper-

iments in the ultrasound regime are generally much easier to perform with respect to their counterpart in the RF regime. Ultrasound experiment can be easily performed indoors and in better controlled environments, such as ultrasound chambers, and do not require a lot of space. In addition to this, data collection is much faster. Gathering the data required to produce the results presented in this thesis took only a few hours and the duration of the experiments depended on the angular resolution required. On the contrary, experiments with real radar targets can be very expensive and time consuming. Scaled targets can be easily made available and more importantly allow manual removal of parts of the target so that classification performance can be assessed as a function of target features (geometrical features).

For all this to be possible an investigation of possible similarities between the electromagnetic regime and the acoustic regime is an imperative. It is, in fact, obvious that the physics of the scattering mechanisms that take place in the ultrasound regime is very different from that related to the RF regime for radar systems. Also, in the ultrasound regime there is no the equivalent of the polimetry (i.e. the use of different electro-magnetic polarisations) in the RF regime, which represent a key degree of freedom for radar systems. This is one of the fundamental differences that might have an impact in the information contained in target echoes. Here, a dataset consisting HRRPs collected by ensonifing a scaled version of a T-55 tank (Figure 10.1 and Figure 10.2) with the acoustic radar are compared to another dataset containing HRRPs of a T-55 Russian tank (Figure 10.3) collected by a real radar and results are discussed. Figure 10.4 shows the image obtained when the unmodified scaled tank was ensonified by the acoustic radar. These were obtained by
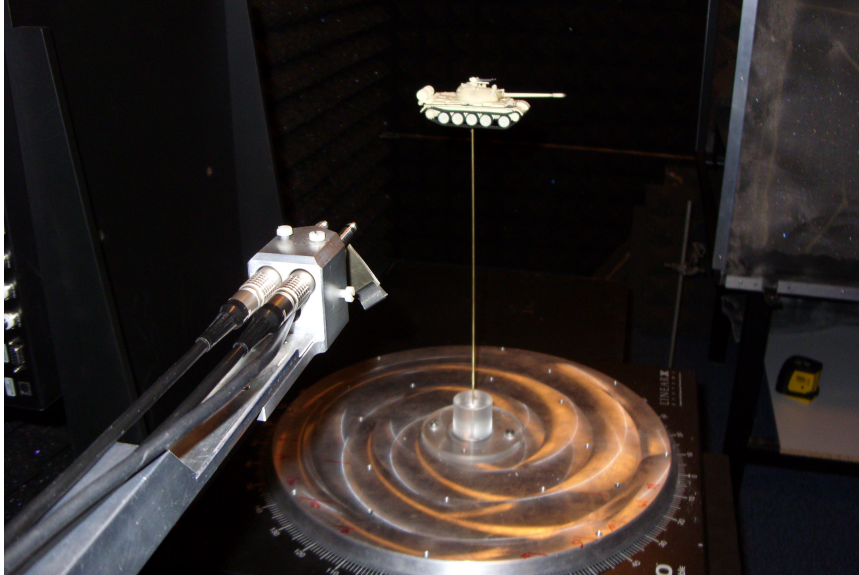
Figure 10.1: Photo of the scaled tank in the ultrasound chamber during the experiments.

Figure 10.2: Photo of the scaled tank.

Figure 10.3: Photo of the Russian T-55 tank.

turning the horizontal turntable from -90 degrees to +90 degrees with a step angle equal to 1 degree. In the image the zero degree line corresponds to the frontal view of the target. The image was normalised to its maximum value. Results show a complex echo structure in which the features of the tank are not as clearly distinguishable as those of the aircraft presented in the previous chapter. Scattering from the gun, looking forward towards the artificial bat-head, is visible between -30 degrees and +30 degrees although its scattering is much weaker than the scattering associated with the body of the tank. The highest scattering occurs at both -90 degrees and +90 degrees, i.e. when the longer side of the tank was facing the arm bringing the artificial bat-head. Figure 10.5 shows the same results when the turret and the gun were manually removed from the scaled tank. As expected, the scattering associated with the gun disappears and the echo structure changes in the area from 20 cm to 21.5 cm between -20 degrees and +20 degrees. No other

198

differences are to be reported. The maximum values in the scattering occur as in the previous case around 20 cm at -90 degrees and +90 degrees.

A cross-correlation analysis as that performed on the scaled aircraft in Chapter 9 was repeated on the tank. HRRPs taken from the same angular perspective were extracted from the two images and cross-correlated. Results, given in Figure 10.6, show that the profiles taken from -90 degrees to about -30 degrees and those taken from +30 degrees to +90 degrees are highly correlated. This suggests that at these angles the characteristic features of the profiles were not highly impacted by removing the turret. On the other hand, between -30 degrees and +30 degrees the cross-correlation function drops. Because the only difference between the two experiments is represented by the missing turret this can only be the cause of the cross-correlation drop. These results are consistent with the qualitative observation that resulted from the comparison between the two images of Figure 10.4 and Figure 10.5.

To make a radar comparison the results obtained with the acoustic radar were compared to those obtained with a step-frequency X-band radar, with a central operating frequency equal to 9.25 GHz, characterised by a range resolution of 30 cm. More information on the data collection can be found in [80]. This represents a good example where the value of ratio between the size of the target and the range resolution, i.e. the number of range cells covering the targets, is comparable in the two cases. In particular, because the size of the scaled tank on its longest dimension is $L = 9$ cm and the range resolution of the acoustic radar is about $R_r = 2$ mm, the number of range cells covering the target N_c that follows the expression $N_c = L/R_r$ results to be equal to 45. In the radar case where the range resolution is about 30
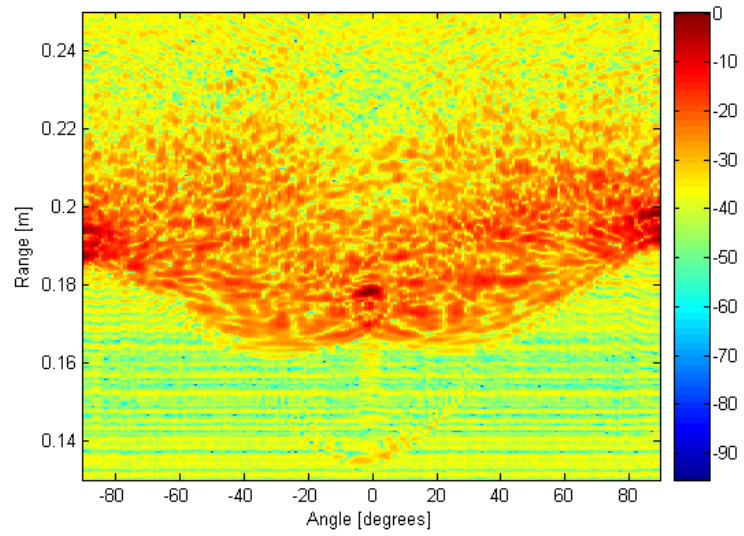
Figure 10.4: HRRPs of the unmodified scaled tank over a angular window between -90 degrees and +90 degrees. Colour scale is [dB].
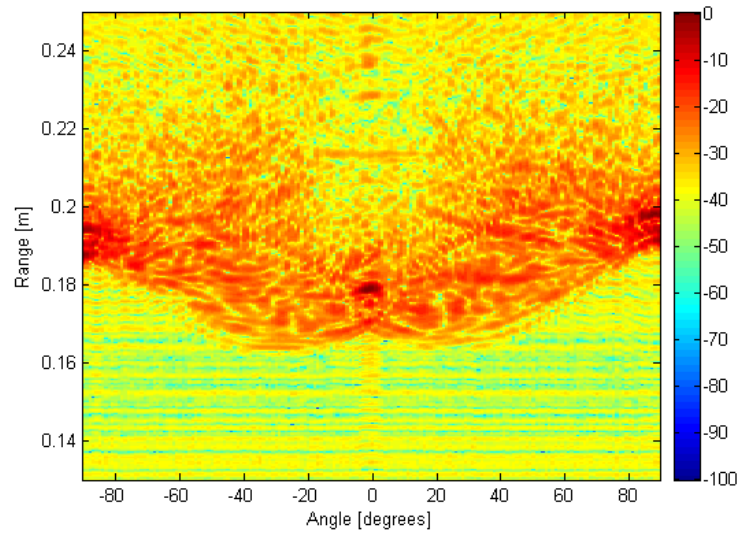
Figure 10.5: HRRPs of the scaled tank without gun over a angular window between -90 degrees and +90 degrees. Colour scale is [dB].
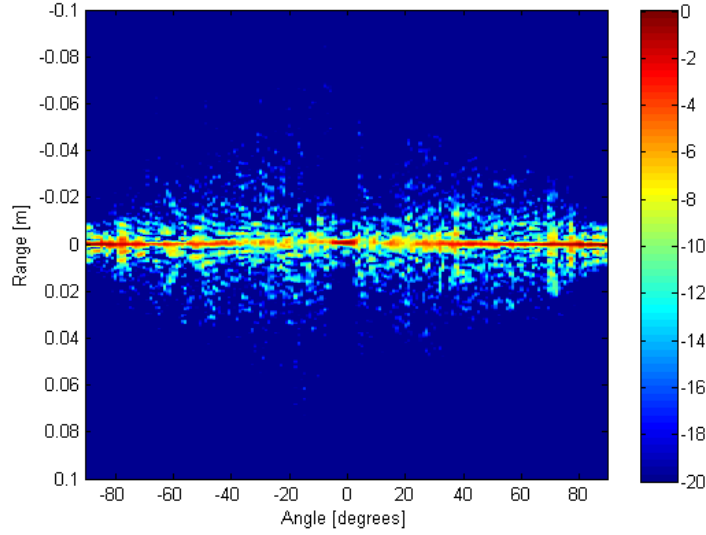
Figure 10.6: Cross-correlation function between the unmodified and modified scaled tanks. Profiles taken from the same angular perspectives were cross-correlated. Colour scale in [dB].

cm and the size of the real tank on its longest dimension about 6.5 m the number of cells that covers the target is about 22. This is comparable with the scaled version of the experiment meaning that, in both case, the same level of detail in the target is achievable. Another parameter that needs to be considered is the number of wavelengths contained in the target, as this is the parameter that defines that reflection properties in the two cases. In the ultrasound regime, the number of wavelengths contained in the scaled target varies between 13 (@50 kHz) and 52 (@200 kHz) while in the radar case the number of wavelength contained in the tank equal to 216. Because of this parameter differs by a factor 10 it is possible that because of the reflection properties the comparison between radar and sonar data may become difficult to sustain. In particular there is the possibility that, in the ultrasound
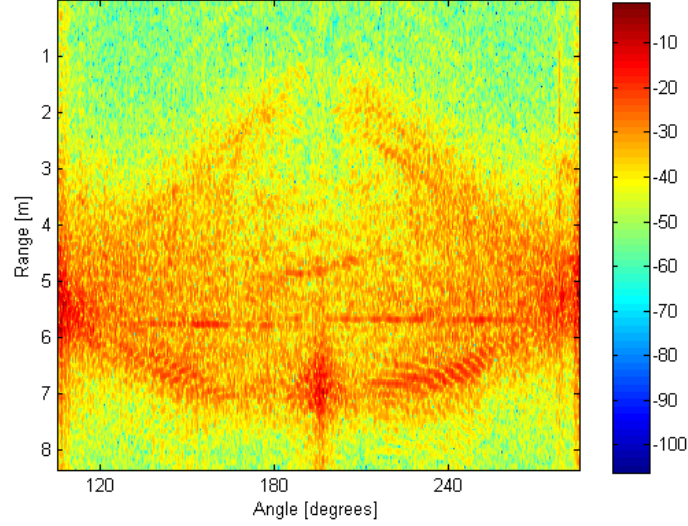
Figure 10.7: HRRPs of the real tank over an angular window between -90 degrees and +90 degrees. Colour scale is [dB].

case, scatterers presenting a dimension which is smaller or comparable to a wavelength can generate interferences that may make the data different.

Results obtained by the radar are given in Figure 10.7. Qualitatively it seems that the properties of the image obtained by the radar are close to those obtained in the ultrasound case. Both cases show their maximum values at -90 degrees and + 90 degrees, and another maximum corresponding to 0 degrees. The structure of the scattering is highly complex in both cases and this does not allow an easy comparison even if the overall behaviour looks alike. To make a quantitative comparison of the data a cross-correlation analysis of each image was carried out. In particular each HRRPs of each image was cross-correlated to any other HRRPs taken from its same image and, mathematically, each element of the cross-correlation matrix C_{ij} was calculated

as

$$C_{ij} = < \hat{x}_i, \hat{x}_j > \; i = 1...N, j = 1...N, \qquad (10.1)$$

where $\hat{x}_i$ is the ith high range resolution profile and $< \; . \; >$ indicates a typical scalar product between vectors. Results obtained for the two dataset representing the unmodified and the modified tank are reported in Figure 10.8 and Figure 10.9 respectively. Figure 10.10 shows the results of the same analysis in the radar case. Results firstly show that differences between the unmodified case and the unmodified case can be slightly seen between -20 degrees and + 30 degrees. In particular when the turret is not present HRRPs de-correlates more slowly at the angle of interest. As expected maximum values are all distributed on the diagonal of the matrix as in this point the cross-correlation function corresponded to the autocorrelation of each single profile. In the ultrasound case the two profiles taken at -90 degrees and +90 degrees, respectively, are highly correlated as well. Results show that in both the ultrasound case and the radar case HRRPs de-correlates quickly with angle. In particular both the result show that a movement of the sensor of a couple of degrees only is enough to obtain a drop in the autocorrelation function. This leads to expect the necessity to increase the number of HRRPs needed to train a classifier that operates with range profiles. It is self evident that a target whose HRRPs decorrelates quickly with angle contains more independent information than a target whose HRRPs decorrelates slowly, and thus results more challenging to be recognised. Results contain another important information on the level of symmetry of the target. Because only one of the two diagonals of the cross-correlation matrix is visible means that

203
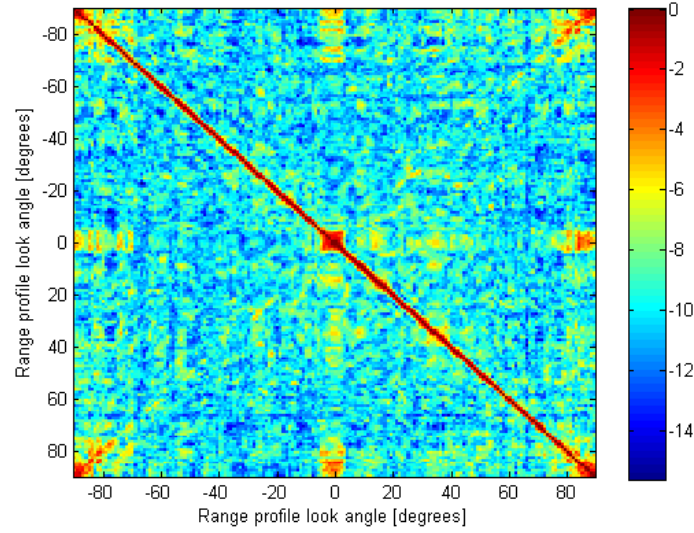
Figure 10.8: Autocorrelation matrix obtained as in Eq. 10.1 for the un-modified scaled tank. Each element i, j is the maximum value of the cross-correlation function between the ith and the jth range profile. Colour scale is in [dB].

specular perspectives are not highly correlated and lead to the conclusion that symmetry of the target is not significant. Symmetric targets should present cross-correlation matrix in which both the diagonals should be well visible.

This is obvious when observing Figure 10.11 showing the cross-correlation matrix related to the unmodified scaled aircraft described in the previous chapter. As expected, because the aircraft is fully symmetrical around the profile collected at 0 degree both the diagonal of the cross-correlation matrix are well visible. In addition to this results show that HRRPs decorrelates more slowly with respect to those of the tank and highlights zones of the targets at high level of correlation that might represents weaknesses in terms of target stealth. In particular HRRPs taken at angles from -60 degrees to +90 degrees result to be high correlated. Finally, results showing the cross-
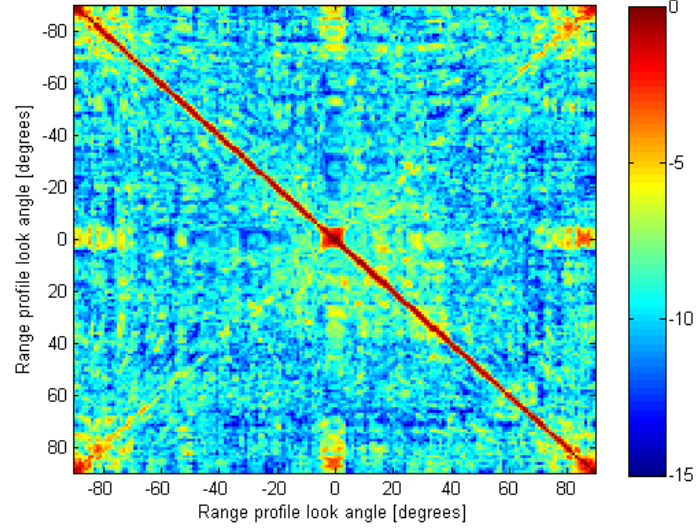
Figure 10.9: Autocorrelation matrix obtained as in Eq. 10.1 for the modified scaled tank. Each element i, j is the maximum value of the cross-correlation function between the ith and the jth range profile. Colour scale is in [dB].
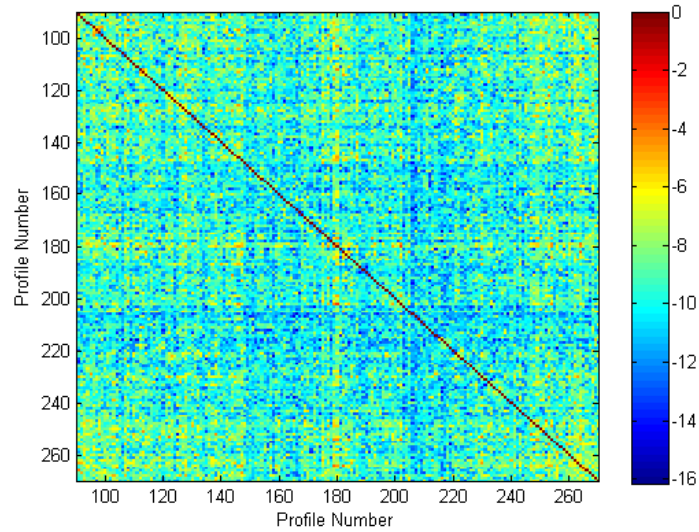
Figure 10.10: Autocorrelation matrix obtained as in Eq. 10.1 for the real tank. Data was collected with a real radar. Each element i, j is the maximum value of the cross-correlation function between the ith and the jth range profile. Colour scale is in [dB].

correlation matrix of the same scaled aircraft when one of the two engines was removed (Figure 10.12) highlight once again the importance of specific features in targets. In particular, in this case, the secondary diagonal in the image disappears as result of the removal of the engine on the symmetry properties of the target. Unfortunately, because RF data of the Boeing 737 are not available it has not been possible to perform a direct comparison between these results and their RF counterpart.

Results show that, for this experiment, ultrasound data and RF data present similar characteristics when the range resolution to size of the target ratio assumes similar values. In particular, the properties of the cross-correlation function between HRRPs taken from different perspective in the RF regime are similar to those of the ultrasound regime suggesting that performance of a classifier is likely to be similar as well. It remains to address the impact of different reflection properties, due to the possible different number of wavelengths contained in the target, on the results. Some scatterers in the ultrasound regime may, in fact, present dimension which are smaller or comparable to the wavelength and can generate interferences that may make the data different. This will have to be taken into account in future works. It is self evident that a greater number of data must be processed before drawing any final conclusions. Once this data becomes available it will be possible to compare classification performance of classifiers testing RF data to that of classifiers testing ultrasound data. Indeed, this is an interesting topic that can have a huge impact on the study of radar and sonar target classification and thus is worth being at the centre of future research works.
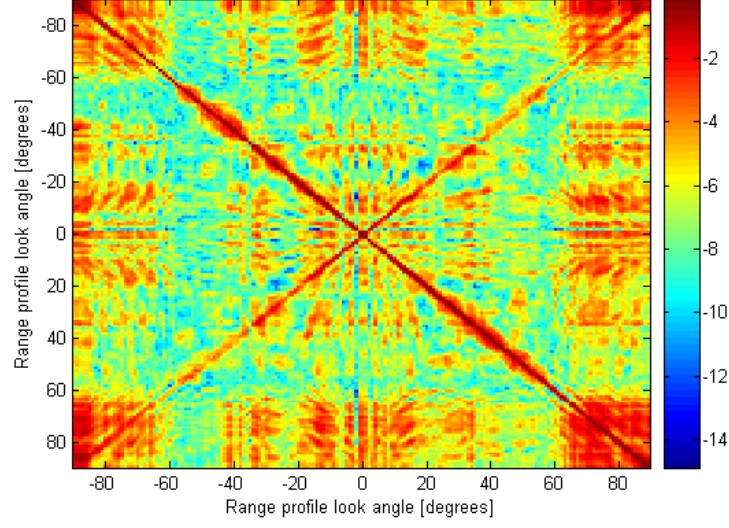
Figure 10.11: Autocorrelation matrix obtained as in Eq. 10.1 for the scaled Boeing 737 described in the previous chapter. Each element i, j is the maximum value of the cross-correlation function between the ith and the jth range profile. Colour scale is in [dB].
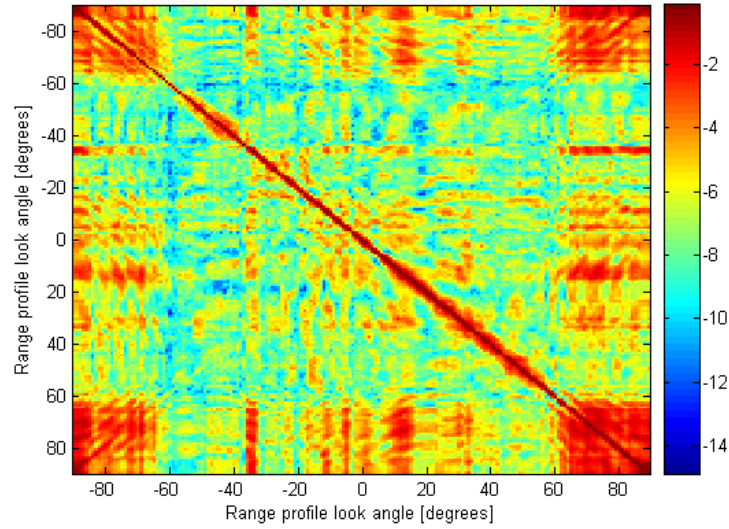
Figure 10.12: Autocorrelation matrix obtained as in Eq. 10.1 for the modified scaled Boeing 737 described in the previous chapter. Each element i, j is the maximum value of the cross-correlation function between the ith and the jth range profile. Colour scale is in [dB].

10.1 Classification of man-made scaled targets

In order to investigate the performance of the bio-inspired classification approach presented in Chapter 8 on man made targets, the same classification performance analysis carried out on the *Cobaea Scandens* flower data, was carried out on the T-55 tank, a M4A3 Sherman scaled tank (Figure 10.13) and a scaled Ford car (Figure 10.14). A photo of the three targets next to each other is given in Figure 10.15, and their geometric dimensions are given in Table 10.1.

HRRPs were collected by transmitting a linear down chirp spanning the frequencies between 200 kHz and 50 kHz towards the targets, which were impaled on a thin pin placed on the horizontal turntable, at a distance of about 21 cm from the artificial bat-head containing the microphone and the loudspeaker. The horizontal turntable was set to rotate with an angular resolution of 1 degrees. A background measurement was subtracted from the echo, at each angular step, and the resulting signal was matched filtered with

Table 10.1: Specifications of the Boeing 737-500 and its 1:400 scaled version. Information taken from www.geminijets.com.

	Length of shortest side	Length of longest side (incl. gun)
T55	4.5 cm	12.5 cm
M4A3 Sherman	3.7	8 cm
Ford Car	3.5 cm	9.9 cm

Figure 10.13: Photo of the scaled M4A3 Sherman tank.

Figure 10.14: Photo of the scaled Ford car.

Figure 10.15: Photo of the scaled M4A3 Sherman tank, the T55 tank and the Ford car next to each other.

Matlab to the analytic signal of the transmitted signal. The analytic signals were obtained from the raw data through a simple Hilbert transform with Matlab. The achieved range resolution was about 2 mm.

Figure 10.16 shows the amplitude of the HRRPs of the T55 tank for the angular perspectives between -90 degrees and +90 degrees. In the image reflections from the gun are visible between -30 and about +20 degrees from 14 cm to 16 cm from the bat head. The strongest return is achieved at -90 degrees and +90 degrees, i.e. when the tank presented its longer sides to the loudspeaker and the microphone. The scattering from the turret is present over all angle between 19 cm and 23 cm. However, this is very complex and the details of the turret, whose dimensions are smaller than the insonifying wavelengths, are not resolved. One scatterer, on the turret can be tracked in the sinogram between -70 and -30 degrees ranging from 23 cm to 19 cm.
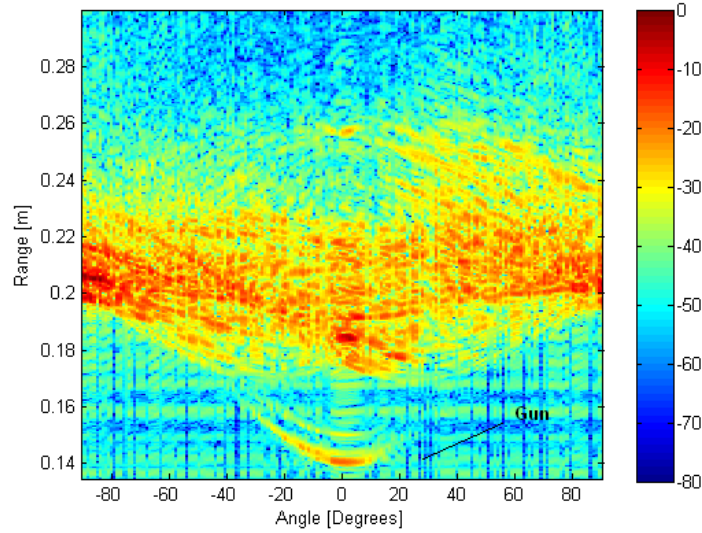
Figure 10.16: Amplitude of the HRRPs of the scaled T-55 tank over a angular window between -90 degrees and +90 degrees. Colour scale is [dB].

This is likely to be generated by the point of junction between the gun and the turret. Another strong contribution, probably due to a reflector located at the base of turret, is visible between +10 and +80 degrees ranging from about 20.5 cm to about 21.cm. Reflections from the back of the tank, that carries two cylindrical tanks, are weak over all this frontal view.

Figure 10.17 plots the amplitude of the HRRPs of the M4A3 Sherman scaled tank versus their corresponding angular perspectives. As for the T-55 tank, the strongest return is achieved at -90 degrees and + 90 degrees. The turret, contributes with a strong return over all angular perspective at a range between 20 cm and 21 cm. For the same reasons discussed above, small details of the turret are not distinguishable. As expected, reflections from the short gun are superimposed with those from the main bulk of the tank, and therefore the gun cannot be not distinguished. The secondary gun of the tank,

211
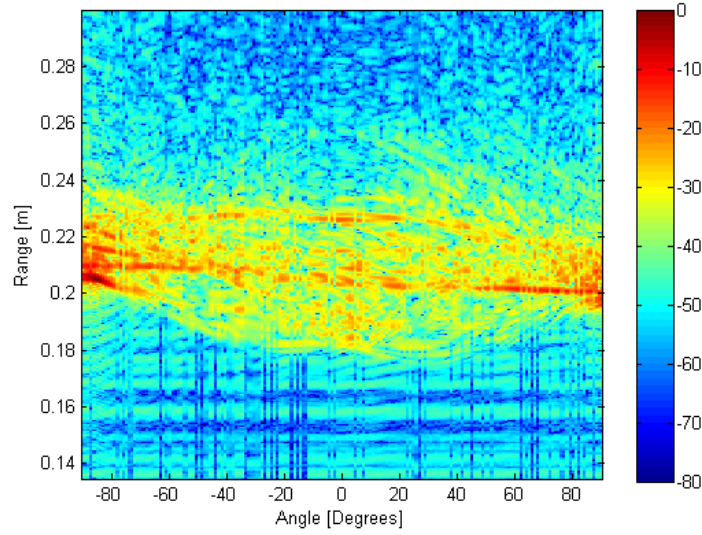
Figure 10.17: Amplitude of the HRRPs of the scaled M4A3 Sherman tank over a angular window between -90 degrees and +90 degrees. Colour scale is [dB].

located on top of the turret, is visible between -10 degrees and +20 degrees at about 23 cm. Reflections from the back are only weakly visible between +15 degrees and +40 degrees ranging from 26 cm to 24 cm. The amplitude of the HRRPs of the scaled Ford car are given in Figure 10.18. The maximum of the return is at -90 degrees and +90 degrees. The front of the car scatters the maximum power between -10 degrees and +10 degrees at a range of about 17 cm from the artificial bat-head. The corner made by the front cowling and the front window of the car is also clearly visible between -20 degrees and +20 degrees at about 20 cm in range. Two additional scatters give a strong contribution at the back of the car. The first one, visible from +5 degrees to about +40 degrees from 23 cm to 22 cm must be the corner made by the end of the roof and the back window. The other scatterer, visible at the same
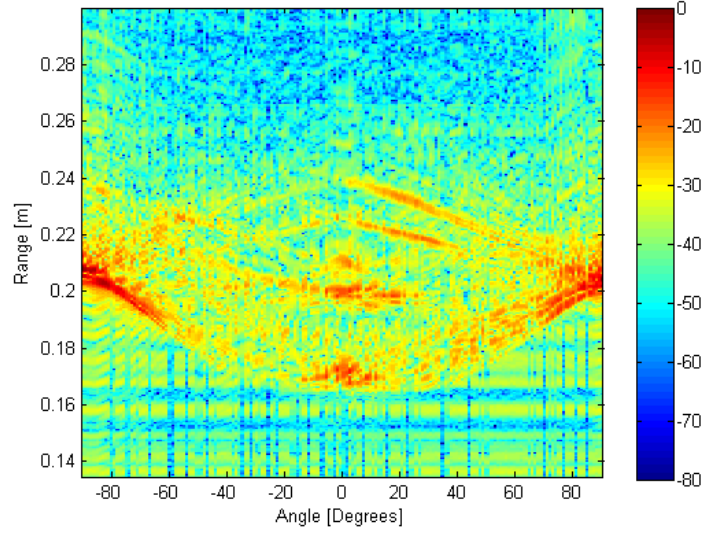
Figure 10.18: Amplitude of the HRRPs of the scaled car over a angular window between -90 degrees and +90 degrees. Colour scale is [dB].

angles and between 24 cm to 22 cm, is likely to be the other corner made by the back window and the back cowling.

Classification performance was assessed in pairs to highlight differences between the targets and to identify the main physical features of the targets that could lead to high level classification performance. In each image, all HRRPs were normalised to mean value equal to zero and mean power equal to unity before classification. 6 HRRPs were extracted from each image to train the classifier leading to a total $N_p = 12$ HRRPs training profiles (because two classes were tested at a time). These corresponded to the 6 angular perspectives that starting from the one gathered at -90 degrees were then separated of 30 degrees. Classification was performed by means of a Knn classifier characterised by a parameter K_n with $n = 3$. The test set was formed by selecting, from each image under test, the profile corresponding

to the perspective at α_0 degrees plus the $(N_{calls} - 1)/2$ profiles collected soon before and soon after it, for a total of $2 * N_{calls}$ test profiles. The separation angle between the test profiles was set to 1 degree and this determined the size of the angular window α around the main looking direction α_0. Each test profile was compared with the training set by calculating the maximum value of the magnitude of its cross-correlation function with each training profile as described in Chapter 8 (Eq. 8.1). For each test profile, between all the $N_p = 12$ maximum values of all the cross-correlation functions, only the $n = 3$ highest values were used to make the decision. Each test profile was assigned to the class that owned the highest number of training profiles between those generating the selected n values. The probability of correct classification was estimated, for each looking angle α_0, as the ratio between the number of correct decisions and the total number of test profiles (N_{calls}). This analysis was then repeated for each looking angle α_0.

Figure 10.19 plots the performance of the classifier when the scaled Ford car was tested against the scaled T-55 tank. The first peak in classification performance (95% correct classification) is achieved at about -50 degrees, i.e. over the angular sector between -60 degrees and -40 degrees. This is the sector where the T-55 tank presents the reflections from the point of junction between the gun and the turret. The second peak in classification performance, with about 80% correct classification, is for $\alpha_0 = 0$ degrees corresponding to the angular window between -10 degrees and + 10 degrees. Over this angular sector, the tank shows clear reflections from the gun and the car shows reflections from the corner reflectors made by the front cowling and the front window. The highest probability of correct classification

(over 95%) is achieved for $\alpha_0 = +50$ degrees, i.e. where the sinogram of the tank presents a strong contribution from the reflector located at the base of turret and the one related to the car contains part of the reflections from the back corner reflectors made by the back cowling and the back window. Classification is poor at -80 degrees and +80 degrees, i.e. when the two targets were facing the artificial bat-head and most of their physical features were masked. Figure 10.20 shows the results of the same analysis when the scaled Ford car was compared to the scaled M4A3 Sherman tank. In this case classification performance are slightly higher on the average. The first peak in performance, with over 95% correct classification, is for $\alpha_o = 0$ degrees (corresponding to the angular window between -10 degrees and +10 degrees). Over this sector, the car shows strong reflections from the corners located at the front cowling and at the front window. The second peak in classification performance, is achieved for α_0 varying between +40 degrees and +50 degrees and corresponds to those angular windows where the scattering from the corner reflectors at the back of the car are dominant. As in the previous case classification performance drops to 50% at -80 degrees and +80 degrees most likely due a masking effect on the features. To conclude this analysis, the same results are given for the case in which the T-55 tank and the M4A3 Sherman tank were compared against each other. On the average classification performance is lower due to close similarities between the two targets. As expected, one of the peak in classification performance is for $\alpha_0=0$, where the sinogram of the T-55 tank clearly presents the gun and that of the M4A3 Sherman tank present a strong scattering from the secondary gun. The other peak in performance (about %80 correct classifi-

cation) is achieved at $\alpha_0 = +50$ degrees. Here, the T-55 tank shows the reflections from the scatterer located at the base of the turret. Finally, another area characterised by high level performance is that between -80 degrees and about -50 degrees. The sector between -50 degrees to -70 degrees contains the scattering from the point of junction between the gun and the turret. At -80 degrees, instead, the two targets face the bat-head and therefore most of their physical features are likely not to be resolved in range. Because, the targets under test are different, and not simply obtained by removing physical parts from an original sample as in the case of the flowers, it remains impossible to conclude that the classifier was always making decision based solely on the physical features of the targets. For example, it is possible that at -80 degrees the classifier was using additional information, such as the total scattered mean power, to decide on the targets.

Results show that, as in the flower case, also for man made targets classification performance can be improved by exploiting those angular windows that contain the information on the main features of the targets. Also, the analysis of classification performance as a function of the looking direction α_0 can allow the identification of these main features. This confirms that, given the knowledge on the targets to be classified, a good strategy aiming at choosing the right trajectories to explore key features is an imperative for high level target classification. How to choose and adapt the trajectory to improve classification performance remains a challenge that will have to be addressed in future works.
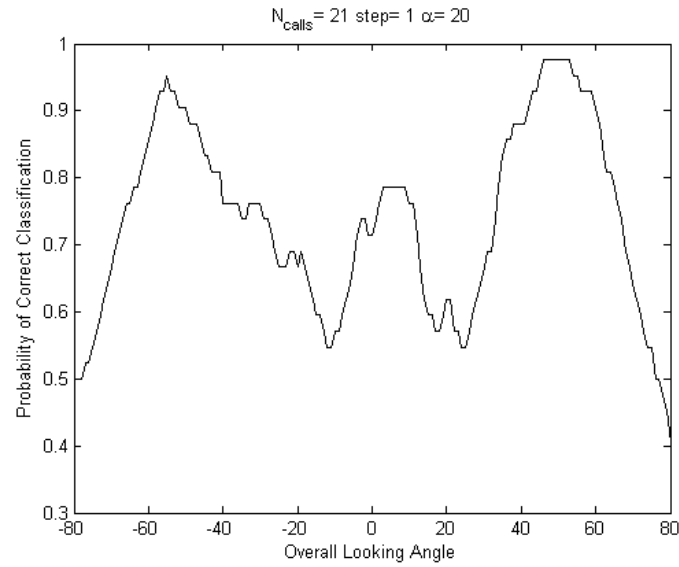
Figure 10.19: Classification performance as a function of look direction angle of a *Knn* classifier testing the scaled T-55 tank and the scaled Ford car (*Ncalls* = 21, α = 20 degrees).
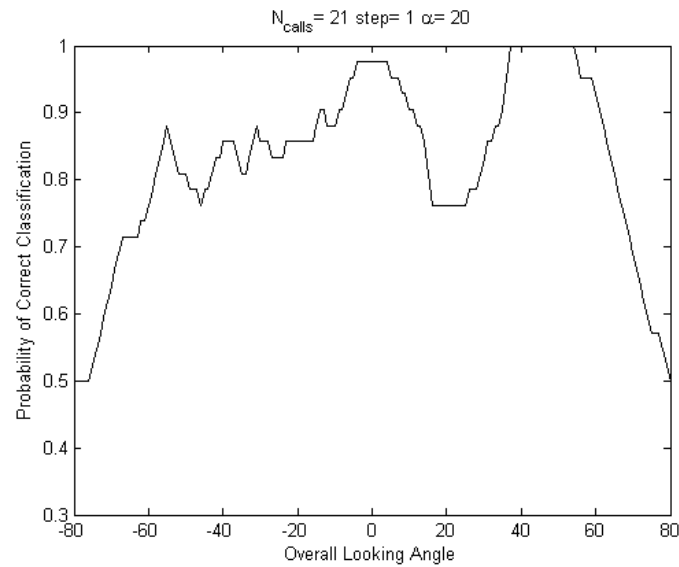
Figure 10.20: Classification performance as a function of look direction angle of a *Knn* classifier testing the scaled M4A3 Sherman tank and the scaled Ford car (*Ncalls* = 21, α = 20 degrees).

217
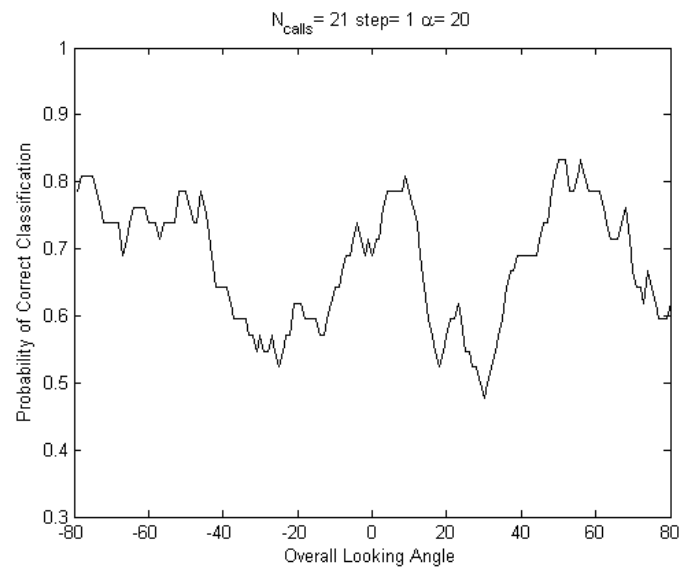
Figure 10.21: Classification performance as a function of look direction angle of a Knn classifier testing the scaled T-55 scaled tank and the scaled M4A3 Sherman tank ($Ncalls = 21$, $\alpha = 20$ degrees).

Chapter 11

Conclusions and suggestions for future work

In this work the methodologies used by nectar-feeding bats to perform the task of classification of bat-pollinated flowers have been investigated. Results have been discussed and related to the task of target classification in radar and sonar systems. In Chapter 4 an example of a series of echolocation calls emitted by a foraging bat has been given with a discussion on similarities and differences with typical radar and sonar waveforms. Results clearly show the ability of bats to intelligently diversify the waveforms they emit for the success of the mission and highlight the presence of harmonics in echolocation calls. The purpose of harmonics is yet unclear and is a fascinating topic that is worth being considered for future research. Here, the effect that multi-components could have on radar and sonar waveforms has been exploited. Results have shown that an intelligent use of multi-component signals can result in advantages on the range cut of the ambiguity function, such as a

drop of the sidelobes.

An acoustic radar fully synchronised with a setup that allows collection of high range resolution profiles of small targets was improved to gather data from two different species of flowers: *Rhytidophyllum auriculatum* and *Cobaea scandens*. A number of experiments aiming at investigating what is the strategy that underpins the process of classification of bat-pollinated flowers by bats have been described together with a discussion of the results. In particular these experiments aimed at exploring the information that bat-pollinated plants display to bats through their flowers and how this information changes depending on their age and maturity stage. Also, the parts of the flowers that plays a leading role in this task were identified and the differences in information as a function of these parts was investigated as well. Results suggest that flower petals can be a very important feature for bat pollinated plants to display information to bats in order to support high recognition/selection performance. The scattering from the petals and the way this changes as a function of the state of the flower could be a way of letting bats know which flower is most suitable for pollination, i.e. holds a nectar reward, and hence play an important role for recognition and selection of the flowers. These results were related to a typical trajectory of a nectar feeding bat in order to understand and make an hypothesis of how bat sample this information in the 3D space. This preliminary analysis showed that the angular perspectives that are exploited are in agreement with the angular window in which features, such as petals, are present in real flowers'echoes. Analysis of an inflorescence of *Rhytidophyllum auriculatum* composed of closed buds an open flowers and Calixes confirmed the hypothesis of the importance of the

trajectory to identify open flowers between clutter and closed buds. Results show that open flowers are much more directional than buds and Calyxes, i.e. visible from a limited number of angular perspectives only. This allow the bat understand the visiting direction into the flower. These results show how nature operates under a high level of space time adaptivity and indeed this is between the current challenges in radar and sonar systems.

Results relating the available information to the the way bats sample this information contain a fundamental limitation that must be addressed in future works. This is represented by the fact that the information available to the bat and the behaviour of the bats in terms of echolocating calls and trajectory separately was gathered in different experiments. It would be of great interest to carry out an experiment where the bat, in the same room with the flower or an object, has the task to detect recognise and approach the target to get the nectar reward. This experiment has to be carried out in a fully controlled environment allowing recording of video and ultrasound information. Doing so, full knowledge of each call emitted by the bat during the mission would be available together with the information on the position where each call was emitted with respect to the position of the targets and, more importantly, to the features of the target. Indeed such experiment is an imperative to corroborate the arguments of this thesis.

This analysis showed that bats gather the information displayed by flowers over a limited angular window. It is likely that they intelligently base their decision by testing the angular perspectives where critical information on the main features of the flowers is available to obtain high level target classification performance. This suggests that a similar approach could be

tested for radar and sonar systems as well. In Chapter 8 a bat inspired approach to radar and sonar target classification is discussed and tested on real data. In particular classification performance of a K_{nn} classifier testing HRRPs measured by a sensor limited to exploit a limited number of angular perspective and emit a small number of pulses only was assessed. Results show that indeed exploiting the angular windows that contain critical features can enhance performance significantly and at the same time show that operating without a specific and intelligent strategy may result in a drop in performance. Indeed these results make worth investigating these concepts further against typical radar and sonar targets. In addition to this, there are still a number of uncertainties that must be addressed in future work. It is self evident that in order to operate this strategy in real radar and sonar scenarios the development of a reliable and automatic algorithms capable of identifying and selecting the angular perspectives that contain the main target features is necessary. These concept require further investigations and results must be corroborated with a greater number of data, and a number of dataset gathered under several conditions. This study suggests that these are fundamental topics that should be targeted by further research on radar and sonar target classification .

The way the bat moves around the target collecting multi perspective information suggests it might even be trying to perform some sort of imaging on the target itself. The frequency of the angular sampling in particular is typical of tomographic imaging techniques and inspired us to an investigation of tomography at this range of ultrasound frequencies in air. This investigation has been carried out on a real scaled radar target in Chapter 9 where multi

perspectives profiles of a scaled Boeing 737 were collected with the acoustic radar. Results confirm the ability of the acoustic radar to capture detailed information of small static targets and in particular allow detection of differences due to small changes in their shape. They also show that ultrasound tomography in air are possible and can lead to good imaging of small static targets. This suggests that ultrasound systems, such as the acoustic radar, might potentially be used in real scenarios to allow detection and classification of very small objects. Because the speed of sound in air at this range of frequencies (typically used by echolocating bats) is only about 343 m/sec the acoustic radar allows a very high range resolution that cannot be easily achieved by other sensors. This could be also used as support to other sensors, such as typical radar systems, to enable a better and more efficient surveillance of high risk areas. Because the results presented in this thesis were obtained by processing data gathered in an ultrasound chamber further investigation aiming at assessing the impact of multipath and clutter on these results are an imperative and represent another potential area of interest of future research. Finally in Chapter 10 it has been investigated whether ultrasound systems, such as the acoustic radar, can be used to gather data of scaled targets in order to carry out a preliminary analysis of classification performance and produce predictions for real radar scenarios that can be validated when data collected by actual radar systems becomes available. A datasets containing HRRPs of a Russian scaled tank is compared to another dataset consisting of HRRPs of Russian T-55 tank gathered by using a real radar systems. Results in the two cases are compared and results show that there are close similarities between the ultrasound case and the radar case.

A discussion on the advantages resulting by using the acoustic radar for this purposes is given as well. Obviously the comparison between the radar case and the ultrasound has been carried out on a limited number of data and a further investigation corroborating the results of this thesis is necessary. Investigation of binaural differences is a key point that has been receiving a growing interest in the last few years. The acoustic radar was developed to allow collection of binaural information and at this stage of our research binaural data is available for most of the experiment presented in this research work. This data has not been fully analysed yet but it remains clear that understanding the role that differences at the two ears play in the task of detection and recognition of targets is an important point that cannot be neglected. For these reasons this will be at the centre of our future research work.

Appendix A

Matlab Code

This appendix contains the Matlab code that has been used to produce the tomographic images presented in this thesis. Following, for completeness, two examples of tomographic images obtained on one the flowers (the fresh unmodified*Cobaea scandens*) and on the scaled T-55 tank are shown.

```
clear all
clc
close all
load('ScaledAircraft.mat'); %File .mat that contains all the HRRPs of the
scaled aircraft
Madd1=zeros(300,180);
Madd2=zeros(300,360);
step=1;
M=[M1;Madd1];
%M=M(:,45:1:135);
S=mean(M')';
```

```
MEA=S*ones(1,size(M,2));

M=M-MEA;

beg=1;

en=300;

i=1;

for i=10:1:30

T=abs(M(beg:en+2*i,:)); % For non-coherent analysis

%T=M(beg:en+2*i,:); % For coherent analysis

R=iradon(T,[-90:89]);

Res=abs(R);

Res=Res/max(max(Res));

figure

imagesc([1:size(R,1)]*343/500e3/2,[1:size(R,2)]*343/500e3/2,20*log10(Res),[-40 0]);

axis xy

xlabel('Range [m]')

ylabel('Cross-Range [m]')

colorbar

end
```
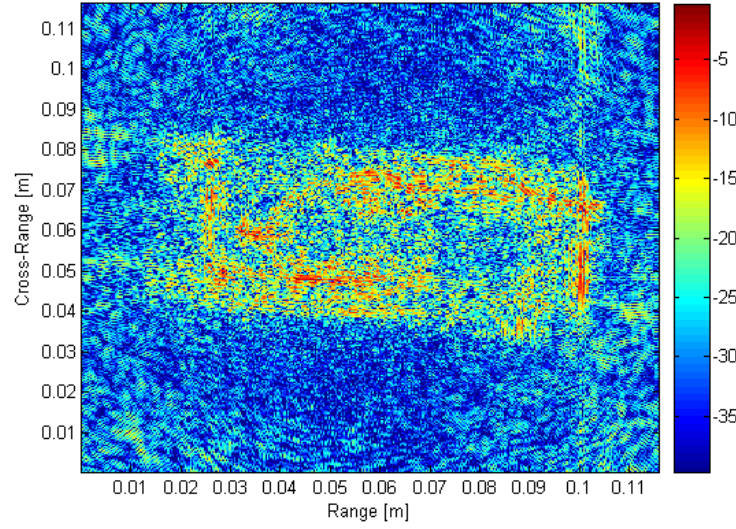
Figure A.1: Tomographic image of the scaled T-55 tank developed by using a complete view of 360 profiles obtained from coherent data. This image was developed by processing the HRRPs of the tank as described in Chapter 9.
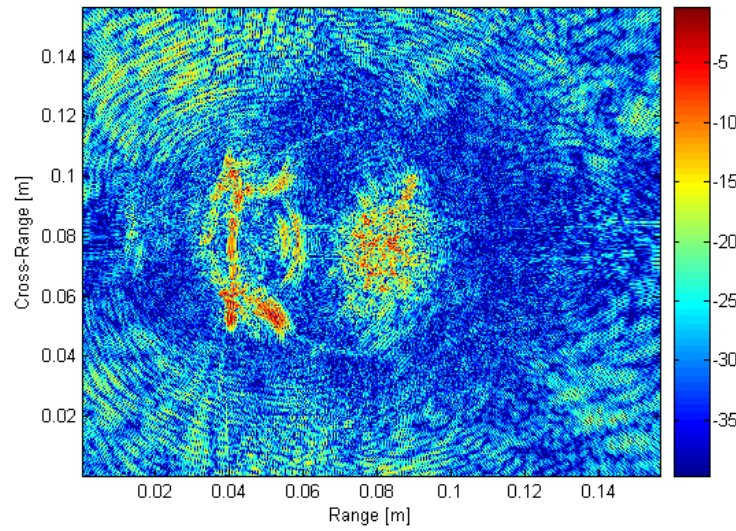
Figure A.2: Tomographic image of the *Cobaea scandens* flower developed by using a frontal view of 180 profiles obtained from coherent data. This image was developed by processing the HRRPs of the flower as described in Chapter 9.

Bibliography

[1] J.-E. Grunwald, S. Schornich and L. Wiegrebe, "Classification of natural textures in echolocation," *Proceedings of the National Academy of Sciences of the United States of America*, vol. 101, pp. 5670–5674, 2004.

[2] D. von Helversen, M. W. Holderied and O. von Helversen, "Echoes of bat-pollinated bell-shaped flowers: conspicuous for nectar-feeding bats?" *Journal of Experimental Biology*, vol. 206, no. 6, pp. 1025–1034, 2003.

[3] G. Jones and E. C. Teling, "The evolution of echolocation in bats," *Trends in Ecology and Evolution*, vol. 21, no. 3, pp. 149–156, 2006.

[4] G. Jones and M. W. Holderied, "Bat echolocation calls: adaptation and convergent evolution," *Proceedings of The Royal Society of London series B-Biological Sciences*, vol. 21, pp. 905–912, 2007.

[5] J. D. Altringham, *Bats Biology and Behaviour*. Oxford University Press, 1996.

[6] M. Vespe, C. Baker and H. Griffiths, "Aspect dependent drivers for multi-perspective target classification," *2006 IEEE Conference on Radar*, pp. 256–260, 24-27 Apr 2006, Verona, NY, USA.

[7] A. Zyweck and R. Bogner, "Radar target recognition using range profiles," *ICASSP-94.*, vol. ii, pp. II/373–II/376 vol.2, 19-22 Apr 1994.

[8] M. Vespe, C. Baker and H. Griffiths, "Multi-perspective target classification," *2005 IEEE International Radar Conference*, pp. 877–882, 9-12 May 2005, Arlington, VA, USA.

[9] G. E. Smith, K. Woodbridge and C. J. Baker, "Micro-doppler signature classification," *CIE '06. International Conference on Radar, 2006.*, pp. 1–4, 16-19 Oct. 2006, Shanghai, China.

[10] V. Chen, F. Li, S.-S. Ho and H. Wechsler, "Micro-doppler effect in radar: phenomenon, model, and simulation study," *IEEE Transactions on Aerospace and Electronic Systems*, vol. 42, no. 1, pp. 2–21, Jan. 2006.

[11] E. Cerrone, C. Baker and Y. Kwag, "Scattering centre extraction for target classification," *EUSAR 2008*, June 2-5 2008, Friedrichshafen, Germany.

[12] R. Duda, P. Hart and D. Stork, *Pattern Classification.* John Wiley and Sons, 2001.

[13] H.-U. Schnitzler, D. Menne, R. Kober and K. Heblich, "The acoustical image of fluttering insects in echolocating bats," *Neuroethology and Behavioral Physiology*, pp. 235–250, 1983.

[14] G. von der Emde and H.-U. Schnitzler, "Classification of insects by echolocating greater horseshoe bats," *Journal of Comparative Physiology A: Neuroethology, Sensory, Neural, and Behavioral Physiology*, vol. 167, pp. 423–430, 1990.

[15] J. Thiele and Y. Winter, "Hierarchical strategy for relocating food targets in flower bats: spatial memory versus cue-directed search," *Animal Behaviour*, vol. 69, pp. 315–327, 2005.

[16] D. von Helversen and Y. Winter, "Acoustic guide in batpollinated flower," *Nature*, vol. 398, pp. 759–760, 1999.

[17] R. Simon, M. W. Holderied and O. von Helversen, "Size discrimination of hollow hemispheres by echolocation in a nectar feeding bat," *Journal of Experimental Biology*, vol. 209, pp. 3599–3609, 2006.

[18] M. I. Skolnik, *Radar Handbook (Second Edition)*. McGraw-Hill, 1990.

[19] P. Tait, *Introduction to Radar Target Recognition*. IEE, 2005.

[20] C. Looney, *Pattern Recognition Using Neural Networks*. Oxford University Press, 1998.

[21] A. Ksienski, Y. Lin and L. White, "Low-frequency approach to target identification," *Proceedings of the IEEE*, vol. 63, no. 12, pp. 1651–1660, Dec. 1975.

[22] M. Van Blaricum, L. Pearson and R. Mittra, "An efficient scheme for radar target recognition based on the complex natural resonances of the

target," *IEEE Antennas and Propagation Society International Symposium, 1975*, vol. 13, pp. 416–419, Jun 1975.

[23] A. Zyweck, "Preprocessing issue in high resolution radar target classification," *PhD Thesis, University of Adelaide*, 1995.

[24] M. Cohen, "An overview of high range resolution radar techniques," *National Telesystems Conference 1991.*, vol. 1, pp. 107–115, 26-27 Mar 1991, Atlanta, Georgia, USA.

[25] C. Smith and P. Goggans, "Radar target identification," *IEEE Antennas and Propagation Magazine*, vol. 35, no. 2, pp. 27–38, Apr. 1993.

[26] H.-J. Li and S.-H. Yang, "Using range profiles as feature vectors to identify aerospace objects," *IEEE Transactions on Antennas and Propagation*, vol. 41, no. 3, pp. 261–268, Mar 1993.

[27] S. Hudson and D. Psaltis, "Correlation filters for aircraft identification from radar range profiles," *IEEE Transactions on Aerospace and Electronic Systems*, vol. 29, no. 3, pp. 741–748, Jul 1993.

[28] A. Zyweck and R. Bogner, "Radar target classification of commercial aircraft," *IEEE Transactions on Aerospace and Electronic Systems*, vol. 32, no. 2, pp. 598–606, Apr 1996.

[29] V. Chandran and S. Elgar, "Pattern recognition using invariants defined from higher order spectra- one dimensional inputs," *IEEE Transactions on Signal Processing, [see also IEEE Transactions on Acoustics, Speech, and Signal Processing]*, vol. 41, no. 1, pp. 205–, Jan. 1993.

[30] J. Tugnait, "Detection of non-gaussian signals using integrated polyspectrum," *IEEE Transactions on Signal Processing, [see also IEEE Transactions on Acoustics, Speech, and Signal Processing]*, vol. 42, no. 11, pp. 3137–3149, Nov. 1994.

[31] X. Liao and Z. Bao, "Circularly integrated bispectra: novel shift invariant features for high-resolution radar target recognition," *Electronics Letters*, vol. 34, no. 19, pp. 1879–1880, 17 Sep 1998.

[32] X.-D. Zhang, Y. Shi and Z. Bao, "A new feature vector using selected bispectra for signal classification with application in radar target recognition," *IEEE Transactions on Signal Processing [see also IEEE Transactions on Acoustics, Speech, and Signal Processing]*, vol. 49, no. 9, pp. 1875–1885, Sep 2001.

[33] X. Liao, Z. Bao and M. Xing, "On the aspect sensitivity of high resolution range profiles and its reduction methods," *IEEE International Radar Conference, 2000*, pp. 310–315, 2000.

[34] L. Du, H. Liu, Z. Bao and M. Xing, "Radar HRRP target recognition based on higher order spectra," *IEEE Transactions on Signal Processing [see also IEEE Transactions on Acoustics, Speech, and Signal Processing]*, vol. 53, no. 7, pp. 2359–2368, July 2005.

[35] M. Cohen, "An overview of radar-based, automatic, noncooperative target recognition techniques," *IEEE International Conference on Systems Engineering, 1991.*, pp. 29–34, 1-3 Aug 1991.

[36] A. Ghaleb, L. Vignaud and J. Nicolas, "Micro-Doppler analysis of wheels and pedestrians in ISAR imaging," *IET Signal Processing*, vol. 2, no. 3, pp. 301 –311, september 2008.

[37] ——, "Micro-Doppler analysis of pedestrians in ISAR imaging," *IEEE Radar Conference 2008. RADAR '08.*, pp. 1 –5, May 2008, Roma, Italy.

[38] P. Sammartino and J. Fortuny-Guasch, "Space and frequency diversity for moving personnel spectrogram estimation," *accepted for IEEE Radar Conference 2010.*, 10-14 May 2010, Arlington, VA, USA.

[39] G. E. Smith, K. Woodbridge and C. J. Baker, "Template based micro-doppler signature classification," *IET Seminar on High Resolution Imaging and Target Classification*, pp. 127–144, 21 Nov. 2006.

[40] H.-U. Schnitzler and E. K. V. Kalko, "Echolocation by Insect-Eating Bats," *BioScience*, vol. 51, no. 7, pp. 557–569, 2001.

[41] H.-U. Schnitzler, C. F. Moss and A. Denzinger, "From spatial orientation to food acquisition in echolocating bats," *Trends in Ecology and Evolution*, vol. 18, no. 8, pp. 386–394, 2003.

[42] B. Tian and H.-U. Schnitzler, "Echolocation signals of the greater horseshoe bat (rhinolophus ferrumequinum) in transfer flight and during landing," *The Journal of the Acoustical Society of America*, vol. 101, no. 4, pp. 2347–2364, 1997.

[43] G. Schuller and G. D. Pollak, "Disproportionate frequency representation in the inferior colliculus of doppler compensating greater horseshoe

bats. Evidence for an acoustic fovea," *Journal of Comparative Physiology*, vol. 132, pp. 47–54, 1979.

[44] J. Ostwald, "Tonotopical organization and pure tone response characteristics of single units in the auditory cortex of the Greater Horseshoe Bat," *Journal of Comparative Physiology A: Neuroethology, Sensory, Neural, and Behavioral Physiology*, vol. 155, pp. 821–834, 1984.

[45] G. von der Emde and H.-U. Schnitzler, "Fluttering target detection in hipposiderid bats," *Journal of Comparative Physiology A: Neuroethology, Sensory, Neural, and Behavioral Physiology*, vol. 159, pp. 765–772, 1986.

[46] R. Kober and H.-U. Schnitzler, "Information in sonar echoes of fluttering insects available for echolocating bats," *The Journal of the Acoustical Society of America*, vol. 87, no. 2, pp. 882–896, 1990.

[47] O. Sotavalta, "The flight tone (wing stroke frequency) of insects," *Acta Entomologica Fennica*, vol. 4, pp. 5–117, 1947.

[48] H.-U. Schnitzler, "Echoes of fluttering insects: Information for echolocating bats," *Cambridge University Press*, pp. 226–243, 1987.

[49] R. C. Roverud, V. Nitsche and G. Neuweiler, "Discrimination of wingbeat motion by bats, correlated with echolocation sound pattern," *Journal of Comparative Physiology A: Neuroethology, Sensory, Neural, and Behavioral Physiology*, vol. 168, pp. 259–263, 1991.

[50] Y. W. Sum and D. Menne, "Discrimination of fluttering targets by the fm-bat *pipistrellus stenopterus*?" *Journal of Comparative Physiology A: Neuroethology, Sensory, Neural, and Behavioral Physiology*, vol. 163, pp. 349–354, 1988.

[51] A. Grossetête and C. F. Moss, "Target flutter rate discrimination by bats using frequency-modulated sonar sounds: Behavior and signal processing models," *The Journal of the Acoustical Society of America*, vol. 103, no. 4, pp. 2167–2176, 1998.

[52] K. Krumbholz and S. Schmidt, "Evidence for an analytic perception of multiharmonic sounds in the bat, megaderma lyra, and its possible role for echo spectral analysis," *The Journal of the Acoustical Society of America*, vol. 109, no. 4, pp. 1705–1716, 2001.

[53] Y. Yovel, M. L. Melcon, M. O. Franz, A. Denzinger and H.-U. Schnitzler, "The voice of bats: How greater mouse-eared bats recognize individuals based on their echolocation calls," *PLoS Computational Biology*, vol. 5, no. 6, pp. 1–10, 06 2009.

[54] J. A. Simmons, N. Neretti, N. Intrator, R. A. Altes, M. J. Ferragamo and M. I. Sanderson, "Delay accuracy in bat sonar is related to the reciprocal of normalized echo bandwidth, or Q," *Proceedings of the National Academy of Sciences of the United States of America*, vol. 101, pp. 3638–3643, 2004.

[55] C. F. Moss and H.-U. Schnitzler, "Behavioral studies of auditory information processing," *Hearing by Bats, Springer-Verlag, New York*, pp. 87–145, 1995.

[56] P. A. Saillant, J. A. Simmons, S. P. Dear and T. A. McMullen, "A computational model of echo processing and acoustic imaging in frequency-modulated echolocating bats: The spectrogram correlation and transformation receiver," *The Journal of the Acoustical Society of America*, vol. 94, no. 5, pp. 2691–2712, 1993.

[57] J. A. Simmons, P. A. Saillant, M. J. Ferragamo, T. Haresign, S. P. Dear, J. Fritz and T. A. McMullen, "Auditory Computations for Biosonar Target Imaging in Bats," *Auditory Computations for Biosonar Target Imaging in Bats, Springer-Verlag, New York*, pp. 401–468, 1996.

[58] D. von Helversen and Y. Winter, "Glossophagine Bats and Their Flowers: Costs and Benefits for Plants and Pollinators," *Bat Ecology, University of chicago Press, Chicago*, pp. 346–397, 2003.

[59] D. von Helversen and O. von Helversen, "Object recognition by echolocation: a nectar-feeding bat exploiting the flowers of a rain forest vine," *Journal of Comparative Physiology A: Neuroethology, Sensory, Neural, and Behavioral Physiology*, vol. 189, pp. 327–336, 2003.

[60] D. von Helversen, "Object classification by echolocation in nectar feeding bats: size-independent generalization of shape," *Journal of Comparative Physiology A: Neuroethology, Sensory, Neural, and Behavioral Physiology*, vol. 190, pp. 515–521, 2004.

[61] M. W. Holderied and O. von Helversen, "'Binaural echo disparity' as a potential indicator of object orientation and cue for object recognition in echolocating nectar-feeding bats," *Journal of Experimental Biology*, vol. 209, no. 17, pp. 3457–3468, 2006.

[62] T. Papadopoulos, R. Allen and S. Haynes, "Determining the binaural signals in bat echolocation," *Advances in Science and Technology*, vol. 58, pp. 97–102, 2008.

[63] P. Woodward, *Probability and Information Theory with Applications to Radar*. New York: McGraw-Hill, 1953.

[64] N. Levanon and E. Mozeson, *Radar Signals*. Wiley, 2004.

[65] J. Kroszczynski, "Pulse compression by means of linear-period modulation," *Proceedings of the IEEE*, vol. 57, no. 7, pp. 1260 – 1266, July 1969.

[66] C. Baker, M. Vespe and G. Jones, "50 million years of waveform design," in *The Institution of Engineering and Technology Forum on Waveform Diversity and Design in Communications, Radar and Sonar, 2006.*, Nov. 2006, pp. 7–21.

[67] M. Vespe, G. Jones and C. Baker, "Lessons for radar," *IEEE Signal Processing Magazine*, vol. 26, no. 1, pp. 65–75, Jan. 2009.

[68] "University of Maryland: BatLab, Auditory Neuroethology Laboratory," *http://www.bsos.umd.edu/psyc/batlab/*.

[69] M. Hurtado and A. Nehorai, "Bat-inspired adaptive design of waveform and trajectory for radar," *42nd Asilomar Conference on Signals, Systems and Computers 2008*, pp. 36 –40, 26-29 Oct 2008, Pacific Grove, CA, USA.

[70] S. Haykin, "Cognitive radar: a way of the future," *IEEE Signal Processing Magazine*, vol. 23, no. 1, pp. 30 – 40, Jan. 2006.

[71] R. C. Roverud, "Harmonic and frequency structure used for echolocation sound pattern recognition and distance information processing in the rufous horseshoe bat," *Journal of Comparative Physiology A: Neuroethology, Sensory, Neural, and Behavioral Physiology*, vol. 166, pp. 251–255, 1989.

[72] H. Griffiths, L. Vinagre and W. Lee, "Developments in radar waveform design," *12th International Conference on Microwaves and Radar, 1998. MIKON '98.*, vol. 4, pp. 56 –76, 20-22 May 1998, Krakow , Poland.

[73] A. Streicher, R. Muller, H. Peremans and R. Lerch, "Broadband ultrasonic transducer for a artificial bat head," *2003 IEEE Symposium on Ultrasonics*, vol. 2, pp. 1364 – 1367, 2003.

[74] *Results of private conversation with Dr. Marc Holderied and Miss. Violene Dapreaux.* School of Biological Sciences, University of Bristol.

[75] K. Ghose and C. F. Moss, "The sonar beam pattern of a flying bat as it tracks tethered insects," *The Journal of the Acoustical Society of America*, vol. 114, no. 2, pp. 1120–1131, 2003.

[76] A. Surlykke, S. Pedersen and L. Jakobsen, "Echolocating bats emit a highly directional sonar sound beam in the field," *Proceeding of the Royal Society B*, vol. 276, pp. 853–860, 2008.

[77] A. Volz, *Echolocation and flight behaviour of neo-tropical nectar-feeding bats (Chiroptera, Glossophaginae) during flower approach.* Master's Thesis, University of Erlangen, 2006.

[78] M. Pinto, "Mine super-classification with auv-based high resolution synthetic aperture sonar," *NATO Workshop on Machine Intelligence For Autonomous Operations*, 7-8 Oct. 2009, Lerici, Italy.

[79] J. Bell, Y. Petillot, K. Lebart, S. Reed, E. Coiras, P. Mignotte and H. Rohou, "Target recognition in synthetic aperture and high resolution sidescan sonar," *The Institution of Engineering and Technology Seminar on High Resolution Imaging and Target Classification*, pp. 99 –106, Nov. 2006.

[80] M. Vespe, C. Baker and H. Griffiths, "Radar target classification using multiple perspectives," *IET Radar, Sonar and Navigation*, vol. 1, no. 4, pp. 300 –307, Aug. 2007.